The
PHILOSOPHICAL MAGAZINE

FIRST PUBLISHED IN 1798

UNIVERSITY OF HAWAII
LIBRARY
AUG 1 '55

L. 46 SEVENTH SERIES No. 377 June 1955

A Journal of Theoretical Experimental and Applied Physics

EDITOR
PROFESSOR N. F. MOTT, M.A., D.Sc., F.R.S.

EDITORIAL BOARD
SIR LAWRENCE BRAGG, O.B.E., M.C., M.A., D.Sc., F.R.S.
SIR GEORGE THOMSON, M.A., D.Sc., F.R.S.
PROFESSOR A. M. TYNDALL, C.B.E., D.Sc., F.R.S.

PRICE 15s. 0d.
Annual Subscription £8 0s. 0d. payable in advance

ED AND PUBLISHED BY TAYLOR & FRANCIS LTD., RED LION COURT, FLEET ST., LONDON, E.C.4

Commemoration Number

To mark the 150th Anniversary of the

PHILOSOPHICAL MAGAZINE

Natural Philosophy through the

Eighteenth Century & Allied Topics

CONTENTS

- The Philosophical Magazine. By ALLAN FERGUSON, M.A., D.Sc., and JOHN FERGUSON, M.A., B.D.
- **Astronomy through the Eighteenth Century.** By Sir H. SPENCER-JONES, F.R.S.
- **Physics in the Eighteenth Century.** By Prof. HERBERT DINGLE, D.Sc.
- **Chemistry through the Eighteenth Century.** By Prof. J. R. PARTINGTON, D.Sc.
- **Mathematics through the Eighteenth Century.** By J. F. SCOTT, Ph.D.
- **Engineering and Invention in the Eighteenth Century.** By Engineer-Captain EDGAR C. SMITH, O.B.E., R.N.
- **Scientific Instruments in the Eighteenth Century.** By ROBERT S. WHIPPLE, M.I.E.E., F.Inst.P.
- **The Scientific Periodical from 1665 to 1798.** By DOUGLAS McKIE, D.Sc., Ph.D.
- **Scientific Societies to the end of the Eighteenth Century.** By DOUGLAS McKIE, D.Sc., Ph.D.
- **The Teaching of the Physical Sciences at the end of the Eighteenth Century.** By F. SHERWOOD TAYLOR, Ph.D.

ALERE FLAMMAM

viii+164 pages

15/6

POST FREE

TAYLOR & FRANCIS, LTD.

RED LION COURT, FLEET ST., LONDON, E.C.4

PRINTERS & PUBLISHERS FOR OVER 150 YEARS

LXVII. *The Production of Hyperons and Heavy Mesons*

By G. D. James and R. A. Salmeron*
The Physical Laboratories, The University, Manchester†

[Received February 21, 1955]

Abstract

A full dynamical analysis of the reaction

$$\pi + N \rightarrow Y + K \quad . \; . \; . \; . \; . \; . \; . \quad (1)$$

is given and it is shown that some of the results apply to the production of hyperons in any collision with a free nucleon at rest. In particular, difficulty is found in accounting for the low-energy hyperons that are frequently observed in both cloud chambers and photographic emulsion. Their existence necessitates a mechanism by which hyperons can lose most of their energy. It is suggested that this process is scattering by nucleons.

19 cloud chamber photographs showing two *V*-events associated with the same nuclear interaction are discussed. In no case do the *V*-events represent the decays of the two secondaries of reaction (1).

The observed frequency of associated *V*-events provides no evidence for or against the hypothesis that heavy unstable particles are always produced in reaction (1) or in similar 'double production' reactions. Because the secondary particles from these reactions are scattered in heavy nuclei it is concluded that the reactions can best be studied in light materials.

§ 1. Introduction

In this paper we discuss the production of hyperons and heavy mesons considering, in particular, the evidence available from a cosmic ray cloud chamber experiment.

Fowler *et al.* (1953, 1954) first observed the double production of hyperons and heavy mesons in collisions between energetic negative π-mesons and free protons. Several events observed in the gas of a hydrogen-filled diffusion cloud chamber were interpreted as examples of the reaction

$$\pi^- + P \rightarrow Y + K$$

where Y stands for a hyperon and K for a heavy meson.‡ Since their discovery of this type of reaction a number of examples of the production of Y- and K-particles in a single nuclear interaction have been reported. These are considered briefly in § 2.

---

* On leave from the Centro Brasileiro de Pesquisas Fisicas, Rio de Janeiro.

† Communicated by G. D. Rochester.

‡ Throughout this paper we use the nomenclature proposed by Amaldi *et al.* (1954).

There is a good theoretical reason for believing that Y- and K-particles should be more readily produced in pairs than singly (Nambu *et al.* 1951, Pais 1952). Their long lifetimes cannot be reconciled with their copious production if they are produced singly. In fact, it may well be that every Y- or K-particle observed experimentally is produced in association with another such particle which generally escapes detection. The experimental evidence for and against this hypothesis is discussed in the later sections of the paper.

When it is realized that some thousands of unstable heavy particles have now been observed in cosmic ray cloud chamber experiments, it appears surprising that so little can be said with confidence about the mechanism of their production. The reasons for this situation are considered in § 5.

§ 2. PUBLISHED EXAMPLES OF ASSOCIATED PRODUCTION

The most important evidence for double production of hyperons and heavy mesons comes from the work with the Brookhaven accelerator summarized by Fowler *et al.* (1955). In interactions between negative π-mesons and protons in hydrogen nine events have been observed that are interpreted as examples of the reaction

$$\pi^- + \mathrm{P} \rightarrow \mathrm{Y} + \mathrm{K}.$$

Only in a few cases could complete dynamical measurements be made and there is some uncertainty in the masses that must be assigned to the secondary particles. In particular, Fowler *et al.* show that in some events the neutral hyperon produced is a Λ^0-particle while in others the measurements are better fitted by assuming a larger mass for the Y^0-particle. It is suggested that a Λ^0-particle could subsequently arise from the rapid γ-decay of the heavier hyperon.

Details have also been published of a further four events that are dynamically compatible with the general reaction

$$\pi + \mathrm{N} \rightarrow \mathrm{Y} + \mathrm{K} \quad . \quad . \quad . \quad . \quad . \quad . \quad . \quad (1)$$

where N represents a nucleon. In each of the four cases the reaction occurs in a complex nucleus. One of the events (Fowler *et al.* 1954) showed the decays of a Λ^0- and a θ^0-particle coming from a nuclear interaction in the wall of a cloud chamber. A similar event was reported by Thompson *et al.* (1954) but in this case the nuclear interaction was caused by a cosmic ray particle. The remaining two events were found by Dahanayake *et al.* (1954) in nuclear emulsion. These events are stars from which a charged hyperon and heavy meson emerge; measurements on both events show that they are compatible with the dynamics of reaction (1).

In addition to the above well-measured examples of double production in reaction (1) there are many examples of associated[*] Y- and K-particles coming from a single nuclear interaction. In nuclear emulsion experiments such association particles have been described by Lal *et al.* (1952) and by Debenedetti *et al.* (1954). In cloud chamber experiments associated pairs of *V*-events are quite frequently observed but the only detailed analysis of such pairs has been made by Ballam *et al.* (1955). In this paper we report measurements on 19 pairs of associated *V*-events.

In cosmic ray experiments on heavy unstable particles production occurs in complex nuclei where scattering might be expected to mask the dynamical relations of the production process. The four examples of reaction (1) that have been observed in heavy nuclei show that this is not always so and, for this reason, we give in § 3 a full analysis of the dynamics of reaction (1). In later sections we compare our experimental observations with the results of this analysis.

§ 3. Dynamics of Double Production Processes

(*a*) *The Interaction* $\pi+\mathrm{N}\rightarrow\mathrm{Y}+\mathrm{K}$

Some features of the dynamics of reaction (1) have been described by Reynolds and Treiman (1954) and by Dahanayake *et al.* (1954). We wish to have a complete description of the reaction in both the laboratory and centre of mass systems of coordinates.

Fig. 1

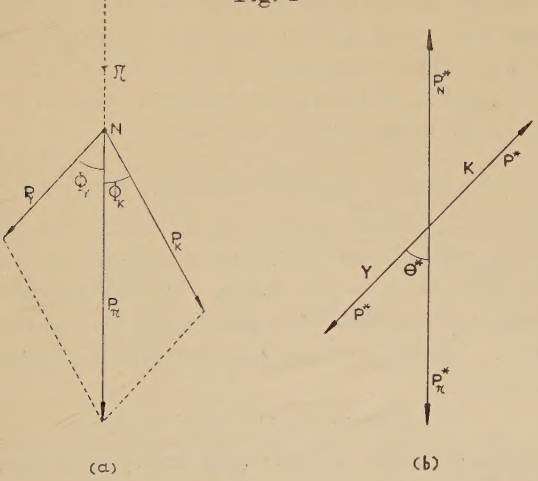

Diagram explaining the nomenclature used in the dynamical analysis of the reaction $\pi+\mathrm{N}\rightarrow\mathrm{Y}+\mathrm{K}$. (*a*) represents the collision in the laboratory system where the nucleon is at rest and (*b*) shows the collision in the centre of mass system.

---

[*] We distinguish between double production and ‘ associated ’ production restricting the former to describe production in a specific reaction such as (1). By associated particles we mean only particles which appear to come from a single nuclear interaction.

Figures 1 (*a*, *b*) show the quantities used to describe the reaction in the two frames of reference. In the laboratory system (in which the nucleon is assumed to be at rest) there are three momenta, p_π, p_Y, and p_K, and two angles, ϕ_Y and ϕ_K. These quantities are, of course, related by the vector equation $p_Y+p_K=p_\pi$. In the centre of mass system the momentum (p^*) of either secondary particle is determined uniquely by p_π and, for a given p_π, the only parameter needed to describe the reaction is θ^*, the angle between the trajectories of the incident π-meson and the emergent Y-particle.

Figure 2 (*a*) shows the variation of ϕ_Y with $1/p_Y$ for different values of p_π and θ^* while figure 2 (*b*) shows the corresponding variation of ϕ_K with $1/p_K$. In calculating these values the masses of the hyperon and heavy meson have been taken to be those of the neutral Λ^0- and θ^0-particles (2181 m_e and 965 m_e).

Figure 2 shows some features which demand particular attention. Most striking are the limits within which p_Y is confined. Under no circumstances can the Y-particle have a momentum of less than 195 MeV/c in the laboratory system nor can its trajectory ever make an angle greater than 57° with that of the incident π-meson. For low values of p_π the limits imposed on p_Y and ϕ_Y are even more restrictive.

A second feature of the dynamics which is apparent from fig. 2 is that the Y- and K-particles produced in reaction (1) cannot have a small angle between their trajectories unless one of their momenta is small. This is better shown in the type of diagram used by Dahanayake *et al.* where the values of p_Y and p_K are plotted for a given value of the total angle $\phi(=\phi_Y+\phi_K)$. This diagram is drawn in fig. 3 for the interesting cases where ϕ is small. It shows, for example, that if ϕ is less than 30° either p_Y or p_K must be less than 6×10^8 ev/c.

(*b*) *More Complex Production Processes*

The limitation of p_Y shown in fig. 2 (*a*) is due to the difference in mass between the target nucleon and the secondary hyperon. It arises because increasing the value of p_π never makes the velocity of the hyperon in the centre of mass system equal the velocity of the centre of mass system in the laboratory. Letting γ_Y and γ_{CM} correspond to these two velocities we find that

$$\gamma_Y/\gamma_{CM}\rightarrow m_N/m_Y \quad \text{as} \quad p_\pi\rightarrow\infty$$

where m_N and m_Y are the nucleon and hyperon masses. To find the minimum value of p_Y we take the difference between these two velocities which leads to the result

$$p_Y\rightarrow\tfrac{1}{2}m_Y(m_Y/m_N-m_N/m_Y).$$

This quantity is equal to 195 MeV/c if m_Y is taken to be 2181 m_e.

In this extreme relativistic approximation the masses of the π- and K-mesons do not enter the calculation of the hyperon momentum and the limiting curve in fig. 2 (*a*) holds for all reactions of the type

$$\mathrm{A+N\rightarrow Y+B} \qquad \ldots\ldots\ldots \quad (2)$$

Fig. 2

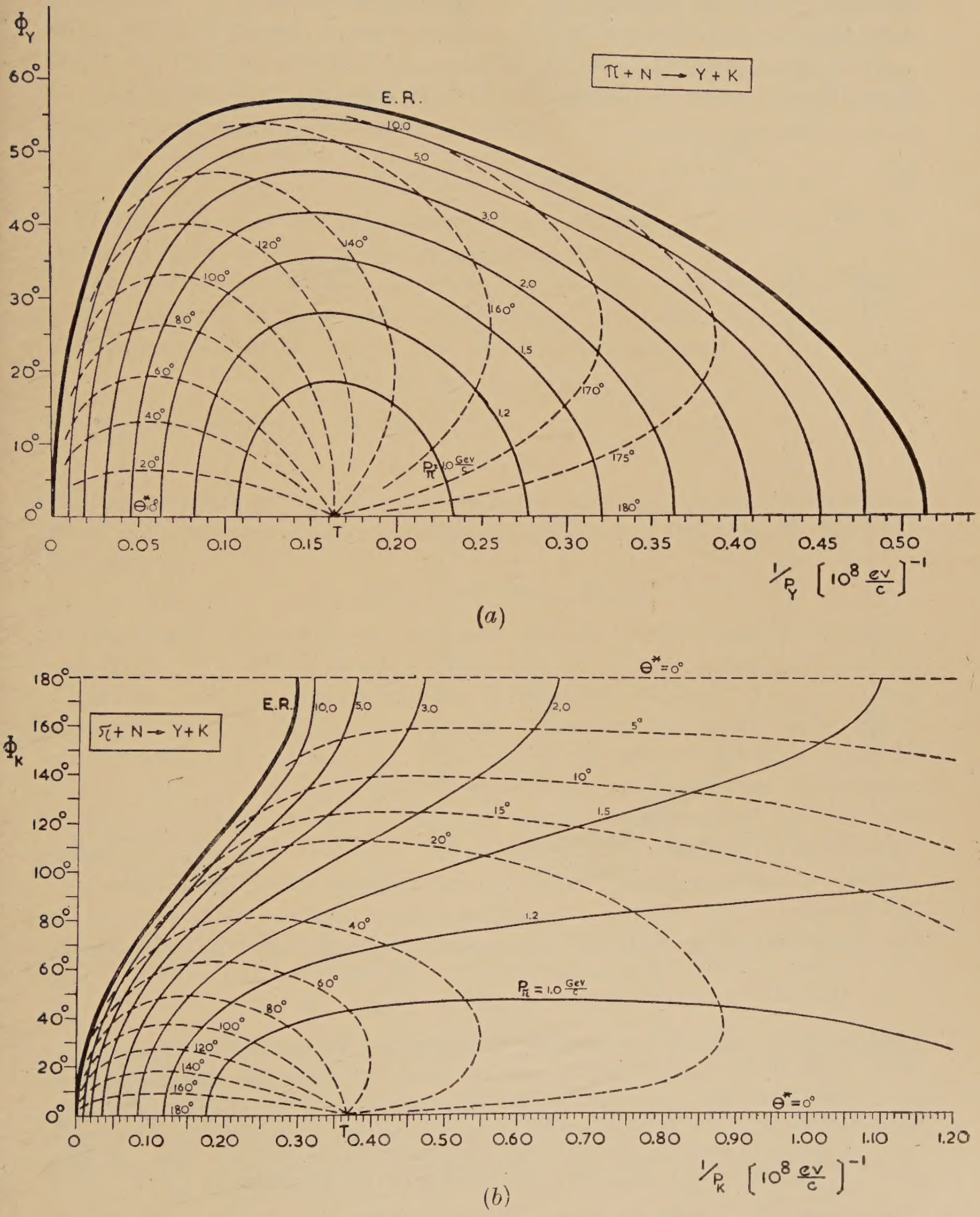

Momenta and angles of emission of the secondaries from the reaction $\pi + N \rightarrow Y + K$. The full lines are curves of constant p_π; the broken lines are curves of constant θ^* (see fig. 1). The value of p_π is given in Gev/c against each solid line and the values of θ^* are given in degrees.

(*a*) shows the variation of ϕ_Y with $1/p_Y$ and (*b*) the corresponding values of ϕ_K and $1/p_K$. The masses of the Y- and K-particles have been taken to be 2181 m_e and 965 m_e.

The solid lines marked E.R. show the limiting angles and momenta as $p_\pi \rightarrow \infty$. These lines represent the limits for any reaction of the type $A + N \rightarrow Y + B + C + \ldots\ldots$ (see text).

whatever the masses of the particles A and B. A full discussion of reaction (2) for all values of p_A is complicated but it is not difficult to show that the minimum value of p_Y occurs when p_A has an extreme value —either the threshold value or infinity. The minimum value of p_Y is then either its value at the threshold of the reaction or 195 Mev/c.

Fig. 3

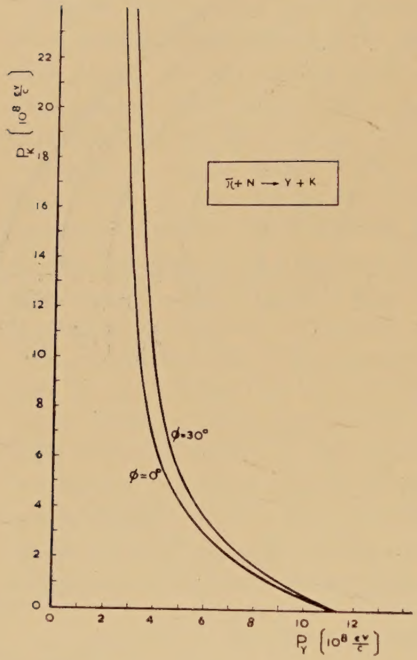

Fig. 4

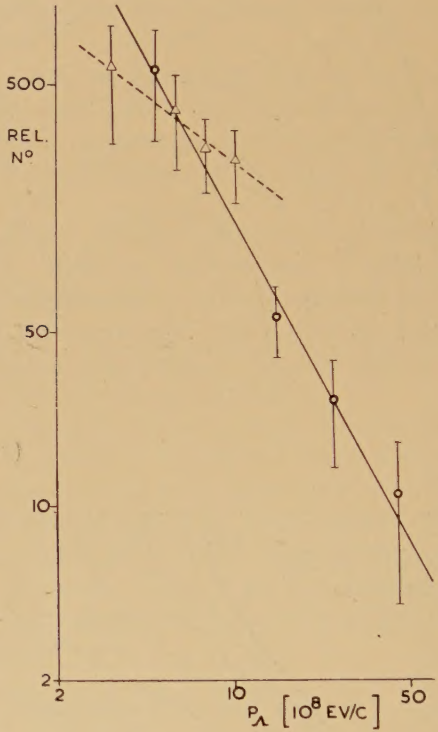

Fig. 3

The variation of p_K with p_Y for constant $\phi(=\phi_K+\phi_Y)$ in the reaction $\pi+N\rightarrow Y+K$. For values of $p_Y > 1{\cdot}15$ Gev/c the angle is never less than 30°.

Fig. 4

Differential momentum spectrum of Λ^0-particles at production. The circles and full line are obtained from our data ; the triangles and interrupted line from the measurements of Gayther and Butler (1955). The two curves are made to coincide at a momentum of 0·7 Gev/c. The total number of events used to obtain this spectrum is only 47. The full line corresponds to a power-law spectrum with an exponent of —2·0.

A further generalization is possible to reactions of the type

$$A+N\rightarrow Y+B+C+D+ \quad . \; . \; . \; . \; . \; . \; . \; . \; . \; . \qquad (3)$$

where A, B, C, D, are arbitrary particles. For a given momentum of particle A the *maximum* value of p^* for the Y-particle occurs when the other secondaries (B, C, D, . . .) have the same velocity ; that is, they behave as a single particle of mass $m_A+m_B+m_C+\ldots$. Since we are interested in the maximum value of p^* when finding the limiting values of ϕ_Y and p_Y, reaction (3) is, for this purpose, equivalent to reaction (2).†

This extension of the argument is of great practical importance since an example has recently been reported of hyperon production in a collision between two nucleons (Block *et al.* 1954). The reaction is interpreted as

$$\mathrm{N}+\mathrm{N}\rightarrow\mathrm{Y}+\mathrm{K}+\mathrm{N}. \qquad \ldots\ldots\ldots (4)$$

In this reaction the momentum of the hyperon is restricted to the region inside the curve (E.R.) shown in fig. 2 (*a*).

The production process discussed by Fowler *et al.* (1955) in which Λ^0-particles result from the rapid γ-decay of heavier hyperons (Σ) is also included as a reaction of type (3) since the reactions

$$\pi+\mathrm{N}\rightarrow\Sigma^0+\theta^0 \quad \text{and} \quad \Sigma^0\rightarrow\Lambda^0+\gamma$$

are together equivalent dynamically to

$$\pi+\mathrm{N}\rightarrow\Lambda^0+\theta^0+\gamma$$

provided that the Σ^0-particle decays before moving a detectable distance. Thus very slow hyperons cannot be produced even in this type of ‘ cascade ’ process.

(*c*) *Effect of the Fermi Energy*

The results shown in fig. 2 apply, strictly, in the nucleon frame of reference. If account is taken of the Fermi energy of a bound nucleon a further Lorentz transformation is required to find the angles and momenta in the laboratory system. This has an appreciable effect on the minimum value of p_Y. If a nucleon is assumed to have a kinetic energy of 10 MEV, it is possible to produce a Y-particle whose momentum in the laboratory system is only 30 MEV/c (corresponding to a kinetic energy of 0·5 MEV). However, the chance of producing such a low-energy Y-particle is extremely small since it demands a head-on collision between a very energetic π-meson and a nucleon of 10 MEV energy followed by the emission of the Y-particle at an angle θ^* greater than 177°.

§ 4. SUMMARY OF EXPERIMENTAL DATA

The observations that are reported here were all made with a large magnet cloud chamber situated at the Jungfraujoch (3580 m). The apparatus has been described by Newth (1954) and a typical system of counter control is shown in the same paper. During the past four years some 70 000 photographs have been taken and about 40% of these show evidence of nuclear interactions in the lead transition layer above the cloud chamber. Most of the photographs were taken with the chamber free from solid material but on occasions a 3 cm lead plate (or, more recently, a 1·2 cm copper plate) was placed across the centre of the chamber.

---

† We are extremely grateful to Mr. B. Powell for making this point clear to us. The argument can be outlined as follows. Let the secondary particles B, C, D, etc. (Y excluded) have a total energy U^* and total momentum p^* in the centre of mass system. The quantity $U^{*2}-p^{*2}$ is equal to U^2, where U is the total energy of the particles B, C, D, etc. in *their* centre of mass system. Thus, if U^* is fixed, the maximum value of p^* is obtained when U is a minimum. This leads directly to the required result.

In table 1 a summary is given of the number of V-events observed. The V^0-events include both Λ^0-decays and θ^0-decays and the $V^{\pm}$-events include, presumably, decays of charged hyperons and heavy mesons. Table 1 gives also the number of photographs which show two associated V-events.

Table 1. Yield of Single and Associated V-Events in Jungfraujoch Cloud Chamber

Site of nuclear interaction	No. of single neutral V-events	No. of single charged V-events	No. of associated V^0+V^0	No. of associated $V^0+V^{\pm}$
Transition layer	750	106	13	6
Inside the chamber	28	9	1*	1

Table showing the yield of V-events in the Jungfraujoch cloud chamber. The events originating in the 25 cm lead transition layer above the cloud chamber are distinguished from those originating inside the cloud chamber. The latter group includes three neutral V-events coming from stars in the chamber gas. The event marked with an asterisk is not discussed further since one of the V-events appears to be neither a Λ^0- nor a θ^0-decay.

A distinction is drawn between nuclear interactions occurring in the transition layer and inside the chamber, since the probability of observing the decay of an unstable particle depends strongly upon the distance of its origin from the illuminated volume of the chamber. Among the particles produced inside the cloud chamber there are three V^0-particles produced in stars in the chamber gas; the remaining particles were produced in the lead or copper plates.

Most of the V-events observed in the Jungfraujoch experiment cannot be classified as decays of a particular type. This is because the momenta of many of the particles involved in the decays are high and the maximum detectable momentum in the chamber is only 4 GeV/c. Newth and James (1953) made a statistical survey of the high-energy neutral V-particles observed and showed that approximately equal numbers of Λ^0- and θ^0-particles decayed in the chamber. From this they showed that comparable numbers of the two types of particle were produced in nuclear interactions above the chamber. In itself, this result is suggestive of some common production process—in fact, it was the starting point of the present work.

Concerning the charged V-decays, it is only possible to say that they include no events that cannot be interpreted as K-meson decays. The majority of the events have been discussed by Buchanan *et al.* (1954) who found no evidence for hyperon decays. This does not necessarily mean that charged hyperon decays are rare ; it may well be that few, if any, satisfy the rather stringent criteria used for classifying charged V-events.

§ 5. ANALYSIS OF RESULTS

(*a*) *The Nature of the Associated V-Events*

The 19 associated pairs of V-events (table 1) merit particular study and the details of these events are set out in table 2. Where possible the neutral V-events have been classified from angle and momentum

Table 2. Measurements of 19 Associated V-Events

Event	V_a		V_b		ϕ (deg.)	n_s	ψ_{ab} (deg.)	ψ_a (deg.)	ψ_b (deg.)
	Nature	Momentum (GeV/c)	Nature	Momentum (GeV/c)					
MJ29	Not Λ^0	$>0{\cdot}8$	?	>1	15	9	46 ± 5	82 ± 5	53 ± 5
NJ42	?	>4	?	$\sim1{\cdot}7$	3	2	86 ± 5	20 ± 5	80 ± 2
NU11	?	>1	?	>1	10	11	4 ± 2	11 ± 5	10 ± 5
OC31	?	?	Not Λ^0	~3	35	8	10 ± 5	0 ± 5	10 ± 5
OC56	?	~3	?	~3	10	12	85 ± 5	80 ± 10	10 ± 10
PH161	Not Λ^0	>4	?	>4	10	20	85 ± 2	85 ± 5	10 ± 5
QL759	?	~5	?	>4	10	10	25 ± 15	79 ± 5	63 ± 15
RJ451	?	~2	?	>2	10	6	57 ± 10	53 ± 10	73 ± 10
RT851	Not Λ^0	$>1{\cdot}5$	?	>2	8	7	43 ± 2	30 ± 5	13 ± 5
SF1841	?	>2	?	>2	0	11	—	—	—
SG75	Λ^0	$0{\cdot}7$	Not Λ^0	$2{\cdot}2$	21	0	88 ± 2	45 ± 10	48 ± 10
SH232	?	~2	Not Λ^0	~3	8	10	89 ± 5	14 ± 5	89 ± 2
SL325	?	>1	Not Λ^0	~2	8	2	31 ± 10	55 ± 10	45 ± 5
RC941	Not Λ^0	~2	V^+	$\sim1{\cdot}3$	15	10	33 ± 5	59 ± 5	29 ± 5
RK829	?	$\sim0{\cdot}8$	$V^\pm$	$>0{\cdot}4$	4	4	21 ± 5	27 ± 5	45 ± 5
RQ31	Not Λ^0	>2	V^-	>1	10	20	—	—	—
SJ388	?	~1	V^+	$>0{\cdot}3$	16·5	3	72 ± 10	70 ± 10	2 ± 10
SL101	?	>2	V^+	$\sim0{\cdot}5$	31	2	53 ± 10	37 ± 10	86 ± 10
SN2069	?	$>0{\cdot}7$	V^+	$>0{\cdot}5$	20	8	61 ± 5	88 ± 5	20 ± 5

The table gives details of the 19 pairs of associated V-events. The first 13 are associated neutral V-events ; the remaining 6 are associated neutral and charged V-events. Columns 2 to 5 give information about the individual V-events. ϕ is the angle between the lines of flight of the two unstable particles. n_s is the number of associated fast charged particles seen in the cloud chamber. ψ_{ab} is the angle between the planes of decay of the two particles. ψ_a and ψ_b are the angles that each plane of decay makes with the plane containing the lines of flight of the two V-particles.

The momenta of the V-particles have been obtained by the method described by Buchanan *et al.* (1954).

measurements as compatible or incompatible with Λ^0- or θ^0-decays. In every case a lower limit to the momentum of the unstable particle could be set. This information is given in columns 2 to 5 of table 2. The sixth column gives the angle (ϕ) between the trajectories of the unstable particles.

From the values of ϕ and the momenta of the unstable particles, it is evident that not one of the 19 pairs is a simple example of double production in reaction (1). Figure 3 shows that for the small values of ϕ observed, one or other of the secondary particles should have a low momentum; all the particles listed in table 2 have high momenta.

Two other processes could account for these associated events. They could result from 'plural' production, each being produced in a separate reaction inside the same nucleus. Little could then be said about the nature of the individual reactions. Alternatively, they could be examples of double production in reactions more complex than (1). In favour of the first interpretation is the high multiplicity of the nuclear interactions with which the events are associated. The number of associated shower particles *seen* in the cloud chamber is given for each case in column 7 of table 2. These figures show clearly that our events are very different from the example of double production observed by Thompson *et al.* (1954), where no additional products of the nuclear interaction were seen. Two of the events are reproduced in Plates 12 and 13.

Nothing can be said with certainty about the second hypothesis that the events are examples of more complex reactions than (1). However, Ballam *et al.* (1955) have found an apparent correlation between the planes of decay of associated V-particles. The existence of such a correlation for our events would be a strong argument for their being examples of double production processes.

In fact, we find no correlation of the decay planes. The last two columns in table 2 give the angles between the plane of decay of either V-particle and the plane containing the paths of the two V-particles (the angle less than 90° is quoted). Ballam *et al.* found that, for the 11 pairs of events they considered, these angles all satisfied the condition that one was more than twice as great as the other. Among our 17 measurable pairs 9 satisfy this condition; this is just what we should expect if the planes were randomly orientated.

We conclude therefore that none of our 19 pairs of V-events shows the decays of the two products of reaction (1). Nor is there any evidence for the associated events resulting from a complex 'double production' process. The most plausible interpretation is that each V-particle was produced in a separate reaction within a nuclear interaction of high multiplicity. Whether or not the individual reactions involved in this plural production are of type (1) we discuss below.

(*b*) *The Frequency of Double V-Events*

The significance of the fact that we do not observe any simple example of reaction (1) can only be assessed if we calculate how many examples we might expect to observe if all Y- and K-particles were produced in this type of reaction. An exact calculation of the experimental bias involved is very difficult, but we give in this section the results of some approximate calculations that are sufficient to indicate the orders of magnitude involved.

Neutral V-decays are much more efficiently observed than are the decays of charged K-mesons. This is because the mean lifetimes of the Λ^0- and θ^0-particles are such that a large fraction of the particles decay within a distance of 10 to 100 cm from their origins (assuming momenta of a few GeV/c). The charged K-mesons have much longer lifetimes and relatively few decay in even the largest cloud chambers. For the charged hyperons the situation is still obscure since the number of identified decays in cloud chambers is very small indeed.

The relatively high probability of observing neutral V-decays suggests the following approach to the calculation of the expected number of double events. We consider only the reactions

$$\pi+\mathrm{N}\rightarrow\Lambda^0+\theta^0 \qquad \text{(1}a\text{)}$$

and

$$\pi+\mathrm{N}\rightarrow\Lambda^0+\mathrm{K}^{\pm}. \qquad \text{(1}b\text{)}$$

For reaction (1a) we find the probability that, having observed one V^0-decay, the other should be seen. For (1b) we find the probability that, having seen the decay of the K-meson, the Λ^0-decay is also seen. These two probabilities both refer to chance of seeing a neutral V-event and can be calculated from the dynamics of reaction (1) using the known properties of the Λ^0- and θ^0-particles. The first probability we call $\mathrm{N}(2V^0)/\mathrm{N}(V^0)$, and the second $\mathrm{N}(V^0+\mathrm{K})/\mathrm{N}(V^0)$.

Values of these two probabilities have been calculated for various parameters of reaction (1) and the results are shown in table 3. Figures are given both for production in the transition material above the chamber and for production in a plate inside the chamber. The advantage to be gained from studying nuclear interactions inside the chamber is obvious.

From table 3 the values of $\mathrm{N}(2V^0)/\mathrm{N}(V^0)$ for production above and inside the chamber are of the order of 2% and 20% respectively. This suggests that 2% of the observed V^0-events from reaction (1a) occurring in the transition layer should be accompanied by a second visible V^0-event. Of the 750 single V^0-events observed we might expect one quarter to be produced in reaction (1a), the remainder being produced in (1b) or in the reactions which result in a charged hyperon. The absence of *any* pair of V^0-events compatible dynamically with (1a) thus suggests either that the reaction is not as important as we have assumed, or that the secondary particles produced suffer scattering sufficient to destroy the dynamical relations of (1). A similar conclusion is reached from considering the other probabilities given in table 3 although it should be emphasized that the statistical weight of all the observations is poor and the possibility of Λ^0- and θ^0-particles decaying into neutral secondaries has not been considered.

Table 3. Expected Frequency of Associated V-Events from $\pi+\mathrm{N}\rightarrow\mathrm{Y}+\mathrm{K}$

Interaction parameters		Site of interaction			
		Transition layer		Inside chamber	
θ^*	p (GeV/c)	$\mathrm{N}(2V^0)/\mathrm{N}(V^0)$ (%)	$\mathrm{N}(V^0+\mathrm{K})/\mathrm{N}(\mathrm{K})$ (%)	$\mathrm{N}(2V^0)/\mathrm{N}(V^0)$ (%)	$\mathrm{N}(V^0+\mathrm{K})/\mathrm{N}(\mathrm{K})$ (%)
90°	1	0·2	5	40	40
	1 to 3	5	4	16	13
0°	1	0·2	6	34	35
	1 to 1·5	0	0	7	20
	1·5 to 3	0	0	20	20
180°	1	2	2	37	37
	1 to 3	2	2	17	22

The calculated probabilities of seeing double events produced in the interaction $\pi+\mathrm{N}\rightarrow\mathrm{Y}+\mathrm{K}$ for various parameters of the reaction. The table gives a probability of seeing the second neutral V-event when one neutral V-event has been seen and also the probability of seeing a V^0-decay when a $\mathrm{K}^\pm$-decay has been seen. The probabilities are given as percentages.

(*c*) *Slow Neutral Hyperons*

The importance of observations of slow hyperons has been pointed out by Reynolds and Treiman (1954). From the discussion in § 3, it is clear that slow hyperons can only arise from reactions (1) or (2) if the hyperon is emitted backwards in the centre of mass system.

Among our events there are three decays of remarkably low-energy Λ^0-particles. One of these has previously been described by Millar and Page (1953). The Λ^0-particle had a momentum of (190 ± 15) MeV/c. The other two events are decays of Λ^0-particles whose momenta are (230 ± 40) and (150 ± 20) MeV/c. Reference to figure 2 (*a*) shows that the conditions necessary to produce such slow Λ^0-particles in reaction (1) are highly improbable. Moreover, the particle of momentum (230 ± 40) MeV/c comes from an interaction in the copper plate across the middle of the chamber and is emitted at an angle of 90° to the path of the primary particle causing the interaction. This makes interpretations of the event as a simple example of reaction (1) almost impossible.

Any or all of these events can, of course, be accounted for by assuming production according to reaction (1) with subsequent loss of energy by scattering of the Λ^0-particle. To obtain more information on this point we have estimated the momentum spectrum of the Λ^0-particles produced in our experiment. Confining attention to particles with near-vertical trajectories, the momenta of a random sample of Λ^0-particles were obtained and, knowing the mass and mean lifetimes of the particles, it was possible to calculate the efficiency of detecting particles of any momentum and hence to find the differential momentum spectrum at production. This spectrum is shown in fig. 4 ; to our results have been added the data of Gayther and Butler (1955) referring to particles of very low momentum.

Figure 4 shows that the momentum spectrum of the Λ^0-particles is similar to that of the charged shower particles in penetrating showers (Barker and Butler 1951). While the observations contain a large statistical uncertainty, there is good evidence that the spectrum rises with decreasing momentum down to the lowest momenta accessible to observation. This is strong confirmation of the results of Ballam *et al.* (1953) and is in complete disagreement with what would be expected from reaction (1) with isotropic emission of the secondary particles in the centre of mass system. The significance of this result is considered in § 6 where the observations of slow Λ^0-particles in photographic emulsion are discussed.

§ 6. Discussion

(*a*) *Hyperon Production*

The most interesting and important point that arises from the foregoing sections is that it is extremely difficult to produce low-energy hyperons in any type of collision with a nucleon at rest. There is, however, strong evidence for the production in nuclear reactions of a large number of slow Λ^0-particles. In addition to our evidence and that of Gayther and Butler which has already been quoted, the results of the Princeton group (Ballam *et al.* 1953) also show a large fraction of low-energy Λ^0-particles.

Photographic emulsion experiments have produced the best evidence for the existence of very slow Λ^0-particles. Danysz and Pniewski (1953 a, 1953 b) first observed a nuclear fragment that disintegrated after coming to rest in the emulsion. They interpreted this as a fragment in which a bound Λ^0-particle took the place of a neutron. Since their discovery many similar events have been observed (Padua Conference Report 1955). The binding energy of the Λ^0-particles in these fragments cannot be accurately found but is certainly not more than a few Mev. These bound particles are therefore good evidence for the formation of very slow hyperons in nuclear interactions.

If every hyperon is produced in a collision with a single nucleon at rest the observations of slow hyperons necessitate some mechanism of energy loss. The simplest mechanism is scattering of the hyperons by the nucleons in the parent nucleus. (In a single elastic scatter nearly all the hyperon energy can be lost. The maximum angle of scatter is, from § 3, 57°.) By assuming that such scattering usually occurs we can explain all the experimental observations of slow hyperons, the existence of bound Λ^0-particles, and the results of Gayther and Butler (1955) who find that there is a considerable fraction of backward-moving slow Λ^0-particles from nuclear interactions in lead.

The four examples of reaction (1) that have been observed in heavy nuclei (see § 2) are clearly cases where neither the Y- nor the K-particle has been appreciably scattered after production. If we assume that both Y- and K-particles have a mean path λ free from scattering in nuclear matter, the probability of both emerging from a nucleus without scattering is $\exp -(l_Y+l_K)/\lambda$ where l_Y and l_K are their paths in the parent nucleus.

Lock and Yekutieli (1952) have discussed the analogous problem of the scattering of recoil protons in nuclear interactions. They found that their experimental observations were fitted by $l/\lambda \sim 2$. If the heavy unstable particles are scattered by the same process as protons we should expect $l/\lambda \sim 2$ for them also (neglecting differences in nuclear radii). Thus the probability of both particles emerging without scattering from a heavy nucleus would be about $\exp(-4)$ or $\sim 2\%$. In this way we can account for the few recorded examples of reaction (1) occurring in heavy nuclei.

(*b*) *The Frequency of Double V-Events*

It was shown in § 5 (*b*) that in our experiment several examples of double *V*-events compatible with (1) should have been observed if all Y- and K-particles were produced in this type of reaction. The calculation ignored the possibility of the secondary particles being scattered. If we assume that only in about 2% of examples of (1) do the secondaries emerge without scattering our failure to observe such an example is not surprising.

In general, the hypothesis that scattering nearly always destroys the dynamical relations of the production processes makes the study of these processes in heavy nuclei almost impossible. Only a study of nuclear interactions in light materials could give a high proportion of valuable dynamical information.

(*c*) *Anisotropy in the Reaction* $\pi+\mathrm{N}\rightarrow\mathrm{Y}+\mathrm{K}$

To account for the large number of slow Λ^0-particles observed in the Princeton experiments Reynolds and Treiman (1954) suggested that there must be a strong anisotropy in the emission of hyperons in reaction (1). If the hypothesis of hyperon scattering outlined above is correct it is unnecessary to assume anisotropy to account for the emission of slow hyperons.

The direct evidence available from completely measured examples of reaction (1) suggests very strongly that anisotropy favouring values of θ^* near to 180° does exist. Table 3 shows that there may be some experimental bias against observing examples of reaction (1) with small values of θ^*. It seems unwise, at present, to combine clear examples of reaction (1) in which scattering is known to be absent with incomplete observations where only p_Y is known.

(*d*) *Polarization Effects in Associated V-Events*

Since our associated *V*-events are interpreted as the products of separate reactions the absence of any angular correlation between their planes is not surprising. What is difficult to explain is the difference between our results and those of Ballam *et al.* (1954). Among the 11 events that these workers considered there were 7 pairs of V^0-events obtained in a cloud chamber experiment very similar to our own. Ballam *et al.* do not publish sufficient information to show whether or not their events could be examples of reaction (1) but, from our experience, it is unlikely that they are. If their 7 examples are added to our 12 measurable pairs of V^0-events we find that 13 pairs satisfy the condition $\psi_1 > 2\psi_2$ while 6 do not. If the planes of decay were randomly orientated we should expect half the pairs to satisfy this condition.

It seems again preferable to discriminate between double events that are dynamically compatible with reaction (1) and associated events that are not. At present, the evidence for anisotropic distribution of the decay planes is meagre for both categories.

§7. CONCLUSIONS

We can summarize the conclusions drawn from this study in the following way.

(i) To account for the copious production of slow hyperons in nuclear interactions some mechanism of energy loss is essential. Scattering of hyperons by nucleons is the simplest mechanism.

(ii) If the hyperon–nucleon scattering cross section is comparable with the nucleon–nucleon scattering cross section, the observed features of hyperon production can all be accounted for without difficulty.

(iii) The study of production reactions such as $\pi + N \rightarrow Y + K$ in heavy nuclei is extremely inefficient since scattering of the secondary particles will usually destroy the dynamical relations of the reaction. The anisotropy of emission in such reactions can only be studied in completely measured examples where scattering is known to be unimportant.

(iv) The statistical analysis of the frequency of associated *V*-events in our cloud chamber does not provide evidence for or against the hypothesis that Y- and K-particles are always produced together. We interpret those associated *V*-events that we observe as examples of ‘ plural ’ production in separate reactions inside the same nucleus. We find no evidence for correlation between the two planes of decay.

ACKNOWLEDGMENTS

Professor P. M. S. Blackett and Dr. G. D. Rochester have provided us with every facility for our work. The experimental results were obtained at the Jungfraujoch Research Station in Switzerland ; we are deeply indebted to the officers of the station and, in particular, to the manager, Mr. Hans Wiederkehr, for making our work possible.

Many colleagues have assisted in the collection and interpretation of observations. We mention particularly Mr. A. H. Chapman, Mr. W. A. Cooper, Dr. E. G. Michaelis, Miss P. Miles, Mr. J. A. Newth, and Mr. B. W. Powell.

We have been greatly assisted by Dr. D. B. Gayther and also by Professor G. T. Reynolds and his colleagues at Princeton who informed us of their work before publication.

One of us (G. D. J.) is grateful to the Department of Scientific and Industrial Research for a maintenance grant; the other (R. A. S.) received a fellowship from U.N.E.S.C.O. during part of the time when this research was done.

REFERENCES

AMALDI, E., ANDERSON, C. D., BLACKETT, P. M. S., FRETTER, W. B., LEPRINCE-RINGUET, L., PETERS, B., POWELL, C. F., ROCHESTER, G. D., ROSSI, B., and THOMPSON, R. W., 1954, *Nature, Lond.*, **173,** 123.

BALLAM, J., HARRIS, D. R., HODSON, A. L., RAU, R. R., REYNOLDS, G. T., TREIMAN, S. B., and VIDALE, M., 1953, *Phys. Rev.*, **91,** 1019.

BALLAM, J., HARRIS, D. R., HODSON, A. L., MARTIN, W., RAU, R. R., REYNOLDS, G. T., and TREIMAN, S. B., 1955, *Phys. Rev.*, **97,** 245.

BARKER, K. H., and BUTLER, C. C., 1951, *Proc. Phys. Soc.* A, **64,** 4.

BLOCK, M. M., HARTH, E. M., FOWLER, W. B., SHUTT, R. P., THORNDIKE, A. M., and WHITTEMORE, W. L., 1954, *Bull. Amer. Phys. Soc.*, **29,** 33.

BUCHANAN, J. S., COOPER, W. A., MILLAR, D. D., and NEWTH, J. A., 1954, *Phil. Mag.*, **45,** 1025.

DAHANAYAKE, C., FRANCOIS, P. E., FUJIMOTO, Y., IREDALE, P., WADDINGTON, C. J., and YASIN, M., 1954, *Phil. Mag.*, **45,** 855.

DANYSZ, M., and PNIEWSKI, J., 1953 a, *Bull. Acad. Polon. Sci.*, **1,** 42; 1953 b, *Phil. Mag.*, **44,** 348.

DEBENEDETTI, A., GARELLI, C. M., TALLONE, L., and VIGONE, M., 1954, *Il Nuovo Cimento*, **12,** 369, 466.

FOWLER, W. B., SHUTT, R. P., THORNDIKE, A. M., and WHITTEMORE, W. L., 1953, *Phys. Rev.*, **91,** 128; 1954, *Ibid.*, **93,** 861; 1955, *Ibid.* (in the press).

GAYTHER, D. B., and BUTLER, C. C., 1955, *Phil. Mag.* (in the press).

LAL, D., YASH PAL, and PETERS, B., 1953, *Proc. Ind. Acad. Sci.*, **38,** 398.

LOCK, W. O., and YEKUTIELI, G., 1952, *Phil. Mag.*, **43,** 231.

MILLAR, D. D., and PAGE, D. I., 1953, *Phil. Mag.*, **44,** 1049.

NAMBU, Y., NISHIJIMA, K., and YAMAGUCHI, Y., 1951, *Prog. Theor. Phys.*, **6,** 615.

NEWTH, J. A., 1954, *Il Nuovo Cimento Suppl.*, **11,** 296.

NEWTH, J. A., and JAMES, G. D., 1953, *Report of the Bagneres Congress.*

PAIS, A., 1952, *Phys. Rev.*, **86,** 663.

PADUA CONFERENCE REPORT, 1954, *Il Nuovo Cimento Suppl.*, **12,** 466.

REYNOLDS, G. T., and TREIMAN, S. B., 1954, *Phys. Rev.*, **94,** 207.

THOMPSON, R. W., BURWELL, J. R., HUGGETT, R. W., and KARZMARK, C. J., 1954, *Phys. Rev.*, **95,** 1576.

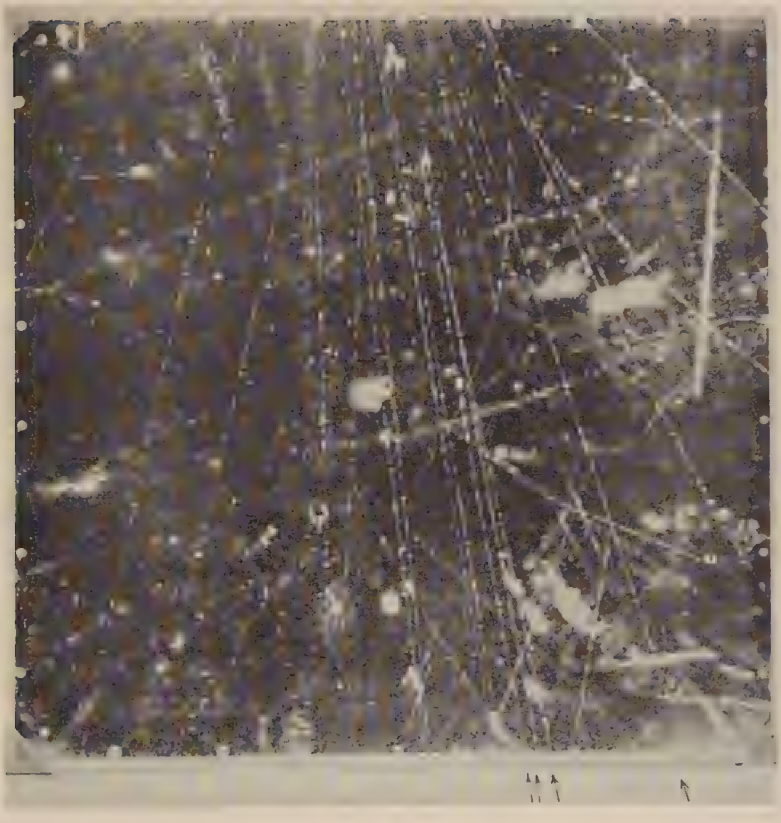

Event PH 161 showing two neutral V-decays among a shower of twenty fast charged particles. The event is described in table 2.

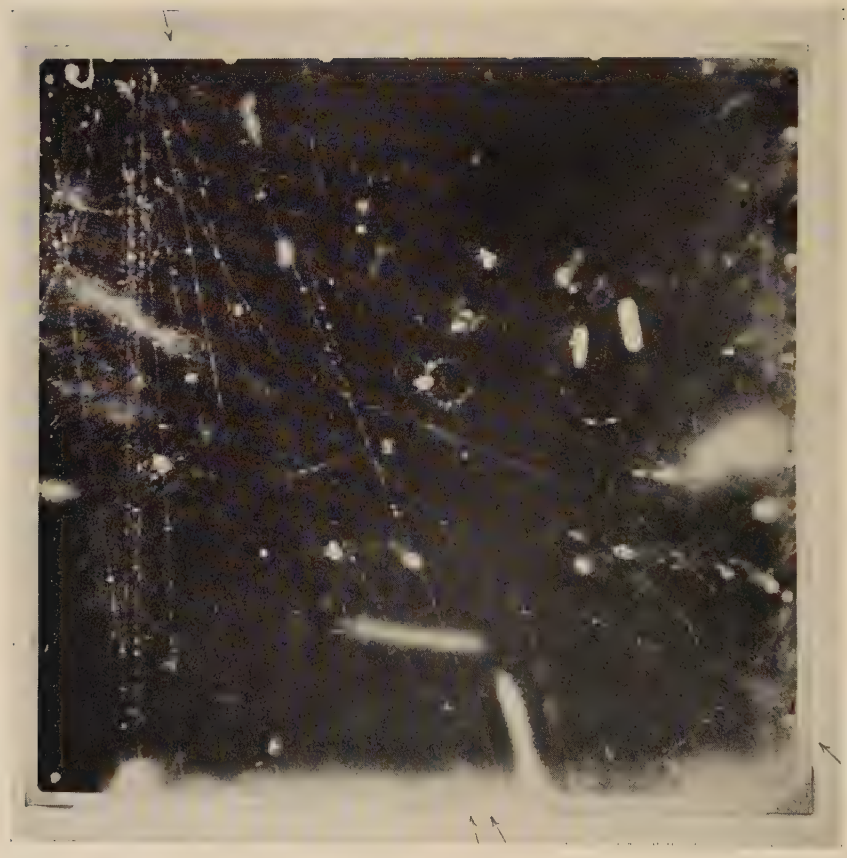

Event RC 941 showing associated neutral and charged V-particle decays. The event is described in table 2.

LXVIII. *Measurement of Ionization in Nuclear Emulsions*

By P. H. Fowler and D. H. Perkins
H. H. Wills Physical Laboratory, University of Bristol†

[Received March 2, 1955]

SUMMARY

The gap-length distribution along the tracks of ionizing particles in nuclear emulsions has been investigated, and shown to be exponential for all values of specific ionization. The coefficient of the exponential, g, is suggested as the most useful measure of the ionization. In the first part of the paper, practical visual methods of measuring g are discussed. Accuracies not far inferior to the maximum possible are obtained by counting the small proportion of gaps of lengths exceeding two or three times the average value. The ratio of the coefficient g in a given track, to that in the track of a relativistic electron, is shown to be independent of degree of development, for particles below six times plateau ionization.

In the second part of the paper, a detailed model is proposed, which is capable of explaining the dependence of g on the velocity and charge of the ionizing particle, and on the development and sensitivity of the emulsion.

List of Symbols Employed

g	Coefficient of the exponent of the gap-length distribution.
g_0	Coefficient of the exponent for track at plateau ionization.
g^*	g/g_0.
B	Blob density (i.e., total number of resolvable gaps per unit length).
B_0	Plateau value of B.
α	Parameter appearing in the empirical relation between B and g, i.e., $B=g \exp(-g\alpha)$. α is nearly equal to u^1 (see below).
l	Minimum chosen gap length, as measured between *inside* edges of developed grains.
H	Density of such gaps per unit length.
s	Projected distance between centres of successive crystals along the path of the particle.
x	Path length of ionizing particle through a crystal.
k	Path length of particle through gelatin between adjacent crystals.
$\bar{k}$, $\bar{s}$, $\bar{x}$	Mean values of k, s, and x.
$1/k_0$	Coefficient of the assumed exponential distribution in s.
u^1	Mean distance between centres of two crystals, which after development can just be resolved in the microscope.

---

† Communicated by the Authors.

$u(n)$	Distance between centres of two developed crystals containing n undeveloped crystals between them.
p	Probability of development of a particular crystal traversed by the ionizing particle.
$\bar{p}$	Mean probability of development of all crystals traversed.
λ	Number of acts per unit length in silver bromide. An ‘ act ’ is defined in § 13.
q	Probability that an act leads to development of the crystal ; it depends only upon degree of development.

§ 1. INTRODUCTION

THE distribution in length of the gaps occurring in tracks of ionizing particles in nuclear emulsions, has formed the subject of a number of recent papers. This distribution may be specified by means of some suitable parameter, e.g. the mean gap length, the blob density or the grain density. It gives a measure of the velocity and charge of the ionizing particle producing the track. It was shown by O'Ceallaigh (1954) that, at least over a limited range of the ionization, the distribution in observed gap length was exponential and that this fact leads to a great simplification in the analysis of the experimental data.

The present paper is divided into two parts. In the first part, observations on the gap-length distribution are described and it is shown that this distribution is exponential over the entire range of ionization which we could measure (between once and several hundred times the minimum value). The coefficient, g, of this exponential appears to be the most useful measure of the ionization in the track. g has been determined as a function of residual range of protons and π-mesons, and as a function of charge for relativistic particles. For values of ionization below about ten times minimum, it is shown that g is nearly proportional to the rate of energy loss of the ionizing particle in the silver bromide crystals which it traverses. Further, over this interval of ionization the value of g/g_0, where g_0 corresponds to minimum ionization, is practically independent of the degree of development of the emulsion. It is shown that g can be determined most rapidly from the ratio of the total number of observable gaps (i.e. the blob density), to the number of gaps of length greater than some optimum value. The value of g so obtained is independent of the mean developed grain size. The statistical errors associated with the measurement of g are discussed and the method is illustrated by a determination of the mass of K-particles. In particular, the determination of masses by this method is shown to be at least as accurate as, and much more rapid than, the photoelectric method over the entire range of ionization considered.

In the second part of the paper, a detailed model is proposed of the formation of developed crystals along a track. It is shown that this model is able to account for the dependence of g upon both the specific ionization and the degree of development of the emulsion or the type of emulsion used.

PART I

§ 2. EXPERIMENTAL RESULTS ON GAP LENGTH DISTRIBUTION

Figure 1 shows the integral gap length distribution observed on the tracks of relativistic cosmic ray particles of different charges. Within the limits of experimental error, these distributions are exponential, and thus

Fig. 1

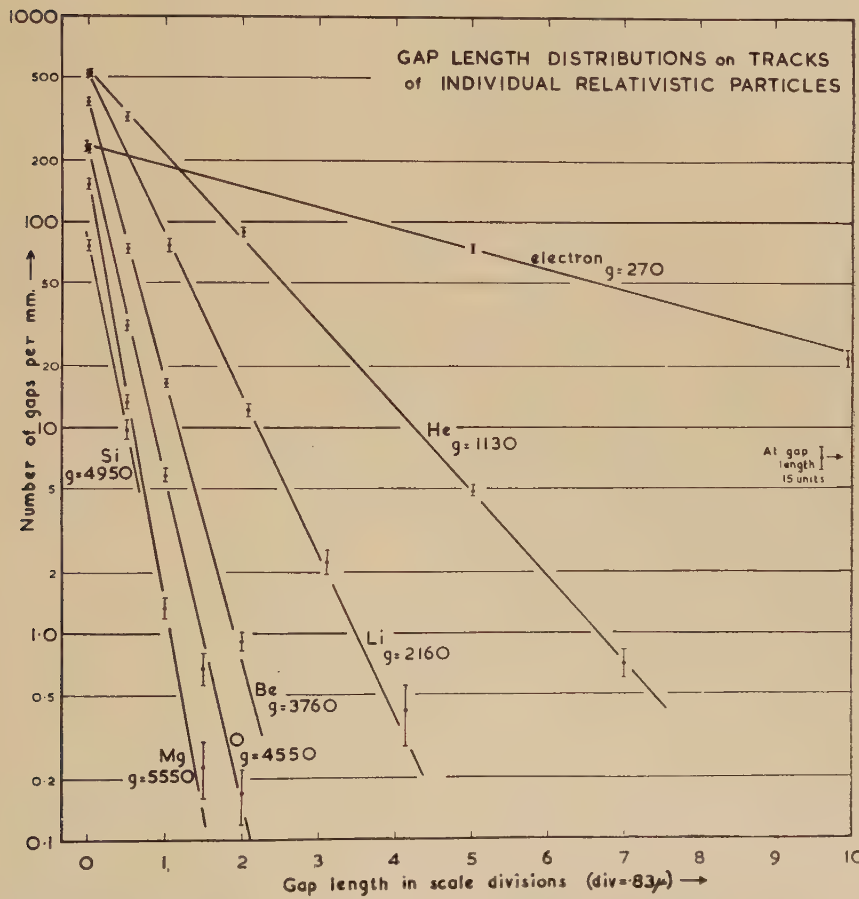

Gap length distribution in tracks of individual relativistic particles in emulsions of Stack 1. As described in the text, the length of each gap is measured between inside edges of the bounding grains. The number per unit length of all visible gaps corresponds to the blob density. Within experimental error, all the points lie on exponential curves.

confirm previous measurements carried out by O'Ceallaigh on lightly ionizing particles. It follows that the ratio of the numbers H_1 and H_2 of gaps of length exceeding l_1 or l_2 per unit length of track, yields a measure of the coefficient of the exponent g :

$$g=\frac{1}{(l_2-l_1)}\log_e\left(\frac{H_1}{H_2}\right). \qquad (1a)$$

The length of gap l is the distance between the inside edges of the developed grains bordering the gap. It should be noted here that we have supposed the gap length to be measured along the track. If however, the track dips at an angle θ to the plane of the emulsion, the projected gap length, l, as observed in the eyepiece scale of the microscope, is related to the true length l_t, by $l_t=l \sec\theta$. Thus, the corrected value of g can be found from eqn. (1a) simply by multiplying by a factor cos θ (O'Ceallaigh 1954).

In general, we have chosen $l_1=0$, corresponding to the smallest resolvable gap, so that $H_1=B$, the blob density as customarily defined ; the density H of gaps exceeding length l is given by

$$H=B\exp(-gl). \qquad (1b)$$

Let g_0 be the value of g for the track of a high energy electron (corresponding to the plateau value of the ionization) in identical conditions of development ; and let $g/g_0=g^*$. Figure 2 shows the observed relation between the quantity g^* and the residual range for protons in G5 emulsion. The measurements were carried out on protons and π-mesons, the equivalent range of a proton being calculated assuming a mass for the π-meson of 273 m_e. The observations were made in two separate stacks of stripped emulsion, each of approximately homogeneous development. In stack 1, the average value of $g_0=270$/mm ; in stack 2, only 180/mm. It will be seen that the values of g^* obtained from the two stacks are practically indistinguishable down to proton ranges of the order of 1 cm, but differ considerably at lower velocities.

It is worth noting here that if instead of measuring the normalized coefficient, g^*, as defined above, one chose to measure the probability of development, normalized to minimum, as described by other workers, the discrepancies between the two stacks would be much greater ($\sim 10\%$ at 1 cm range).

The value of the exponent of the gap length distribution for relativistic heavy primaries is shown in fig. 3, plotted against Z^2. It is clear that g tends to a limit as Z^2— and hence the specific ionization of the particle— becomes very large. This limiting value of g, $\simeq 5000$/mm, is the same for both stacks despite the large difference in development. In a detailed model to be described in Part II, we make the assumption that this value corresponds to the exponential distribution of gelatin gaps between the silver bromide crystals, when all these crystals have been developed.

In fig. 4 are shown the experimental values of blob density B, plotted against the density H of gaps longer than 4·17 μ. Each point corresponds to an observation on a single track in a particular emulsion of the stack. The number of blobs counted for each point was ~ 400, the number of

Fig. 2

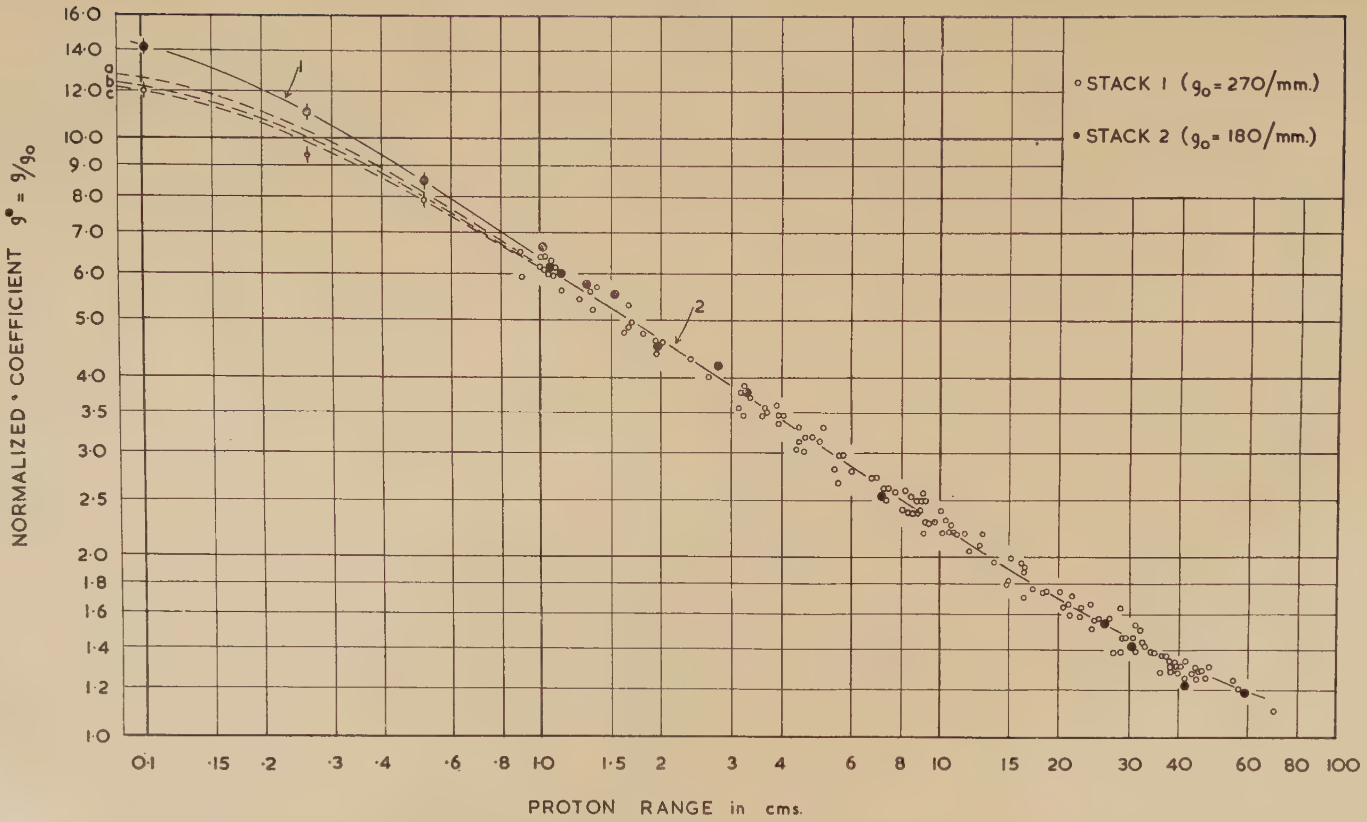

Relation between normalized coefficient g^* of the gap-length distribution, and the residual range R of protons. For R greater than 1 cm, each point corresponds to a single observation in one emulsion. For smaller values of R, each point represents a group of some fifteen observations taken from different tracks in different emulsions. For explanation of curves see § 13.

gaps ~60. The range of g covered by these measurements was from 270–1200/mm.

§ 3. ANALYSIS OF THE EXPERIMENTAL RESULTS

With the help of the results of fig. 4, we find an empirical relation between B and g :

$$B = g \exp(-g\alpha). \quad . \quad . \quad . \quad . \quad . \quad . \quad . \quad . \quad (2)$$

α is a parameter which is determined largely by the developed grain size, and to a lesser extent by the optical resolution of the microscope and the convention employed by a particular observer.

Fig. 3

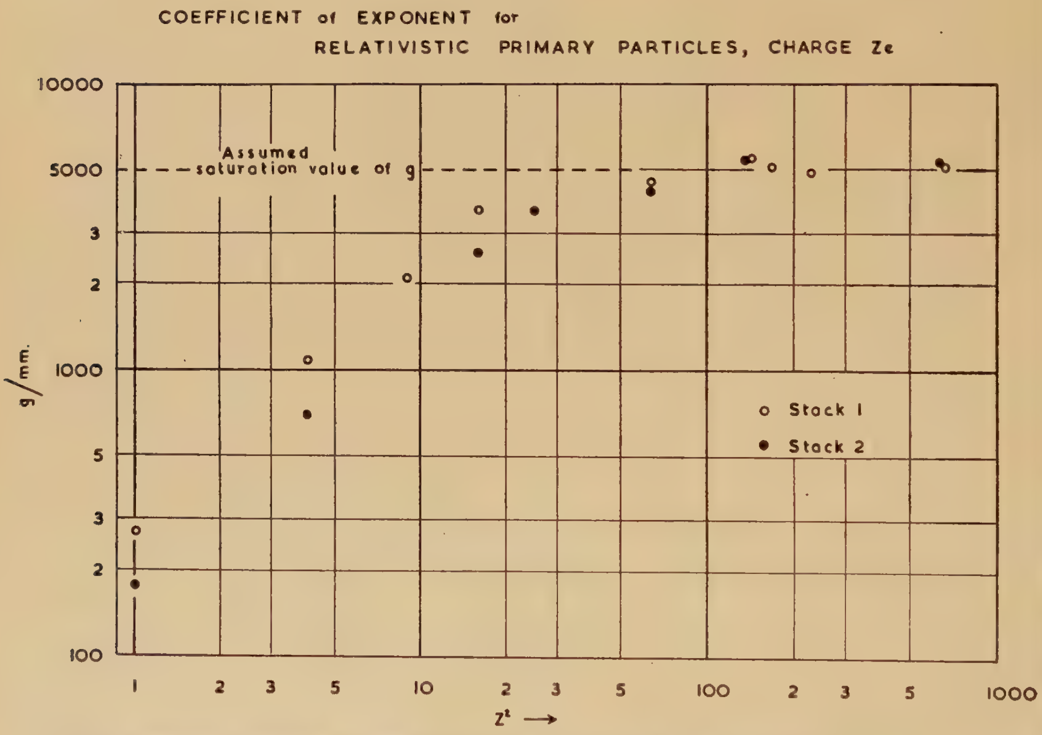

The measured values of the coefficient g, observed on individual relativistic particles, plotted against the square of the nuclear charge Z, as estimated from δ-ray counts.

In fig. 4, curves, 1, 2, and 3 show the relation between B and H calculated from eqns. (1*b*) and (2) for values of $\alpha=0{\cdot}60$, $0{\cdot}65$ and $0{\cdot}70\,\mu$ respectively. It will be seen that the shape of the calculated curves is in good agreement with the observations and the best fit is obtained for $\alpha=0{\cdot}65\,\mu$. The spread of the individual experimental points in this diagram is consistent with the statistical errors arising from the number of blobs and gaps counted (§ 5).

In Part II, with the help of detailed models of the distribution of crystals along the tracks of ionizing particles, we show that α can be identified with the mean separation of the centres of two crystals, which upon development are just resolved. Further, we show that eqn. (2) will be accurate to about 1% for all values of $g < 1200$/mm.

Fig. 4

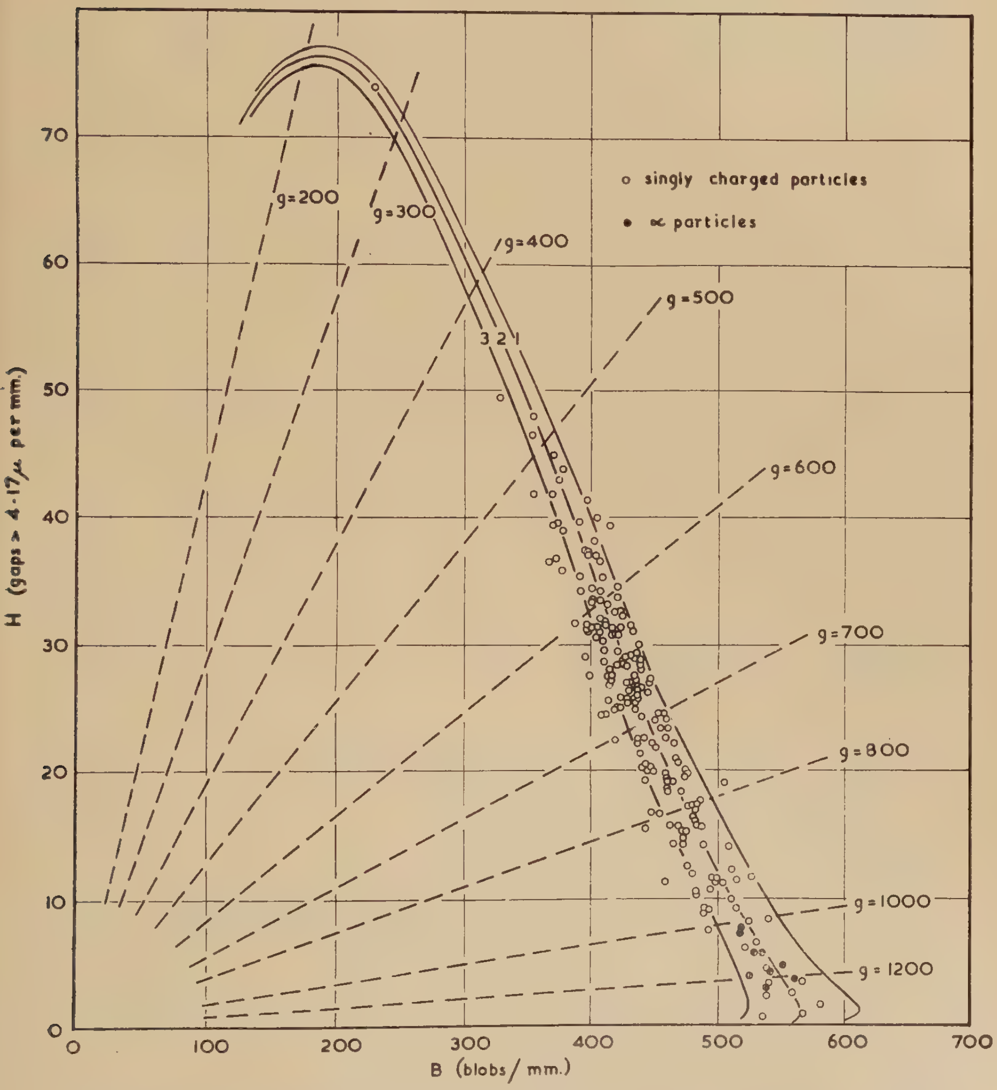

Blob density B, plotted against the density of gaps exceeding 4·17 μ. Each point corresponds to an individual track in a single emulsion, the mean number of blobs per point being ~400, of gaps ~60. Curves (1), (2) and (3) represent the empirical relation between B, g and H (eqn. 2) for α=0·60, 0·65, and 0·70 μ respectively.

Thus in stack 1, from which the above measurements were taken, α is independent of both the coefficient g and of casual variations in development from one emulsion to another. α, however, can depend on the conditions of development, for a similar analysis carried out in stack 2 gives a value of $0{\cdot}74\,\mu$ for this quantity.

§ 4. MEASUREMENT OF LOW VALUES OF g AND NORMALIZATION

In order to determine g when g is less than ~ 550/mm it is sufficient to measure the blob density B alone. The reasons for this are as follows. Blob counting is both reliable and rapid for lightly ionized tracks, since the proportion of developed grains which are close to each other is small. Further, any small variations in the developed grain size and/or optical conditions have, for the same reason, a trivial effect (§ 5(*c*)). The appropriate value of g has been calculated from B using eqn. (2) and the best value of $\alpha=0{\cdot}65\,\mu$ given above.

In order to determine g_0 throughout the stack, blob counts were made on relativistic electrons in cascade showers, in each emulsion, as a function of depth. The value of B_0 in a given emulsion varied by $\sim 7\%$ between top and bottom. Approximately 4000 blobs were counted in each emulsion of the stack. g_0 was calculated from B_0 and so determined to a statistical accuracy of less than 2%. No significant differences were found in the variation of B_0 with depth in the various emulsions. Furthermore, variations of B_0 over the surface area (150 cm^2) of a given emulsion were found to be less than the statistical error of the blob counts (3%).

§ 5. STATISTICAL ERRORS ASSOCIATED WITH DETERMINATION OF g

In order to calculate the accuracy expected in individual determinations of the coefficient g, we quote here an approximate form of the result derived in the Appendix. Let σ be the standard deviation associated with the number of gaps counted, N_H. Then

$$\sigma\sqrt{(N_H)} \simeq H\sqrt{\left(\frac{\bar{t}^2}{(1-\epsilon)}+\frac{1}{g^2}\right)} \qquad . \quad . \quad . \quad . \quad . \quad (3)$$

where $\bar{t}=1/H-1/g-(l+\alpha)$, and is the mean distance between the centres of those crystals which upon development form the end of one gap and the beginning of the next.

l is the length of the gap as previously defined, and ϵ is the ratio of the number of gaps exceeding the minimum length l to the total number of developed grains in the track. The statistical error in a determination of blob density B can be obtained by substituting $l=0$ and $B=H$ in (3).

Expression (3) is sufficiently accurate in practice for all values of g and l, but the complete expression is given in the Appendix.

As can be seen from (3), when the mean separation of the gaps $\bar{t}$ becomes very large compared with $1/g$, then $\sigma\sqrt{(N_H)}\rightarrow 1$; the gaps are distributed at random. However, for the values of B and H commonly measured, $\sigma\sqrt{(N_H)}$ and $\sigma\sqrt{(N_B)}$ are significantly less than unity. $\sigma\sqrt{(N_H)}$ in fact passes through a minimum of $\sim 0{\cdot}52$ when $(l+\alpha)g\simeq 1{\cdot}0$.

(*a*) *Determination of g from B and H*

In order to determine the optimum value of the minimum gap length, a detailed calculation must be made. This must take into account not only the statistical fluctuations of B and H given by eqn. (3), but also the correlation between the fluctuations of H and those of B when taken over the same section of track.

As a result, we find that the theoretical optimum value of l occurs when $gl \sim 2{\cdot}0$, for all values of g. The accuracy does not vary appreciably in the interval $1{\cdot}5 < gl < 2{\cdot}5$. The actual expression for the statistical error in g is somewhat complex, but is represented approximately by

$$dg/g = \frac{1}{\sqrt{(N_H)} \cdot \log_e B/H} . \qquad \qquad (4)$$

This expression is in fact a slight overestimate of the error, but is sufficiently accurate in practice provided $B/H > 4$, and $N_B > 4N_H$. It will be noted that the expression (4) is that which would have been obtained by assuming that $\sigma\sqrt{(N_H)} = 1$ always, and not as given by (3); that the correlations between B and H could be ignored; and that the statistical errors in B are negligible.

In considering the optimum value of lg, we must also take into account the following practical considerations. In scrutinizing gaps of length close to the limiting value l, there will be a number of decisions to make. One cannot therefore exclude the possibility of a small temporary bias which might vary from track to track, and possibly be different for blobs and gaps. The proportion of such decisions is of course independent of the gap length chosen. The effect which the actual assignment of borderline gaps produces on the value of g obtained is clearly inversely proportional to l. Furthermore, the larger the value of l chosen the fewer the gaps that have to be counted and the more rapidly the measurements are completed.

Thus we feel that the best value of l to use in practice is that which gives $lg \simeq 2{\cdot}5$. l is of course chosen to be an integral number of eyepiece scale divisions.

(*b*) *Determination of g from B alone*

When the determination of g depends on a blob count alone, (§ 4), and if N_B is the number of blobs counted, then for low values of g,

$$\sigma\sqrt{(N_B)} \to B/g$$

and

$$\frac{dg}{g} \simeq \frac{1}{\sqrt{(N_B)}} \frac{\exp(-g\alpha)}{(1-g\alpha)} . \qquad \qquad (5)$$

For such low values of g, as can be seen from (5), the fractional error in g is close to $1/\sqrt{(N_B)}$. For $g\alpha > 0{\cdot}35$, the error in g rapidly becomes larger, and as mentioned previously, much more sensitive to real fluctuations in α and more dependent on decisions regarding borderline gaps. Hence one should not rely on blob counts alone for the determination of values of $g\alpha$ greater than 0·35. We recommend that any tracks for which the dip correction exceeds the standard deviation in g, should be measured using B and H and not B alone, for all values of g.

(*c*) *Comparison of the Present Method with a Mean Gap-Length Determination*

In discussing the accuracy attainable by the present method, we must compare it with the maximum precision which it is possible to attain. The greatest precision would presumably be achieved by measuring the length of each individual gap along the track. Since the gap length distribution is exponential, the precision with which the coefficient g could be determined (e.g. by finding the mean gap length) would then be $dg/g=1/\sqrt{(N_B)}$.

On the other hand, the precision in g obtained by the method described in this paper is given with sufficient accuracy by eqn. (4). With $\log_e B/H=2{\cdot}5$, we thus obtain as much as 55% of the total information available in the track by *counting* (as opposed to measuring) the long gaps, amounting to only 8% of the total, and by *counting* a sample of the blobs (such that the number of blobs counted is large compared with the number of long gaps).

§ 6. SUMMARY OF PROCEDURE FOR DETERMINING g^*

It is now perhaps convenient to summarize the procedure that we have adopted for determinations of g^*.

(1) The plateau blob density B_0 must be measured in each emulsion, by counts on relativistic electrons. The dependence of B_0 on depth must be investigated and this is more conveniently achieved by gap counts on tracks of relativistic α-particles rather than on those of electrons, since more information is available per unit length of track. We have found that the depth dependence in a given batch of emulsions processed in a similar manner is quite uniform, but this point must be checked.

(2) Measurement of the parameter α (or better, u^1, as defined in Part II, eqn. (14)). α or u^1 can be most readily found by measurement of blobs and gaps on protons of 1 cm range, where B is near its maximum value for average conditions of development. We find that α is nearly constant in a given batch of emulsions. It may differ slightly however from one observer to another. These two points must also be investigated.

(3) From the values obtained for α (or u^1) and B_0, g_0 is obtained from eqn. (2) at a given depth in a particular emulsion.

(4) Measurement of g :

(*a*) For lightly ionizing particles, when $g\alpha<0{\cdot}35$, g and hence g^* is most conveniently determined from blob counts alone.

(*b*) For values of $g\alpha>0{\cdot}35$ we have determined g from counts on blobs and gaps. The gap-length is chosen such that $lg\sim 2{\cdot}5$ and the number of blobs counted is about four times the number of gaps.

(5) For blob counts alone, the fractional standard deviation in g is $\simeq 1/\sqrt{(N_B)}$. For blob and gap counts combined, the corresponding error is

$$\simeq \frac{1}{\sqrt{(N_H)}\,.\,\log_e B/H},$$

provided that the number of blobs counted is more than about four times the number of large gaps. In addition, normalization errors must be taken into account. As a check in estimating the accuracy in mass determinations on long tracks by this method, the final error in mass should also be obtained from the internal fluctuations of the individual measurements about the mean value.

§ 7. DETERMINATION OF THE MASS OF INDIVIDUAL PARTICLES BY MEASUREMENT OF g AND RESIDUAL RANGE

Figure 2 shows that for values of the residual range R of a proton in the interval 1–40 cm, $g^* \propto R^{-0\cdot42}$. Thus, neglecting errors in determination of the range of a particle and straggling, the statistical error in mass M resulting from a determination of g^* is

$$\frac{dM}{M}=\frac{1}{0\cdot42}\frac{dg^*}{g^*}.$$

In order to illustrate the accuracy of the technique, we describe measurements on three heavy mesons observed in stack 1. Their ranges at emission were 9·1, 7·2 and 7·1 cm. Some fifteen determinations of g^* were made on each track, and the mean value $\overline{M^{-0\cdot42}}$ was computed from the various mass values, suitably weighted according to the number of blobs and gaps counted and including statistical errors in normalization of individual emulsions. We obtained :

$$M_X=942\pm24\ m_e\,; \quad M_Y=1022\pm30\ m_e\,; \quad M_Z=1020\pm24\ m_e.$$

On coming to rest, particle X decayed into two π^+ and one π^--meson, and was a τ^+. Particles Y and Z were K-mesons each giving rise to a singly charged relativistic particle, too steep for identification.

The time required for the determination of the mass of each particle was less than two days for a single observer. This does not take into account time required for calibration of the emulsions.

Methods so far described for the visual measurement of the gap distribution have effectively involved the estimation of the lengths of all individual gaps, and have proved very time-consuming. In the present method, the proportion of gaps which must be scrutinized carefully is small, and for a given statistical accuracy the actual number of gaps counted is reduced by a factor of more than five. The increased speed of measurement that results appears to be one of the chief advantages of the present method.

The photometric method gives a measure of the density of a track, which is substantially free from subjective errors. It has been chiefly advocated on this account. The accuracy claimed for mass determinations on long tracks by the photoelectric method is no greater than that obtained by the technique we have described ; but the time required for these measurements is at least ten times as long.

PART II

§ 8. BASIC ASSUMPTIONS FOR MODELS OF GRAIN PRODUCTION

The primary factor which determines the characteristics of a track is the number of silver bromide crystals developed. In this paper, we shall consider only those grains which lie along the path of the ionizing particle, hence no account will be taken of grains produced by δ-rays.

Let p be the probability of development of any individual crystal, and let $\bar{p}$ be the average probability of development taken over all crystals traversed by the particle. If the crystal is not traversed by the particle we assume $p=0$. We assume further that for a given value of the average probability $\bar{p}$, the probability of development p of any one crystal is independent of whether or not its immediate neighbours are developed. We must emphasize that for the moment we have made no assumptions as to how p might vary from one crystal to another, with degree of development or with the specific ionization of the particle producing the track. Thus, the probability per unit length of obtaining n undeveloped crystals bounded by two developed ones is

$$\pi(n)=\bar{p}^2\frac{(1-\bar{p})^n}{\bar{s}} \quad . \quad . \quad . \quad . \quad . \quad . \quad . \quad . \quad (6)$$

where $\bar{s}$ is the mean spacing between crystals traversed by the particle.

The second important factor determining the track characteristic is the distribution of the crystals along the path of the particle. The simplest model which can be advanced is that in which the distance between the centres of consecutive crystals is assumed to be a constant, $\bar{s}$. It will be shown that this model is inconsistent with the experimental evidence.

In a model which we advance later (§ 10) account is taken of a distribution in spacing s of neighbouring crystals traversed by the particle.

§ 9. CONSTANT SPACING MODEL

Provided that the centre of a developed grain coincides with the centre of the crystal from which it was formed, the distance between the centre of two developed grains, containing n undeveloped crystals between them, is $(n+1)\bar{s}=L$, let us say.

Thus, the differential distribution of gaps per unit length is a discontinuous function of the form

$$\frac{\bar{p}^2(1-\bar{p})^{(L/\bar{s}-1)}}{\bar{s}}$$

which exists only for integral values of $L/\bar{s}$. This distribution has an exponential 'envelope' of coefficient $\log_e (1-\bar{p})/\bar{s}$.

The gap length which has actually been measured is between the edges of developed grains. Fluctuations in developed grain size (and any displacement of the centre of a grain from the centre of the crystal from which it was formed), result in a smearing out of the above distribution, to a considerable extent. Such an effect is easily capable of accounting for the fact that the observed gap distribution is not noticeably irregular. Thus for the larger gap lengths, the integral distribution changes from a step-function to a function with an exponential envelope with the same coefficient as above, with only a slight ripple. For the values of gap length displayed in fig. 1, we can for all practical purposes identify the experimental slope with the coefficient of the exponent of the envelope ; thus we have

$$g=\frac{\log_e(1-\bar{p})}{\bar{s}} \quad . \quad . \quad . \quad . \quad . \quad . \quad . \quad . \quad . \quad (7)$$

We have seen, from fig. 3 that g appears to tend to a limiting value, 5000/mm, at high ionization. Taking $\bar{s}=0{\cdot}40\,\mu$ we have, according to the above formula, $\bar{p}$ tending to 0·86. This value of $\bar{s}$ is taken to agree with the mean diameter of silver bromide crystals measured with the electron microscope.

It is of course possible to employ a model in which 14% of the crystals are completely incapable of development. Calculations which we have made suggest that such a model would be capable of explaining all our experimental results. However, we prefer to explain the saturation of g entirely in terms of fluctuations in the individual values of the spacing, s.

§ 10. VARIABLE SPACING MODEL

O'Ceallaigh (1954) was the first to make allowance for the fluctuations in the spacing between individual crystals. He concluded, under reasonable assumptions, that such fluctuations would not appreciably affect the exponential nature of the gap length distribution. He gave no details of any effects which these fluctuations might have on the actual value of the coefficient, g. As we shall show, these are appreciable.

As indicated above, we assume that in both the stacks employed, practically all crystals traversed by particles of $Z\geqslant 12$ will have been developed. It follows therefore that the gaps observed in these tracks must be those between consecutive crystals. The distribution of such gaps is observed to be exponential, with a coefficient which we shall call $1/k_0=5000$/mm. We therefore assume that the distribution of length s between centres of successive crystals is of the form

$$f(s)\,ds=1/k_0 \exp\left[-\frac{(s-\bar{x})}{k_0}\right]ds \quad . \quad . \quad . \quad . \quad . \quad (8)$$

for all values of $s>\bar{x}$, the mean path of the ionizing particle through a crystal. Thus the mean path length between centres of successive crystals will be $\bar{s}=k_0+\bar{x}$.

It is known that at normal humidities the emulsion consists of nearly equal volumes of silver halide and gelatin. Thus the mean path of the particle through a crystal is very nearly equal to the mean value of the path k in the gelatin between two crystals, i.e. $\bar{x}=\bar{k}=k_0=0\cdot20\,\mu$. The value of $\bar{x}$ so found is consistent with that expected for crystals of diameter $0\cdot30\,\mu$, as observed in electron microscope measurements. These values of k_0 and $\bar{x}$ are to be compared with those of $0\cdot1\,\mu$ and $0\cdot3\,\mu$ respectively, taken by O'Ceallaigh. O'Ceallaigh's model was based on the simplifying assumption that all traversals of crystals were along a diameter.

For large values of s, formula (8) will result in an exponential distribution of the gelatin gaps between the developed crystals, as is observed. The true distribution however will not cut off sharply at $s=\bar{x}$, since individual values of both x, the path of the particle through an individual crystal, and k, the path of the particle in the gelatin between adjacent crystals, will fluctuate. From consideration of the geometry involved—assuming no aggregation of crystals—the fraction of crystals along the path of a particle for which $s<\bar{x}$ would be unlikely to exceed 5%. Thus for the purpose of the detailed analysis which follows, it will be assumed that the distribution in s is rigorously given by eqn. (8).

The distribution $F_n(u)\,du$ of the distance u between the centres of two crystals which after development bound a gap containing n undeveloped crystals, is then

$$\begin{aligned} F_n(u)\,du &= (w^n/n\,!)\exp(-w)\,du \quad \text{for } w>0 \\ &= 0 \qquad\qquad\qquad\qquad\quad\;\; \text{for } w<0 \qquad . \;\; . \;\; . \quad (9) \end{aligned}$$

where $w=u/k_0-(n+1)$, and is the path length of the particle through the gelatin in the gap in units of k_0. The probability per unit length of obtaining n such undeveloped crystals bounded by two developed ones is $\pi(n)=\bar{p}^2(1-\bar{p})^n/\bar{s}$. Thus the contribution to the total gap distribution for each value of n is $\pi(n)F_n(u)\,du$. The form of this expression, for different values of n and for $\bar{p}=1-1/e$, is shown in fig. 5 (curves 1, 2, 3 and 4).

The total differential gap length distribution is obtained by summing over all values of n

$$\phi'(u,\bar{p})\,du=\left\{\sum_n\frac{\bar{p}^2(1-\bar{p})^n}{\bar{s}}\,.\,F_n(u)\right\}du. \quad . \;\; . \;\; . \;\; . \quad (10)$$

The integral distribution $\phi(u,\bar{p})$ of gaps exceeding u can be obtained in a similar manner, though the expressions are more cumbersome.

Both $\phi(u)$ and $\phi'(u)$ may be shown to become exponentials as $u\to\infty$. Thus the integral distribution becomes

$$\phi_{u\to\infty}(u,\bar{p})=\frac{\bar{p}^2\exp[-g(u-k_0)]}{\bar{s}gk_0(2-gk_0)} \quad . \;\; . \;\; . \;\; . \;\; . \;\; . \quad (11)$$

where the coefficient g is given by

$$(1-gk_0)\exp(-gk_0)=1-\bar{p}. \quad . \;\; . \;\; . \;\; . \;\; . \;\; . \;\; . \;\; . \quad (12)$$

More generally, if we longer assume $\bar{x}=k_0$, we have instead of (11) and (12)

$$\phi_{u\to\infty}(u,\bar{p})=\frac{\bar{p}^2}{\bar{s}}\,\frac{\exp\,[-g(u-\bar{x})]}{gk_0(1+\bar{x}/k_0-g\bar{x})} \quad . \;\; . \;\; . \;\; . \;\; . \quad (11a)$$

and

$$(1-gk_0)\exp\,(-g\bar{x})=1-\bar{p}. \quad . \;\; . \;\; . \;\; . \;\; . \;\; . \;\; . \quad (12a)$$

Expressions (12) or (12*a*) are to be compared with (7) where the spacing is assumed to be constant.

Fig. 5

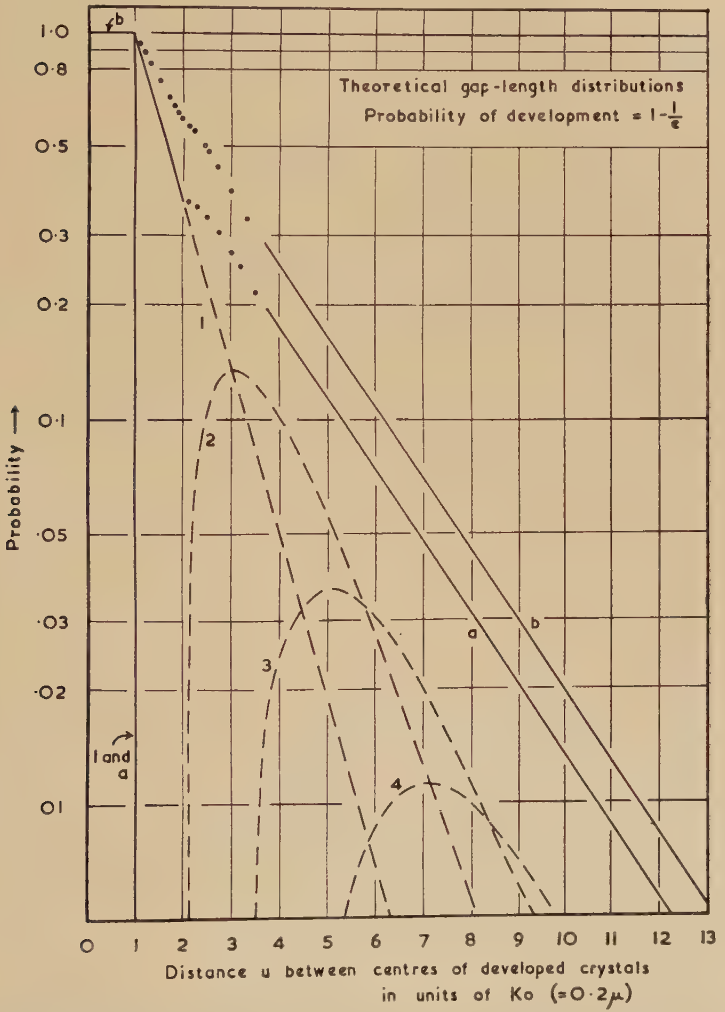

Theoretical gap-length distribution (see § 10). Curves 1, 2, 3 and 4, show the differential gap-length distribution corresponding to gaps containing 0, 1, 2 and 3 undeveloped crystals. Curve (*a*) denotes the total differential distribution, (*b*) the integral distribution. For $u>4k_0$, both are sensibly exponential.

The full-line curves (*a*) and (*b*) in fig. 5 represent the asymptotic expressions for $\phi'(u, \bar{p})$ and $\phi(u, \bar{p})$ normalized to unity at $u=k_0$—eqn. (11). For values of $u<4k_0$, the points represent the result of the numerical evaluation of eqn. (10). For $u>4k_0$, corresponding to nearly all visible gaps, the analytic expression (11) and the results of the numerical calculation are practically indistinguishable. They depart significantly for smaller values of u, however.

Let us now neglect all fluctuations of the size of the developed grains, and of the displacement of their centres from those of the original crystals, as in § 8. Hence, all separations between developed crystals which exceed a certain value u^1, will give rise to a visible gap. Then the blob density will be $\phi(u^1, \bar{p})$ equals B_1, say. Using the asymptotic expression (11), for this quantity, we obtain

$$B_1 = g \exp(-gu^1)\left[1+\frac{11g^2k_0^2}{48}+\frac{5}{96}g^3k_0^3+\ldots\right] . \quad . \quad . \quad (13)$$

The series in brackets rapidly converges, and reaches a maximum value of $e/2$ when $gk_0=1$, as can be readily seen by substitution in (11) and (12). For small values of g it is clear that the expression (13) tends to the empirical expression (2) for the blob density, and furthermore that α is to be identified with u^1, which must be very nearly equal to the diameter of the developed grains as measured under normal optical conditions of the microscope.

A further effect which should now be taken into account arises from fluctuations in developed grain size. Such variations are clearly visible in any track. The distribution in the observed diameters of single grains appears to be approximately Gaussian. The standard deviation ρ in stack 1 was found to be close to $0{\cdot}14\,\mu$. The technical details and analysis of such measurements have been described by Della Corte, Ramat and Ronchi (1953 a).

It can be shown that the effect of the distribution in developed grain size is to increase the predicted values of both B and H by a factor of approximately $(1+g^2\rho^2/4)$. We have no means of measuring the component along the track of displacements of the centre of the developed grain relative to the centre of the crystal from which it was formed; but clearly, such displacements will result in an effective increase in the value of ρ to be used. The new expression for the predicted blob density, taking into account such fluctuations, is

$$B_2 = B_1(1+g^2\rho^2/4) \quad . \quad . \quad . \quad . \quad . \quad . \quad . \quad . \quad . \quad (14)$$

B_1 being given by (13).

§ 11. COMPARISON OF THE VARIABLE SPACING MODEL WITH EXPERIMENT

Figure 6 shows the experimental values of blob density B, plotted against the coefficient g of the exponent of the gap-length distribution. The observations cover singly-charged particles of velocity β between 1·0 and 0·18, relativistic and slow α-particles, and a selection of heavier relativistic cosmic ray nuclei. The points labelled 'fast protons' are mean values taken from fig. 4. The points for slower protons and that for slow α-particles are also averages over a number of tracks. The points corresponding to multiply charged particles refer to individual tracks averaged over several emulsions.

Fig. 6

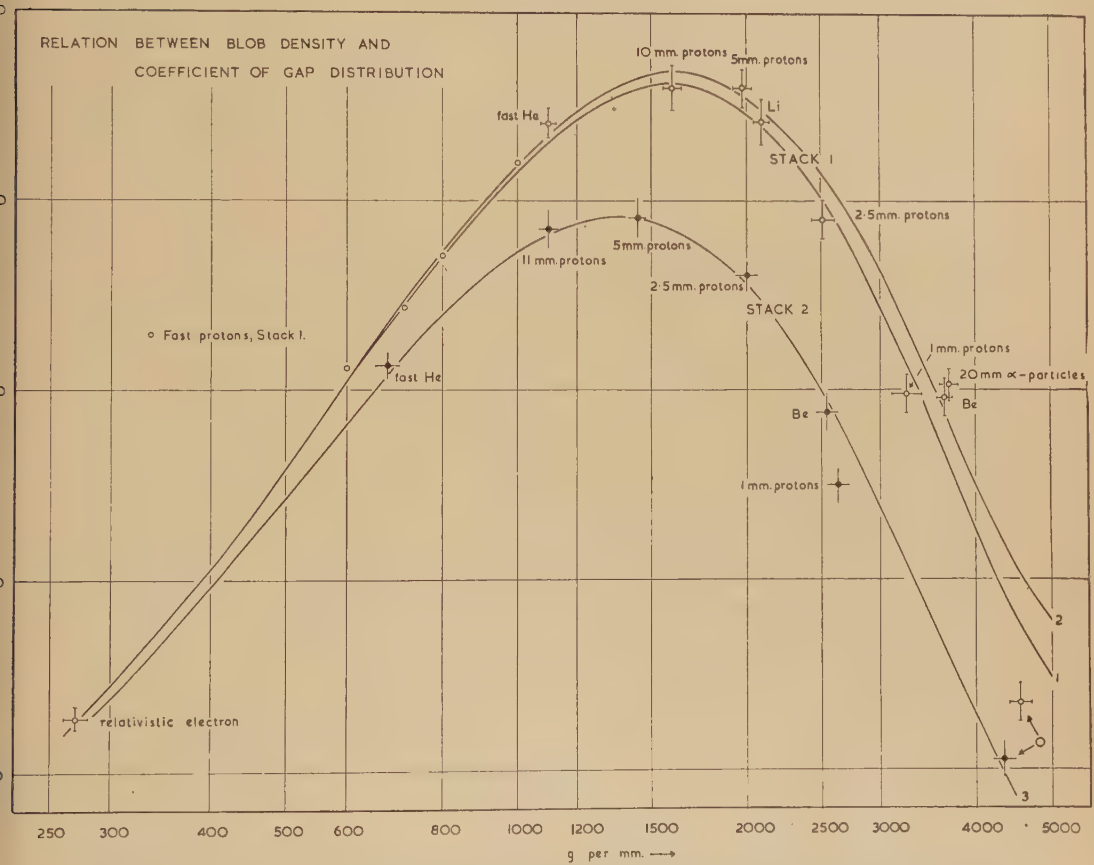

Relation between blob density B and the coefficient g, for the two stacks investigated. Curves (1), (2), and (3) show the predicted variation of these quantities, according to the variable spacing model (§ 10). In Stack 1, the points for heavy primary particles are taken from the results of fig. 1.

The curves (1) and (2) in fig. 6 show the predicted variations of B_1 and B_2 with g according to (13) and (14) respectively, for a value of $u^1=0{\cdot}67\ \mu$. Both curves are in good agreement with the experimental data from stack 1. The best value of u^1 is thus slightly different from the value of $0{\cdot}65\ \mu$ used for α in the empirical formula (2), Part I.

In the same diagram we show some representative points taken from tracks in stack 2. Curve 3 shows the variation of B_1 with g, for a value of $u^1=0{\cdot}76\,\mu$.

The average values found for u^1 in each stack are consistent with the mean values of the diameter of individual developed grains, as directly estimated. Such an estimate is, in fact, quite difficult to make and it appears that the most satisfactory way of determining the effective grain diameter, u^1, is to measure the values of B and g for protons of $\sim$ 1 cm range, where B is close to its maximum value for normal conditions of development.

It should be pointed out here that the values of B and H observed along the tracks of particles of $Z>8$ are considerably lower than those predicted (see fig. 1). This we attribute to obscuration of parts of the track by the presence of δ-rays, which becomes serious for high values of Z.

§ 12. INFLUENCE OF FLUCTUATIONS FOR SMALL VALUES OF g

Taking into account the fluctuations described above, it can be shown that for low values of $\bar{p}$ the coefficient g can be approximated by the expression

$$g=\gamma\left[1-\frac{\gamma\,.\,k_0{}^2}{2\bar{s}^2}\right],$$

where $\gamma=\log_e(1-\bar{p})/\bar{s}$, and is of course the value which g would have had in the absence of fluctuations. This expression has a more general validity in that it is true whatever the form of the distribution of path length of the ionizing particle through either the silver bromide crystals or the intervening gelatin. $k_0{}^2$ should now be considered as the mean square deviation in individual values of the crystal spacing about the mean value $\bar{s}$.

§ 13. VARIATION OF THE PROBABILITY OF DEVELOPMENT p WITH IONIZATION

So far we have not considered how p might vary with ionization or degree of development, except in so far as we have assumed that it tends to unity as the specific ionization becomes very large (see § 10).

In considering the variation of g with the velocity and charge of the ionizing particle, it will have been noticed (i) that the value of g^* for a relativistic α-particle is very nearly equal to four in both stacks investigated (fig. 3); (ii) that for proton ranges exceeding 1 cm the values of g^* for the two stacks are almost indistinguishable, despite the large difference in development; (iii) that for singly-charged particles g appears to vary approximately as dE/dR, the total rate of energy loss of the ionizing particle.

It is natural to attempt to explain the variations of g in terms of the energy lost by the ionizing particle in individual silver bromide crystals, i.e. the *local* ionization as distinct from the total rate of energy loss of the particle.

On traversing the crystal, the charged particle produces a certain number of knock-on electrons, and excitations. If such knock-on electrons are below a certain critical energy, we shall call them 'acts'. These acts will be distributed very nearly at random, since the number of atoms traversed per crystal is large. From any one act, one obtains a distribution in the number of free electrons liberated in the same crystal. δ-rays of more than a certain critical energy will contribute very little to the ionization in the crystal from which they originate. We shall therefore neglect their contribution. This critical energy for δ-rays will be about 2 kev for emulsions with crystal diameters of about $0{\cdot}3\,\mu$. This is much less than the maximum δ-ray energy for the slowest particles investigated ($\beta=0{\cdot}18$). *Hence we feel it is reasonably close to the truth to assume that the distribution of the number of electrons resulting from an act, is independent of the charge and velocity of the primary particle for all tracks considered, and hence to assume that the number of acts per unit length is proportional to the local ionization produced.*

Let the average probability of development of the crystal as the result of a single act be q. q depends upon the degree of development and emulsion sensitivity. We assume however that it is independent of the size of the crystal and the position of the act in it. This seems reasonable in view of the fact that the spatial distribution of the secondary ionization in the crystal about the path of the particle will be sharp. In any case, variations in q from this cause or from variations in intrinsic sensitivity of the crystal can be allowed for in terms of an extra variation of the path length x through the crystal.

Let λ be the average number of acts per unit length in the silver bromide. For a given value of x the distribution in the number of acts per crystal will be very nearly Poissonian, and therefore the fraction of those crystals with path length x which are developed is

$$p=[1-\exp(-\lambda xq)].$$

We can obtain the average probability of development $\bar{p}$ for all crystals traversed by integrating this quantity over all values of x—or more accurately all values of the product xq.

We shall now calculate $\bar{p}$ for three possible distributions in x, as follows :

(a) $x=\bar{x}$ and is constant for all crystals traversed.

(b) The crystals are spheres of equal diameter $3\bar{x}/2$, distributed at random about the path of the particle.

(c) The emulsion consists of spherical crystals of different diameter, all values of the diameter up to $2\bar{x}$ being equally probable (per unit volume of emulsion).

All three models have the same value, $\bar{x}$, for the average path length of the particle through a crystal. Let us write $\lambda\bar{x}q=y$ and let $f(x)\,dx$ be the distribution of the possible values of x. Then :

(*a*) $1-\bar{p}=\exp(-y)$,

(*b*) $f(x)\,dx=\frac{8x}{9\bar{x}^2}dx$ and $1-\bar{p}=\frac{8}{9y^2}\left[1-\left(\frac{3}{2}y+1\right)\exp(-3y/2)\right]$

$$=\exp\left[-(y-y^2/16+\frac{y^3}{240}-\ldots)\right],$$

(*c*) $f(x)\,dx=\frac{3}{2}\frac{x}{\bar{x}^2}\,.\,(1-x/2\bar{x})\,dx$

$$\text{and } 1-\bar{p}=\frac{3}{2y^2}\left[\left(1-\frac{1}{y}\right)+\left(1+\frac{1}{y}\right)\exp(-2y)\right]$$

$$=\exp\left[-\left(y-\frac{y^2}{10}+\text{terms in } y^4 \text{ and higher}\right)\right].$$

Model (*a*) has been proposed by a number of authors, but would appear to be an over-simplification. Model (*b*) first proposed by Demers (1947) appears at first sight to be very plausible ; for it is known that the silver bromide crystals are indeed nearly spherical, and that the dispersion of their diameters is not large. However this model must certainly represent an underestimate of the fluctuations involved which are those of the product xq. We therefore feel that model (*c*) is preferable, bearing in mind that there may be a distribution in the intrinsic sensitivity q of the crystals.

It is now possible, at least in principle, to decide between the above three models by comparing their predictions of how g should vary with the development factor q, for a given value of ionization and therefore λ.

In fig. 2, the full line (1) is a smooth curve drawn through the experimental points of stack 2, for $R<1$ cm. From any given value of g_2, the coefficient g in stack 2, we can calculate the corresponding quantity g_1 for stack 1, for each of the three models. The results are shown in the dashed curves (*a*), (*b*), and (*c*) of fig. 2. It is apparent that model (*c*) predicts differences between the values of g^* in the two stacks in good agreement with experiment, though neither model (*a*) nor (*b*) could be excluded with confidence. The reason for this is of course that in the region of high ionization, where the three models diverge considerably from one another, the coefficient g becomes insensitive to variations in $\log_e(1-\bar{p})$, as a result of the saturation due to the gelatin gap distribution. If however, one knew with confidence the variation of λ with velocity, one could decide among the three models quite easily.

§ 14. VARIATIONS OF λ WITH RANGE OF PROTONS

Using model (*c*), we have determined $y=\lambda q\bar{x}$ as a function of range R from the experimental points for stack 1, fig. 2. Making use of an extrapolated range–energy relation which takes into account the long-range point of Heinz (1954), we have found that y and therefore λ, the number of acts per unit length in silver bromide, varies very closely as $1/\beta^2$. The curve (2) in fig. 2 shows the relation to be expected between g^* and R assuming λ to be proportional to $1/\beta^2$ in the range interval 1–60 cm. Models (a) and (b) give essentially the same result. The curve has been normalized at the energy used by Heinz ($R=24{\cdot}2$ cm). It is interesting to note that the local ionization in the silver bromide crystals can be computed under reasonable assumptions, and also turns out to be very closely proportional to $1/\beta^2$ in this range.

From this experimental fact that λ is proportional to the local ionization in the crystal, it appears that the processes of recombination of ions resulting from separate acts have little effect.

For values of $\beta>0{\cdot}7$, λ is certainly no longer proportional to $1/\beta^2$. For if it were valid up to $\beta=1$, it would predict a value of $g^*=2{\cdot}12$ for $R=24{\cdot}2$ cm, as compared with the observed value of 1·59; and further, there would be no ‘ trough ’ at $\beta\sim 0{\cdot}95$.

To investigate the variation of λ at low velocities, measurements must be made in less sensitive enulsions, such as C2. Observations that have been published (Peters 1952, Dainton, Fowler and Kent 1952) suggest that λ indeed still varies as $1/\beta^2$.

§ 15. VARIATION OF λ WITH CHARGE Z

From the foregoing discussion, one might expect that the quantity λ, the number of acts per unit length in silver bromide, should be proportional to Z^2. This is indeed approximately true. Careful measurements on the tracks of two extremely energetic α-particles gave a value of $g^*=4{\cdot}10\pm0{\cdot}05$. Hence the value of λ must lie between 4·3 (model (a)) and 4·55 (model (c)) times the value for a relativistic electron. This appears significantly greater than 4·0. Similarly, the value of λ for an extremely energetic lithium nucleus was $\sim$ 10 times the minimum value. Furthermore, in numerous measurements on α-particles of whatever energy, no case has been found in which $g^*<3{\cdot}9$.

From these provisional results, it would appear that there is little or no ‘ trough ’ in the curve of ionization versus energy for α-particles and that λ/λ_0 is significantly greater than 4·0. Further observations are being made to investigate this point.

§ 16. COMPARISON OF THE PRESENT RESULTS WITH THOSE OF OTHER WORKERS

The distribution of gaps along the tracks of ionizing particles in G5 emulsions has previously been studied by numerous workers. Among them are Menon and O'Ceallaigh (1954), O'Ceallaigh (1954), Hull, Happ and Morrish (1952), Herz and Davis (1954), Blatt (1954) and Della Corte *et al.* (1953 a, 1953 b, 1954).

In the papers of Della Corte *et al.*, and Herz and Davis, the models assumed constant crystal spacing as described above (§ 9). Such models, as we have seen, fail simply because even when the ionization is very large, there is still a residual gap-length distribution, the greatest gap-lengths observed being far in excess of the mean spacing between consecutive crystals. As mentioned earlier one could however explain such gaps on the assumption that 14% of the crystals are completely incapable of development. This state of affairs we consider most improbable.

In the papers of Della Corte *et al.* the probability of development appears to have been mistakenly identified with the reciprocal of the mean gap-length (i.e. the coefficient of the exponent of the distribution). This led them to assume a dependence of the mean enlargement of a crystal after development upon the probability of development. Our experimental evidence shows that this is not the case, at least up to values of ionization equal to those of relativistic oxygen nuclei. In leaving out of consideration the distribution in gelatin gaps between crystals, they have also had to appeal to recombination of the ions liberated in the crystals, in order to account for the saturation of the mean gap length at high values of ionization.

As mentioned above, the effect of fluctuations in the gelatin gap between crystals had previously been considered by O'Ceallaigh. He, however, took a value of $1/k_0$, the reciprocal of the coefficient of the exponential gap distribution between successive crystals, of $0{\cdot}1\ \mu$, in place of the value $0{\cdot}20\,\mu$ we have derived from the observations in heavily-ionizing tracks. There also appears to be an error in O'Ceallaigh's calculated gap length distribution. His distribution has a maximum at $u \sim 5k_0$–$10k_0$ instead of increasing continuously down to the minimum allowed value of u.

Blatt (1954) has carried out an extensive theoretical treatment of the gap-length distribution according to a number of possible models. Comparing his results with a preliminary measurement of a single track, he had concluded that models based on variable crystal spacing were unacceptable. He has used for u^1, the distance between centres of grains corresponding to the minimum detectable gap, the developed grain diameter as directly measured. The reason for the alleged discrepancy appears to us as likely to have arisen from the difficulty of eliminating systematic errors from this direct measurement. Thus, he has taken a value of $u^1=0{\cdot}65\,\mu$, whereas a value of $0{\cdot}80\,\mu$ would give agreement with the variable spacing models.

ACKNOWLEDGMENTS

We should like to express our sincere thanks to Dr. C. S. Davis of the Department of Mathematics of this University for the proof of the asymptotic form of the gap distribution given in eqns. (11) and (12). This obviated the necessity of exhaustive numerical computation which we had already performed. Our thanks are also due to Professor C. F. Powell for his interest during the course of the work.

REFERENCES

BLATT, J. M., 1954, *University of Sydney Mimeographed Report.*

DAINTON, A. D., FOWLER, P. H., and KENT, D. W., 1952, *Phil. Mag.*, **43**, 729.

DELLA CORTE, M., 1954, *Il Nuovo Cim.*, **12**, 28.

DELLA CORTE, M., RAMAT, M., and RONCHI, L., 1953 a, *Il Nuovo Cim.*, **10**, 509; 1953 b, *Ibid.*, **10**, 958

DEMERS, P., 1947, *Canad. J. Research*, A, **25**, 223.

HAPP, W. W., HULL, T. E., and MORRISH, A. H., 1952, *Canad. J. Phys.*, **30**, 699.

HEINZ, O., 1954, *Phys. Rev.*, **95**, 610.

HERZ, A. J., and DAVIS, G., 1954, *University of Sydney Mimeographed Report.*

MENON, M. G. K., and O'CEALLAIGH, C., 1954, *Proc. Roy. Soc.*, A, **221**, 292.

O'CEALLAIGH, C., 1954, *CERN Report*, B.S. 11.

PETERS, B., 1952, *Progress in Cosmic Ray Physics* (North Holland Publishing Company), p. 191.

APPENDIX

Calculation of Statistical Errors Associated with Blob and Gap Counts

Let us consider the distribution in length, t, of the interval between the centre of the grain terminating one gap, and that of the grain beginning the next gap. The density of gaps is H, the minimum length measured between centres of the bounding grains is $l+u^1$. The mean length of all such gaps is $l+u^1+1/g=\bar{l}$, say. Let G be the number of developed crystals per unit length of track. $G=p/\bar{s}$, and can be found from eqn. (12) in terms of g. The interval, t, can be composed of any number of grains, n. The distribution of the frequency of occurrence of different values of n is a geometric progression :

$$\psi(n)=\xi(1-\epsilon)^{n-1}$$

where ξ and ϵ are constants given by the conditions

$$H=\sum_{1}^{\infty}\psi(n)\ =\xi/\epsilon$$

and

$$G=\sum_{1}^{\infty}n\psi(n)=\xi/\epsilon^2.$$

Hence

$$\epsilon=H/G \quad \text{and} \quad \xi=H^2/G.$$

Let μ be the mean value, and η the standard deviation about this mean value, of the distance between those adjacent grains, whose separation is less than $l+u^1$ (i.e. whose separation is not large enough to count as a gap). If there are n grains in the interval t, the mean value of t is $(n-1)\mu$, and the standard deviation about this mean value is $\eta\sqrt{(n-1)}$.

We now require the total square deviation about the mean value of the quantity t, for all values of n. Let us first sum the squares of the individual standard deviations about $t=0$, over all values of n. The contribution from those intervals containing n grains is

$$\psi(n)[(n-1)\eta^2+(n-1)^2\mu^2].$$

Hence the total square deviation about $t=0$ is

$$Y^2=\sum_1^\infty \xi(1-\epsilon)^{n-1}[(n-1)\eta^2+(n-1)^2\mu^2]/\sum_1^\infty \psi(n)$$
$$=\frac{\eta^2(1-\epsilon)}{\epsilon}+\frac{\mu^2(1-\epsilon)(2-\epsilon)}{\epsilon^2}.$$

The mean length of the interval t is

$$\bar{t}=\sum_1^\infty \psi(n)(n-1)\mu/\sum_1^\infty \psi(n)=\frac{\mu(1-\epsilon)}{\epsilon}.$$

Thus the total square deviation about the mean, $\bar{t}$, is

$$Y^2-\bar{t}^2=\frac{\eta^2(1-\epsilon)}{\epsilon}+\frac{\mu^2(1-\epsilon)}{\epsilon^2}=\frac{\eta^2(1-\epsilon)}{\epsilon}+\frac{\bar{t}^2}{(1-\epsilon)}.$$

So far, we have only considered fluctuations in t, the distance between the end of one gap and the beginning of the next. The total square deviation about the mean, of the distance from the beginning of one gap to the beginning of the next, is clearly $(Y^2-\bar{t}^2)+1/g^2$. This follows because the distribution of gap length is exponential, with coefficient g, and the standard deviation about the mean gap-length $\bar{l}$ is $1/g$. The mean separation between beginnings of successive gaps being $1/H$, we have for the standard deviation in H,

$$\frac{dH}{H}=\frac{1}{\sqrt{(N_H)}}\cdot H\sqrt{(Y^2-\bar{t}^2+1/g^2)}$$
$$=\frac{H}{\sqrt{(N_H)}}\sqrt{\left(\frac{\bar{t}^2}{(1-\epsilon)}+\frac{1}{g^2}+\frac{\eta^2(1-\epsilon)}{\epsilon}\right)},$$

where N_H=number of gaps counted. The quantity η depends on the model of crystal separation employed, and is zero for the constant-spacing model. The term involving η for any model is always small in comparison with the sum of the other two terms under the square-root. ϵ is equal to (H/G) from above, and so depends slightly on the model used. $\bar{t}$ is the mean length of an interval and is therefore $1/H-\bar{l}$.

The above formula, with the term involving η^2 neglected, is given in Part I.

LXIX. *The Radioactivity of* ^{183}Ta, ^{185}Ta, $^{183\text{m}}$W *and* $^{185\text{m}}$W

By A. J. Poë
Atomic Energy Research Establishment, Harwell*

[Received January 13, 1955]

Abstract

The following radiation characteristics of the neutron excess tantalum isotopes ^{183}Ta and ^{185}Ta and of the isomers $^{183\text{m}}$W and $^{185\text{m}}$W have been determined :

	^{183}Ta	^{185}Ta	$^{183\text{m}}$W	$^{185\text{m}}$W
Half-life	5·0±0·1 days	49·5±1·5 min	5·5 sec	1·62±0·05 min
β-energy (Mev)	~0·15, 0·6	~0·15, 1·72	—	—
γ-energy (kev)	110, 160, 210, 240, 320	125, 175, 235	105, 155	130, 165

^{185}Ta does not decay to any appreciable extent via the isomer $^{185\text{m}}$W and the 175 kev gamma-ray from ^{185}Ta is not the same as the 165 kev gamma-ray from $^{185\text{m}}$W. The 125 kev gamma-ray from ^{185}Ta and the 130 kev gamma-ray from $^{185\text{m}}$W are probably the same and due to transition to the ground state of ^{185}W. Unless there is an undetected rate-determining transition the 165 kev gamma-ray from $^{185\text{m}}$W is then due to the isomeric transition and from half-life and K conversion considerations it may be classified as E3. Similarly the 155 kev gamma-ray in $^{183\text{m}}$W is probably from the rate-determining transition.† The classification of the $^{183\text{m}}$W isomeric transition type on the basis of K conversion measurements is not unambiguous.

§ 1. Introduction

The neutron excess radioactive isotopes ^{183}Ta and ^{185}Ta have been described previously. Butement (1950 and 1951) obtained half-lives of 116 hours and 48 minutes for tantalum isotopes produced by (γ, p) reactions on tungsten, and assigned them to ^{183}Ta and ^{185}Ta respectively. Duffield *et al.* (1950) irradiated tungsten enriched in the ^{186}W isotope with x-rays of energy up to 23 Mev and detected a 46-minute half-life tantalum activity, confirming the assignment to ^{185}Ta. This had a beta-disintegration energy of 1·7 Mev and a conversion electron energy of 75 kev. They also found a 1·85-minute half-life in the tungsten which they assigned to an

---

* Communicated by the Author.

† But see note added in proof (p. 619).

isomeric state of ^{185}W, a 75 kev conversion electron again being associated with the decay. Moses and Martin (1951) also found the 48-minute tantalum activity after high energy x-ray irradiation of tungsten and detected a 150 kev beta-disintegration or conversion electron in addition to a 1·6 Mev beta-disintegration. The 150 kev and 1·6 Mev disintegrations were found not to be in coincidence. They also found an activity with a 6-day half-life which had a beta-disintegration energy of 0·6 Mev.

The work described in this paper was undertaken to examine the radiations from ^{183}Ta and ^{185}Ta in greater detail. Work on the isomers ^{183m}W and ^{185m}W is also described. During the course of this investigation the assignment of the 5-day activity to ^{183}Ta was confirmed by Mihelich (1953) and DuMond *et al.* (1953) who detected it after irradiation of tantalum in a high flux of thermal neutrons, the ^{183}Ta being produced by double neutron capture. The latter authors found the half-life to be $5{\cdot}2 \pm 0{\cdot}1$ days and described the gamma-ray spectrum in great detail.

§ 2. Experimental Techniques

The tantalum isotopes were prepared by irradiation of tungstic acid with fast neutrons, generated in the Harwell cyclotron, of energy up to 50 Mev which produced (n, p) and (n, pn) reactions in the tungsten. The tungstic acid was then dissolved in sodium hydroxide solution and the tantalum coprecipitated with ferric hydroxide by the addition of a solution containing a few milligrams of ferric chloride. After washing with sodium hydroxide solution the precipitate was dissolved in hydrochloric acid and reprecipitated from a solution of inactive sodium tungstate acting as a hold-back.

The radiation characteristics were examined by aluminium absorption, beta- and gamma-ray scintillation spectroscopy and coincidence counting techniques. The anthracene crystal in the beta-particle scintillation spectrometer was a cylinder 0·5 in. long and 1·5 in. in diameter. The spectrometer had a resolution of 20% for the 624 kev conversion electron from a ^{137}Cs–^{137m}Ba source. The main source of error in the measurement of beta-disintegration energies was in the initial calibration with a conversion electron of known energy, the final Fermi plot derived from the beta-particle spectrum usually being very close to a straight line.

Conversion electrons were examined by absorption of those electrons which were in coincidence with beta-decay. The sample was mounted over a small hole in a 1 mm thick brass plate placed between two end-window Geiger counters, the brass absorbing most of the particles which would otherwise have been scattered from one counter into the other, thereby producing a spurious coincidence.

The gamma-ray scintillation spectrometer had a resolution of 10% for the photoelectric absorption peak from the 661 kev gamma-ray from ^{137}Cs–^{137m}Ba. The sodium iodide crystal used was a cylinder 1·0 in. long and 1·5 in. in diameter.

§ 3. RESULTS

(*i*) ^{183}Ta

The half-life of this isotope was found to be 5·0±0·1 days from the beta- and gamma-ray decay of ten samples followed for several months. After subtraction of the long-lived activity, which accounted initially for about 5% of the counting rate, the decay of the ^{183}Ta was accurately measurable for about five half-lives.

Aluminium absorption experiments indicated a rather indeterminate low energy component of 0·1–0·2 MeV in addition to the maximum beta-particle energy of 0·6 MeV. The low energy component accounted for 30–40% of the total beta-particle counts.

Scintillation spectrometer studies of the gamma-ray spectrum of a tantalum source after shorter-lived activities had decayed away indicated gamma-ray energies of 60, 110, 160, 210, 240 and 320 kev with approximate relative intensities 25 : 5 : 5 : 3 : 10 : 7, each of which decayed with a 5-day half-life. The 60 kev component is very probably the K x-ray. This spectrum agrees with the results of DuMond *et al.* (1953) allowing for the relatively much poorer resolution of the scintillation spectrometer. The group of gamma-rays of energy close to 145 kev reported by DuMond *et al.* was not resolved but could have been present up to an intensity of 2·5 relative to the 240 kev gamma-ray intensity of 10.

(*ii*) ^{185}Ta

The half-life of ^{185}Ta was measured by following the decay of those beta-particles which passed through 500 mg/cm^2 of aluminium. This was sufficient aluminium to absorb all the beta-particles from longer-lived isotopes present and the long-lived background of gamma-radiation amounted to about 10% of the initial counts. The average half-life resulting from six determinations was 49·5 minutes, all the results lying within 1·5 minutes of this value.

The beta-particle spectrum was examined by aluminium absorption and scintillation spectroscopy. The former indicated, in agreement with previous published work, a maximum beta-particle energy of 1·7 MeV and a low energy component of about 0·15 MeV which amounted to about 30% of the total count. The absorption curve of those particles which were in coincidence with beta-particles of energy >0·2 MeV showed mainly the 0·15 MeV component. This is therefore a conversion electron from a transition in ^{185}W which is in coincidence with the beta-disintegration of ^{185}Ta. The absorption of those beta-particles which were in coincidence with the total gamma-radiation was indistinguishable from the normal beta-particle absorption, which is a further indication of a transition in ^{185}W which is in coincidence with the beta-disintegration of ^{185}Ta.

The beta-particle spectrum measured with the scintillation spectrometer is shown in fig. 1 together with the corresponding Fermi plot. W is the total energy of the electrons in mc^2 units. $N(W)$ is the number of electrons with energy between $W-\frac{1}{2}x$ and $W+\frac{1}{2}x$, where x is the channel-width of the pulse analyser in energy units. θ is the Fermi beta-disintegration function calculated by Bleuler and Zünti (1946). The plot of $[N(W)/\theta W^2]^{1/2}$ against kinetic energy is very close to a straight line, the deviation at the maximum energy being probably due to statistical line broadening (Palmer and Laslett 1951). The average of five closely concordant results for the maximum beta-particle energy was 1·72 MEV.

Fig. 1

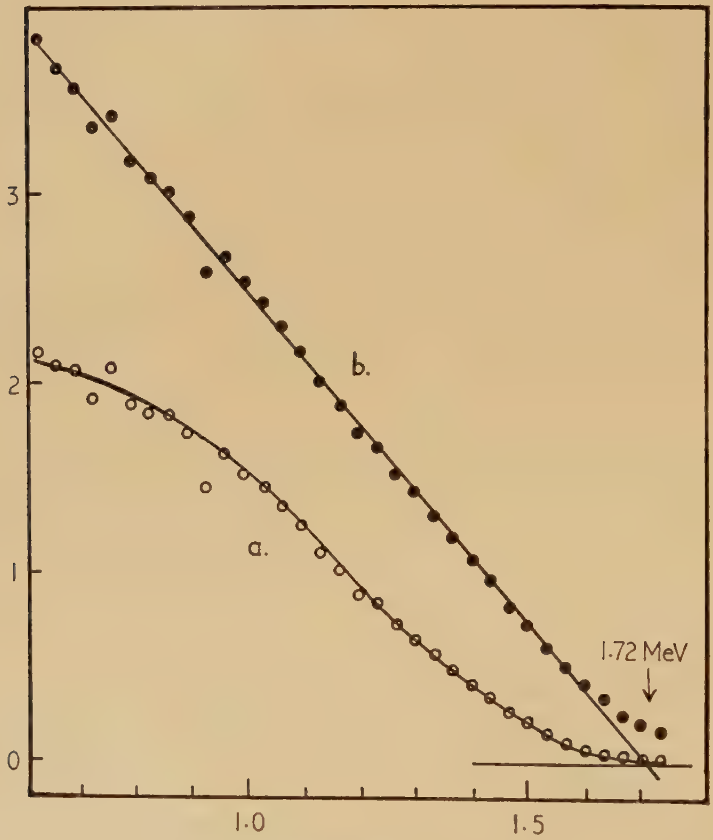

Energy MEV

Beta-particle energy of 49·5 min ^{185}Ta (*a*) $N(W)\times10^{-3}$, (*b*) $[N(W)/\theta W^2]^{1/2}$.

The gamma-ray spectrum is shown in fig. 2 and indicates gamma-rays of 125, 175 and 235 kev and also a 60 kev component (presumably the K x-ray) in the approximate relative intensities, referred to the 175 kev gamma-ray, of 4 : 10 : 2·5 : 14. The sample for this work was prepared by irradiation of tungstic acid enriched in ^{186}W and the spectrum of longer-lived activities was weak and easily corrected for.

(*iii*) ^{185m}W

The ^{185m}W isomer was prepared by irradiation of tungsten metal with neutrons of energy up to 50 MeV in the cyclotron. A half-life of 1·62±0·05 minutes was obtained from the gamma-ray decay.

The mass assignment of this isomer to ^{185m}W was made by Duffield *et al.* (1950) on the basis of its production from tungsten enriched in ^{186}W by irradiation with x-rays of up to 23 MeV. The possibility of a theoretically unlikely assignment to ^{186m}W has been tested by measuring the change with neutron irradiation energy of the relative yields of 1·6-minute activity from two tungstic acid samples, one enriched in ^{184}W and the other in ^{186}W. The ratio of the amounts of ^{184}W in these two samples was 58 : 1 and of ^{186}W was 1 : 16. If the 1·6-minute isomer were ^{184m}W or ^{186m}W the yields from the two samples after irradiating and counting under identical conditions would be in one of the ratios 58 : 1 or 1 : 16, and there would be no change in the ratio with change in the energy of the irradiating neutrons. If the isomer were ^{185m}W the ratio of the yields would be between 58 : 1 and 1 : 16, depending on the relative cross sections of the reactions ^{184}W(n, γ)^{185m}W and ^{186}W(n, 2n)^{185m}W under the conditions of the irradiation. At low neutron irradiation energies the (n, γ) reaction will become increasingly more probable relative to the (n, 2n)

Fig. 2

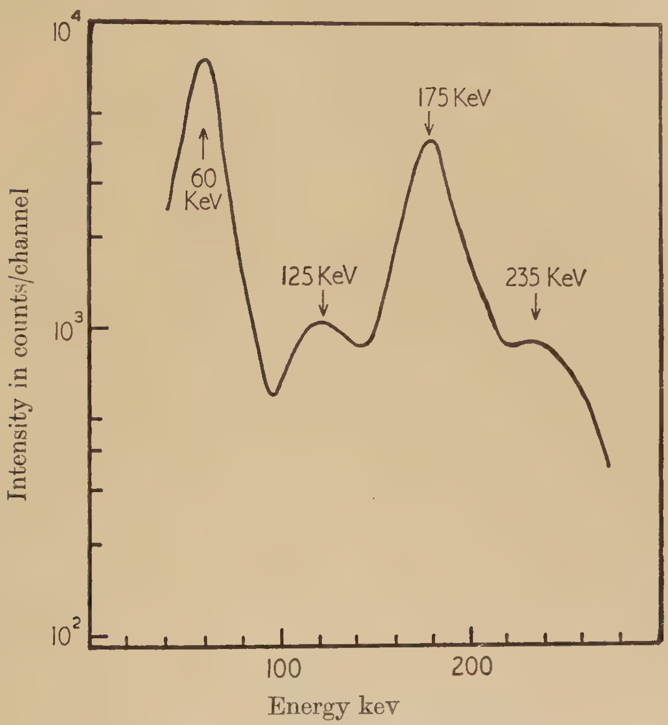

Gamma-ray energy spectrum of 49·5 min ^{185}Ta.

reaction as the irradiation energy is decreased, and the ratio of the yields of the isomer from the two samples will move away from 1 : 16 towards 58 : 1.

The ratios obtained from neutron energies $\ngtr 20$, $\ngtr 15$ and $\ngtr 10$ Mev were 1 : 11, 1 : 4·7 and 1 : $\lesssim$0·3 respectively, the yields having been measured by counting only those gamma-rays of energy between 40 and 250 kev. (The gamma-ray spectrum of the 1·6-minute isomer is described below.) The irradiations were all monitored using the 12·8-hour activity induced in copper foils. Irradiation of $CaCO_3$ containing a mass of oxygen equal to that in the tungstic acid samples showed that no correction for the counts from the annihilation radiation from ^{15}O was necessary. The isomer is therefore almost certainly ^{185m}W.

Attempts were made to separate off any of the ^{185m}W isomer formed after beta-decay of ^{185}Ta using a Deacidite F–F anion exchange resin. This was used in two ways. In one the cyclotron-produced tantalum activities were dissolved in a little 3M HCl : 0·5M HF solution and mounted on a column of resin 5 cm long and 1 cm in diameter. This column was eluted at 20-minute intervals with 5 ml. of the HCl : HF solution and the solution obtained transferred to the counter in less than one minute. These samples were counted in fixed geometry with a scintillation spectrometer adjusted to count gamma-rays between 40 kev and 250 kev. In the other method the tantalum activities were dissolved in 10 ml. of the 3M HCl : 0·5M HF solution and shaken for 15 minutes with 5 g of the resin. The solution was then filtered from the resin and counting begun within 75 seconds of the separation. In both methods the total activity of the initial sample was measured in the same geometry before mounting on the resin and allowance for the decay made so that the 49·5-minute ^{185}Ta activity was known at the time of each attempted ^{185m}W separation.

With tracer activities of tungsten and tantalum under the conditions described above, not less than 10% of the tungsten activity and only up to 0·4% of the tantalum activity was eluted from the column, and not less than 15% of the tungsten and only up to 0·6% of the tantalum was extracted from the resin by shaking for 15 minutes. Similar results were obtained with the elution of carrier free ^{181}W from the column.

In the experiments with cyclotron produced tantalum activities no short-lived decay of the extracted samples was observed. The difference between the first count after separation and a count after all the ^{185m}W would have decayed was of the same order as the probable errors involved in the counting. Knowing the total activity on the resin the activity of the samples obtained was that expected if only tantalum activities were present. The proportion of gamma-ray counts from 49·5-minute ^{185}Ta which are due to decay from the meta-stable ^{185m}W level must therefore be very small. Assuming that 10% of the available ^{185m}W was eluted from the column and that 15% was extracted from the resin by shaking with acid, the average of fifteen values for the proportion of ^{185m}W counts in ^{185}Ta is 0·1% with a probable error of ±0·5%. The detection efficiency, by gamma-ray counting, of the ^{185m}W decay may well be lower than that of ^{185}Ta decay. The proportion of ^{185}Ta disintegrations which lead to ^{185m}W may therefore be somewhat higher than the proportion of ^{185}Ta gamma-ray counts which are due to ^{185m}W decay.

Coincidence measurements described above (3 (*ii*)) provide additional evidence that the ^{185}Ta beta-transition does not go directly to the ^{185m}W isomer. The gamma-ray spectrum of those gamma-rays which were in coincidence with the 1·7 Mev beta-disintegration of ^{185}Ta was indistinguishable from the normal spectrum.

The gamma-ray spectrum of a tungsten sample measured two minutes after irradiation, using a thirty-channel pulse analyser, is shown in fig. 3.

Fig. 3

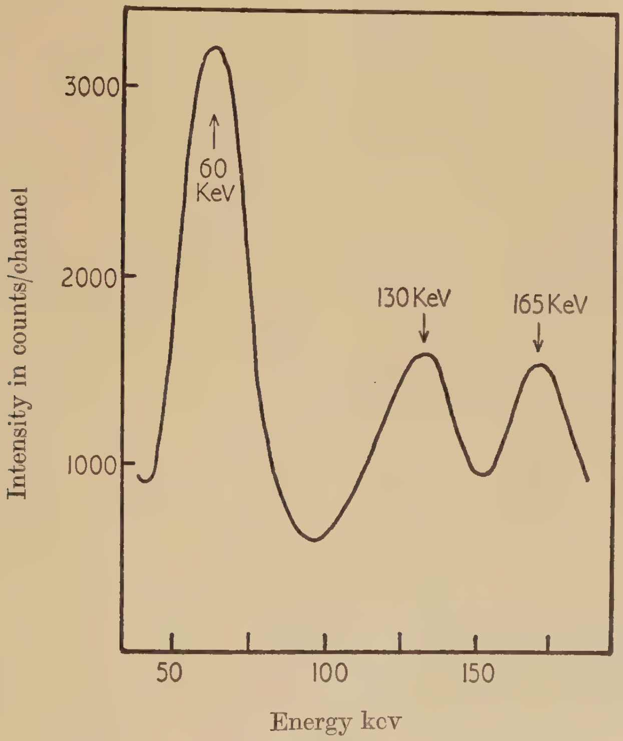

Gamma-ray energy spectrum of 1·6 min ^{185m}W.

There is a 60 kev K x-ray and 130 and 165 kev gamma-rays in the relative intensities, after small corrections for background and long-lived activities, of 2 : 1 : 1. The spectrum of gamma-rays in coincidence with the 165 kev gamma-ray was measured with two scintillation counters placed with the two crystals close together. One counter was connected to a single-channel pulse analyser which only accepted pulses from 165 kev gamma-rays, and the other to a one hundred channel pulse analyser which only accepted gamma-ray pulses which were in coincidence with the 165 kev gamma-rays detected by the other counter. The resulting spectrum consisted only of the x-ray and the 130 kev gamma-ray. The 165 and 130 kev gamma-rays are therefore in coincidence.

Low lying excited states of the tungsten isotopes of mass 182, 183, 184 and 186 have been shown by Coulomb excitation to be 101, 103, 112 and 124 kev respectively above the ground state (McClelland, Mark and Goodman 1954, Huus and Bjerregaard 1953). It therefore seems probable that the 125 kev gamma-ray from ^{185}Ta and the 130 kev gamma-ray from ^{185m}W are the same, and due to transition to the ground state of ^{185}W. It may then be concluded that the 165 kev gamma-ray from ^{185m}W is the rate-determining step in the isomer. The 175 kev gamma-ray from ^{185}Ta must then be from another transition involving other excited levels in the ^{185}W nucleus, since it is in coincidence with the ^{185}Ta beta-disintegration. It is possible, however, that there may be an as yet undetected rate-determining transition in the isomer, in which case the 165 kev gamma-ray could account for part of the 175 kev gamma-ray observed in the ^{185}Ta spectrum up to an extent equal to the intensity of the 125 kev gamma-ray (see figs. 2 and 3).

Assuming, however, that the 165 kev transition is the rate-determining transition in the ^{185m}W isomer, the half-life and energy define it as E3 or M3 (Goldhaber and Hill 1952). According to the calculations of Rose *et al.* (1951) the K conversion coefficients of 165 kev E3 and M3 transitions are 0·7 and 27 respectively.

The K conversion coefficient, as indicated by the gamma-ray : x-ray intensity ratio, cannot be greater than 2 and the E3 assignment for the 1·6-minute ^{185m}W isomeric transition is therefore strongly favoured. The 1·6-minute isomer is therefore probably a 165 kev E3 transition followed by a 130 kev transition to the ground state.

(*iv*) ^{183m}W

The half-life, mass assignment and conversion electron energy of this isomer have been reported by der Mateosian *et al.* (1949). The half-life and energy identify the transition as E3 or M3 (Goldhaber and Sunyar 1951), and unpublished work by der Mateosian and Goldhaber indicating that mainly L x-rays arise in the conversion supports an E3 transition type assignment (Goldhaber and Hill 1952).

The isomer has been prepared in this laboratory by irradiation of tungsten with fast neutrons in the cyclotron, and the gamma-ray spectrum measured using a scintillation spectrometer and a single-channel pulse analyser. Pulses from the amplifier were fed into the pulse analyser and also directly into a scaler. The samples were removed from the cyclotron and counted from ten to twenty, sixty to seventy and eighty to ninety seconds after the end of the irradiation. The ratio of the number of counts of a given energy from the isomer to the total number of counts from the isomer was thereby obtained. Each irradiation gave one point on the spectrum which was covered after about twenty such irradiations.

The spectrum so obtained indicated gamma-rays of 105 and 155 kev together with the K x-ray in the approximate relative intensities 2·5 : 1 : 10. The decay of each of these components was followed separately and indicated a half-life of about 5·5 seconds. Campbell and Goodrich (quoted by Hollander, Perlman and Seaborg 1953) have reported gamma-rays of 0·12 and 0·17 Mev for this isomer.

Following similar arguments to those used for $^{185\mathrm{m}}$W, the 105 kev gamma-ray is probably due to transition to the ground state. The 155 kev gamma-ray is therefore associated with the isomeric transition unless there is an undetected rate-determining transition. The K conversion coefficients for E3 and M3 transitions of this energy are 0·8 and 32 respectively (Rose *et al.* 1951). The K conversion coefficient of the 155 kev transition, as indicated by the x-ray : gamma-ray intensity ratio, could be as high as 10.* On this basis therefore the choice between a transition type assignment of E3 or of M3 cannot be made with certainty, although by analogy with $^{185\mathrm{m}}$W an E3 assignment is favoured in agreement with the conclusions of der Mateosian and Goldhaber quoted above.

ACKNOWLEDGMENTS

Acknowledgments are gratefully made to Dr. F. D. S. Butement for suggesting this work and for helpful discussions and advice, to the members of the Cyclotron Group for carrying out irradiations and to Mr. R. B. Thomas for much assistance with the experimental work.

---

* *Note added in proof.*

A detailed level scheme for ^{183}W recently given by Murray *et al.* (Murray, J. J., Boehm, F., Marmier, P., and DuMond, J. W. M., 1955, *Phys. Rev.*, **97**, 1007) shows that decay to the ground state from the 99·07 kev level reached by Coulomb excitation can occur by a 52·59 kev–46·48 kev cascade as well as directly. The 60 kev component from $^{183\mathrm{m}}$W must, therefore, be partly due to these two low energy gamma-rays. Consideration of the ^{183}W level scheme suggests that the 155 kev gamma-ray from $^{183\mathrm{m}}$W may well not be from the rate-determining transition whose energy and exact transition type are, therefore, still uncertain. The $^{185\mathrm{m}}$W decay scheme is probably also more complex than suggested above.

REFERENCES

BUTEMENT, F. D. S., 1950, *Nature, Lond.*, **165**, 149 ; 1951, *Proc. Phys. Soc.* A, **64**, 395.
BLEULER, E., and ZÜNTI, W., 1946, *Helv. Phys. Acta*, **19**, 375.
DER MATEOSIAN, E., and GOLDHABER, M., 1949, *Phys. Rev.*, **76**, 187A.
DER MATEOSIAN, E., GOLDHABER, M., and SMITH, A., 1949, *Argonne National Laboratory Classified Report*, ANL–4237.
DUFFIELD, R. B., HSAIO, L., and SLOTH, E. N., 1950, *Phys. Rev.*, **79**, 1011.
DUMOND, J. W. M., HOYT, H. C., MARMIER, P. E., and MURRAY, J. J., 1953, *Phys. Rev.*, **92**, 202.
GOLDHABER, M., and HILL, R. D., 1952, *Rev. Mod. Phys.*, **24**, 179.

Goldhaber, M., and Sunyar, A. W., 1951, *Phys. Rev.*, **83,** 906.
Hollander, J. M., Perlman, I., and Seaborg, G. T., 1953, *Rev. Mod. Phys.*, **25,** 469.
Huus, T., and Bjerregaard, J. H., 1953, *Phys. Rev.*, **92,** 1579.
McClelland, C. L., Mark, H., and Goodman, C., 1954, *Phys. Rev.*, **93,** 904.
Mihelich, J. W., 1953, *Phys. Rev.*, **91,** 427.
Moses, A. J., and Martin, D. S., 1951, *Phys. Rev.*, **84,** 366.
Palmer, J. P., and Laslett, J. L., 1951, *U.S. Atomic Energy Commission Unclassified Report*, A.E.C.U., 1220.
Rose, M. E., Goertzel, G. H., Spinrad, B. I., Harr, J., and Strong, P., 1951, *Phys. Rev.*, **83,** 79.

LXX. *Some Magnetic Properties of Dilute Ferromagnetic Alloys : I*

By G. Bate, D. Schofield and W. Sucksmith
University of Sheffield*

[Received January 13, 1955]

Summary

The theory of the coercivity of non-spherical, single domain particles of ferromagnetic material in a non-magnetic matrix has been developed independently by Néel (1947) and Stoner and Wohlfarth (1948). Appropriate conditions for the study of the growth of these domains are to be found in suitable dilute ferromagnetic alloys where there is an increase of solubility of the ferromagnetic constituent with temperature. Such characteristics are found in the copper rich alloys of copper–cobalt and copper–iron. The magnetic properties of appropriate alloys with increase of heat treatment are followed from the normal paramagnetism of the solid solution to the ordinary magnetization curve of the precipitated ferromagnetic. At a suitable stage a maximum in the coercivity is found which the writers believe to be associated with single domain precipitates. The characteristics of the hysteresis loops at this stage indicate the presence of high coercivities of more than 1000 oe.

§ 1. Introduction

In low fields changes in magnetization in ferromagnetic materials occur by two distinct processes ; by domain wall movements in which the volumes of the domains change and by rotation of the domain magnetization vector. Various theories (e.g. Becker, Kersten, Néel) have been put forward to provide the mechanism whereby the free magnetic energy controls the position of the domain boundary but in their present form these theories cannot easily account for coercivities of more than some hundreds of oersteds. However, because of the large energy changes accompanying rotational processes, in the absence of wall movements high coercivities may be associated with irreversible rotational operations.

Single domains were first predicted by Frenkel and Dorfman (1930) who suggested that in small particles the formation of a domain wall may be energetically unfavourable and that such a region would be magnetically uniform. Theoretical analyses by Néel (1947) and independently by Stoner and Wohlfarth (1948) have shown that coercivities of several thousand oersted can be attributed to shape anisotropy. The theoretical maximum coercivities associated with crystal, shape and

---

* Communicated by the Authors.

strain anisotropies with complete orientation of the anisotropy axes are shown in table 1 (Kittel 1949); for a body containing randomly orientated particles, the values of coercivity are reduced by a factor of 0·48. Single domain theories of coercivity are applicable to very finely divided powders and to heterogeneous alloys in which magnetic 'islands' are dispersed in a non-magnetic matrix.

Table 1

Anisotropy	Crystalline	Shape	Strain
Fe	500	10700	600
Co	6000	8800	600
Ni	135	3150	4000

From the results of experiments on finely divided powders, summarized by Weil (1951), it appears that there is good evidence for the crystalline and shape anisotropy mechanisms of hysteresis although the values of coercivity are less than would be expected from theoretical considerations. Little work has been published on suitable heterogeneous alloys, though Constant and his collaborators (1939, 1943) investigating the low field properties of impure copper and brass reported coercivities of about 100 oersted.

A preliminary investigation by Sucksmith (1952) into the variation in magnetic properties of stainless steel magnetic recording wire, 12% Cr, 12% Ni, rest Fe, with heat treatment and cold work, showed that it was desirable to study very dilute two-phase alloys in which interaction effects were negligible and the growth of ferromagnetic regions controllable by heat treatment. The required characteristics appeared to be present in copper rich alloys of copper–cobalt and copper–iron in which the solubility of the ferromagnetic component rises from a very low value at room temperature to 3–4% at 1000°c. Thus, the rapid quenching of alloys of compositions of up to 3% cobalt or iron produces a supersaturated single phase condition which can be transformed into the two-phase equilibrium state by appropriate heat treatment. The present paper contains an account of an investigation into the variation with heat treatment of the magnetic properties of copper–cobalt and copper–iron containing small percentages of ferromagnetic component.

In the determination of the hysteresis loops of such materials with very low intensities of magnetization, induction methods are unduly difficult, chiefly due to inadequate sensitivity, and the utilization of 'traction' methods appears to offer the best prospect of success. Two different methods have been investigated: (i) the couple due to a transverse field acting upon the moment of a specimen and (ii) the force exerted on a magnetized specimen due to a field gradient. Though the main interest lies in the low field characteristics, a few high field results obtained on a paramagnetic balance are given.

§ 2. MEASUREMENT OF HYSTERESIS LOOPS

Preparation of the Alloys

The alloys were prepared by melting the constituents in alumina crucibles in a high frequency induction furnace *in vacuo* or in an atmosphere of argon at a pressure of 5 cm of mercury.

Heat Treatment

The ingots were forged at 900°C into bars approximately 1 cm × 1 cm × 7 cm. The specimens for magnetic measurements were discs 5 mm diameter and 0·5 mm thick. A scratch on the surface of each disc provided a reference mark. Heat treatment was carried out with the specimen sealed in a short length of pyrex tubing in a furnace maintained at a constant temperature to ±1°C. After heat treatment the surfaces of the specimens were dull but in no case did appreciable oxidation take place and comparison of results from control experiments on specimens annealed *in vacuo* indicated that errors from this source were negligible.

Determination of Hysteresis Loops

Constant and collaborators (1939, 1943) used a method which consists of measuring the couple exerted on a specimen by a small field applied perpendicular to the magnetizing field. Preliminary experiments showed that in our experiments this method was unsatisfactory, and some discussion of this method is presented in the Appendix. On the other hand, the technique described below was adopted and found to be satisfactory.

If a ferromagnetic specimen in a field H_x is subjected to a field gradient dH_x/dx, the force exerted on the specimen is

$$F_x = J_x v \frac{dH}{dx} x.$$

With representative values for volume and intensity, in a field gradient of 10 oe cm^{-1}, the force to be measured is of the order of 10^{-3} dynes. Such small forces of this magnitude are most easily measured by a torsion balance. A schematic arrangement of the apparatus is shown in fig. 1.

The disc specimens were held in a recessed hole at the end of a perspex arm 5 cm long and counterbalanced by a glass weight. Considerable care was taken to keep the moment of inertia of the balance as small as possible and by using a simple damping vane immersed in a light oil to ensure that the system was near critical damping.

The balance arm was suspended from the torsion head by a phosphor bronze wire 5 cm long, the torsion constant of which was determined by a separate experiment from the period of oscillation of a metal annulus of calculable moment of inertia attached to the suspension wire. To cover the range of intensities four gauges of phosphor bronze wire from

0·025 mm to 0·06 mm diameter were required. The balance was protected from draughts by enclosing the torsion system in a rectangular box which also limits the swing of the arm. The rotation of the balance and torsion head were determined by the use of small galvanometer mirrors attached to the balance arm and torsion head.

Fig. 1

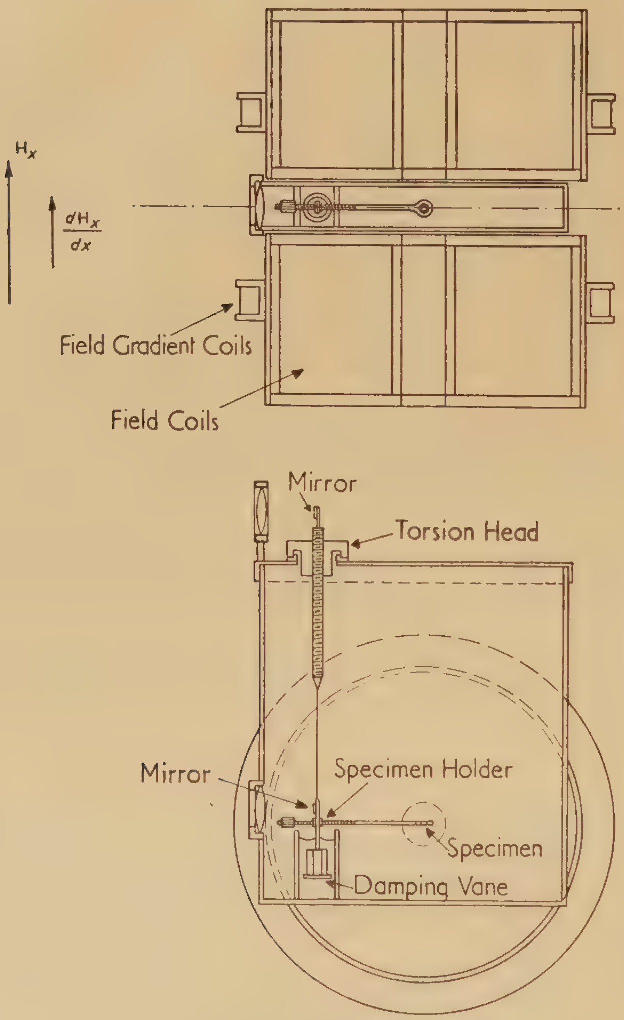

Arrangement of Apparatus.

The magnetizing field was furnished by two coils rigidly fixed to a base plate with the inner faces 1 in. apart. The field at the mid-point of the axis determined by a search coil and ballistic galvanometer was 101 oe/amp ; a maximum current of 8 amp could be passed for a few minutes. The gradient coils were mounted in the Gaugain–Helmholtz position co-axially on the magnetizing coils and symmetrically about the mid-plane of the magnetizing system. The coils connected in series opposition were usually excited by a current of 3 amp which by calculation produced a field gradient of 7·02 oe cm^{-1} at the position occupied by the specimen. Experiment proved that the hysteresis loops were independent of the magnitude of the field gradient used in the determination.

Experimental Procedure

The specimen was magnetized to saturation in a small electromagnet capable of producing about 5000 oe and then transferred to the torsion balance. The orientation of the disc was adjusted so that the direction of this magnetization and the applied field in the hysteresis loop apparatus were collinear. The magnetization curve was obtained by a step by step reduction of the field from a large positive value to suitable negative values, the field gradient being kept constant. At each value of the magnetic field, the torsion head was adjusted to return the specimen to the predetermined zero. By the switching on of a suitably small field gradient, the specimen was deflected and again brought back to the zero by rotation of the torsion head. From a knowledge of the rotation of the head the force exerted on the specimen and hence the intensity of magnetization could be calculated. No correction was necessary for the demagnetizing effects because of the very low intensities.

Experimental Results

In each binary system measurements of the variation of magnetic properties of a series of alloys 0·7% to 2·0% for copper–cobalt and 0·3% to 1·5% for copper–iron with time of heat treatment at 350°c, 400°c and 470°c in the former case and 500°c, 600°c and 800°c in the latter were carried out.

Fig. 2

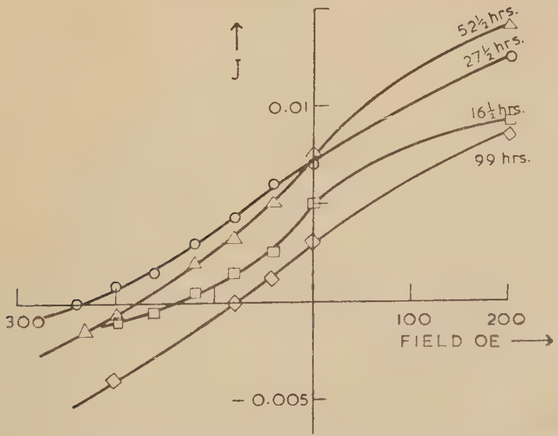

J–H Curves of 1% Co–Cu alloy. Heat treated at 350°c.

In the quenched state, the alloys exhibited paramagnetism almost independent of field and with a mass susceptibility of about 10^{-6}. On heat treatment development of curvature in the $J-H$ graph took place whilst the order of magnitude of the susceptibility indicated the presence of ferromagnetism.

Fig. 3

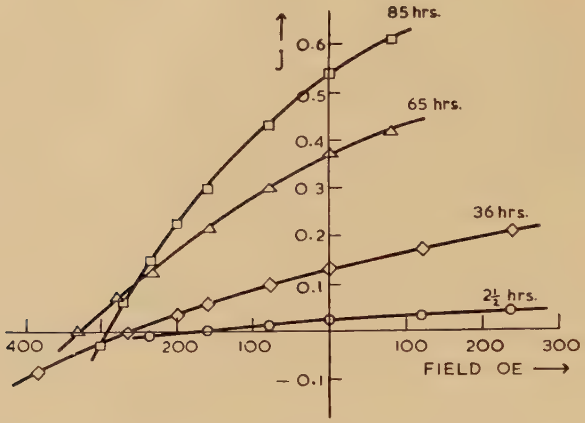

J–H Curves of 1% Fe–Cu alloy. Heat treated at 650°c.

Fig. 4

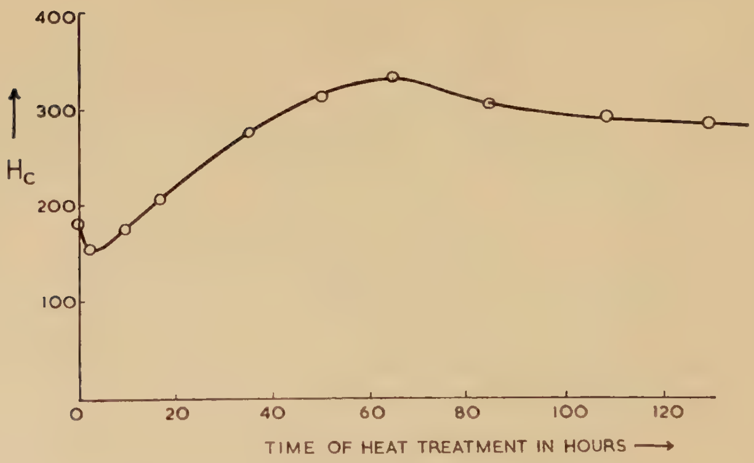

Coercivity *v*. Time at 650°c for 1·0% Fe–Cu alloy.

The changes in magnetization curves with time of heat treatment for typical alloys 1% Cu–Co heat treated at 350°c and 1% Cu–Fe annealed at 650°c are shown in figs. 2 and 3. In copper–cobalt alloys with continued heat treatment the coercivity increased, reached a maximum and then decreased. The iron alloys behaved similarly except that an initial decrease in coercivity was always observed (fig. 4).

Though the largest coercivities observed were 250 oe and 400 oe for Cu–Co and Cu–Fe respectively, it was found that fields of several thousand oersteds were required to develop maximum coercivity and remanence. Figure 5 gives the results on a typical specimen of copper–cobalt, a specimen with a coercivity of 74 oe, though the hysteresis loops show unusual features.

Fig. 5

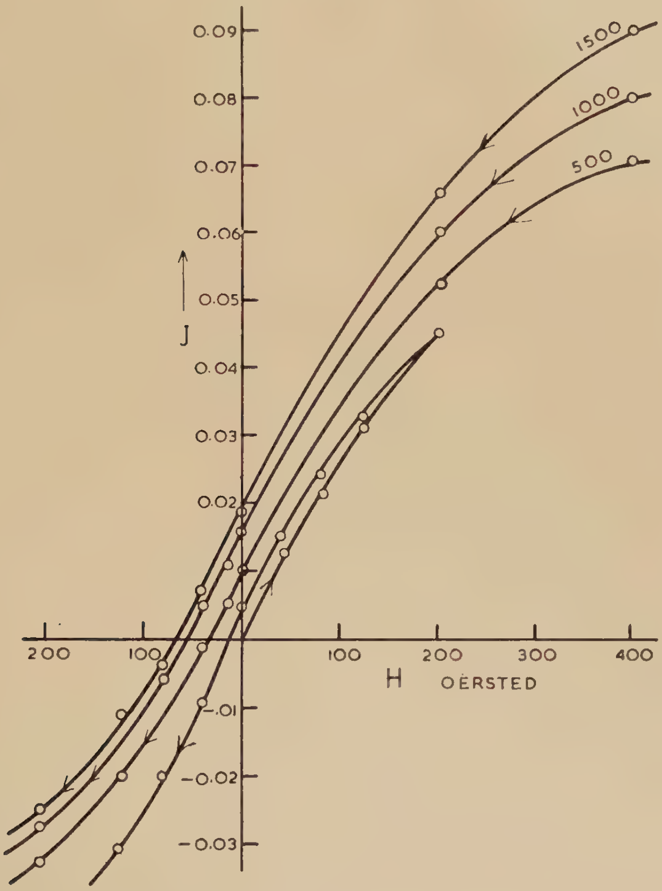

J–H Curves for $1\frac{1}{2}\%$ Co–Cu alloy heat treated for $31\frac{1}{2}$ hrs. at 350°c. Magnetization fields shown on curves.

Whilst in normal ferromagnetics the application of a maximum reverse field not much greater than the coercive field is adequate to delineate a hysteresis loop and to change the sign of the remanent magnetization, such a field applied to these alloys only produced a slight diminution of the magnitude of the remanence, and fields up to 1500 oe were required to reduce the remanence to a zero value, whilst to reverse the remanence in both magnitude and direction called for fields of about 5000 oe. Figure 6 gives data on a 1% copper–cobalt alloy, the coercivity of which under similar conditions to those shown in fig. 5 were of the order 150 oe.

The approach to saturation in high fields was relatively slow, and we are indebted to Dr. J. Crangle of this department for high field data. Above about 3000 oe it was found that the increase of magnetization with field was approximately linear up to about 15 000 oe.

Fig. 6

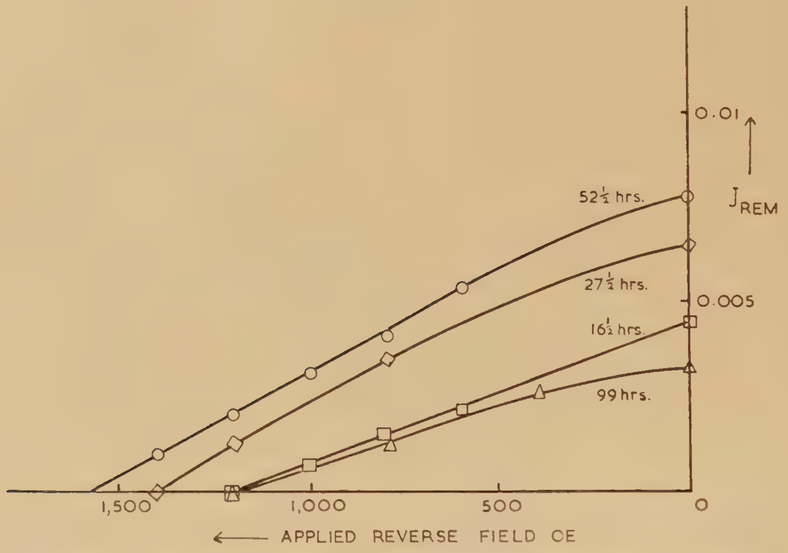

Permanent Magnetization of 1% Co–Cu alloy, heat treated at 350°c.

§ 3. Discussion

When compared with the behaviour usually associated with bulk ferromagnetic materials some of the characteristics of these alloys appear anomalous. One feature of all the magnetization curves is that the remanent intensity is a small fraction of the intensity in high fields. A second unusual characteristic is that, though in general a field about four or five times the coercive force should be adequate to saturate even a permanent magnet material, some of these alloys required fields in excess of twenty times of coercivity to exhibit maximum remanence and coercive force. In addition, in fields of several thousand oe, the magnetization of the alloys increases approximately linearly. This field independent incremental susceptibility was also characteristic of similar alloys investigated by Bitter and others (1939, 1941). In both cases it was found that this susceptibility increased with time of anneal.

It is possible to draw a generally satisfactory picture of the processes involved, though the details are more obscure. As the heat treatment commences upon the solid solution, the iron or cobalt atoms are so widely dispersed that the cooperative phenomenon of ferromagnetism is impossible. As the heat treatment progresses, atoms of the ferromagnetic element diffuse and aggregate to form regions of higher concentration. As these nuclei grow, the threshold of ferromagnetism is reached with the formation of single domains and the theories of Stoner and Wohlfarth and Néel may become applicable. During this stage we get the gradual transition of paramagnetism to ferromagnetism with marked increase of coercivity owing to the shape anisotropy of non-spherical single domains in the non-magnetic matrix of copper. It is to be expected that differences in behaviour will be observed according to the crystal structure relationships of the two phases. Work on other suitable binary alloys of all three ferromagnetics are in progress to try and elucidate further this aspect of the problem. The case of cobalt binary alloys is particularly complicated since this element has two crystalline structures, face-centred-cubic and close packed hexagonal, both of which are ferromagnetic and can exist at temperatures up to about 400°c.

As heat treatment continues the volume of a ferromagnetic region increases until it is energetically more favourable for the region to divide into two or more domains. Changes of magnetization of such a multidomain region proceeds by the movement of domain walls such that the component of magnetization in the direction of the field increases. This process gives rise to low coercivities and in small, approximately spherical particles the changes may be almost completely reversible.

It is obvious that nuclei will develop at different rates owing to local variations in concentration so that the processes described above will be simultaneous and composite magnetization curves will result from the various stages of aggregation, ranging from paramagnetism through a wide range of ‘ hard ’ and ‘ soft ’ hysteresis curves. From the composite magnetization curves it is not possible to separate the hard and soft components but the presence of a ‘ hard ’ magnetic component is indicated by the large fields required to produce maximum remanence and coercivity and the high reverse fields necessary to reduce to zero or change the direction of the remanent magnetization. The low ratio of remanent to saturation magnetization can be safely regarded as a consequence of the range of properties of the aggregates. Only a relatively small percentage of these make substantial contributions to the area under the hysteresis loop.

Thus heat treatment of the supersaturated alloys causes the atoms of the ferromagnetic material to aggregate, eventually reaching the critical size of ferromagnetism and being sufficiently small, form single domains which will exhibit a large coercivity if the regions depart from spherical shape. With further heat treatment the particles continue to grow and become multidomain. On this basis the variation of coercivity with heat treatment is readily explained ; as the proportion of regions behaving as single domains increases the coercivity rises, reaches a maximum and falls as the fraction of multidomains increases.

The workers wish to place on record their thanks to the British and Allied Industries Electrical Research Association, whose financial support enabled this work to be carried out.

APPENDIX

From the definition of intensity of magnetization, the couple M exerted on a ferromagnetic specimen of volume v in a field H at an angle θ to the direction of magnetization is given by

$$M = HvJ \sin \theta.$$

If a specimen is placed with the direction of magnetization, J_x, collinear with the magnetizing field, H_x, the resulting couple is zero. The application of a small transverse field, H_y, exerts a couple which when the specimen is returned to the zero is $J_x v H_y$.

Fig. 7

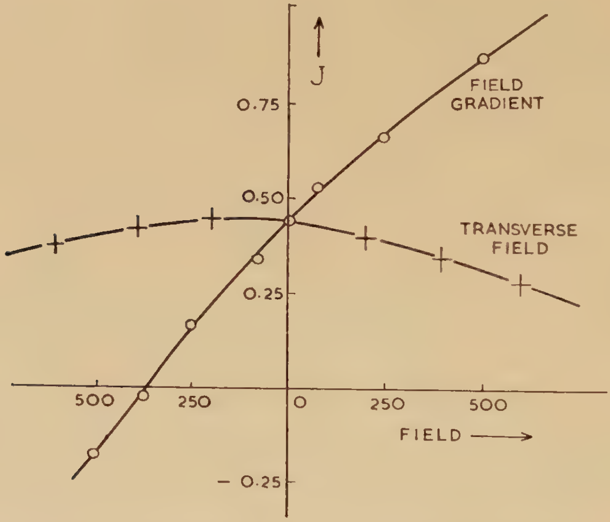

J–H Curves by the two Methods. 1% Fe–Cu—Heat treated for 70 hours at 650°c.

A technique for determining hysteresis loops based on this system has the merit of simplicity and experiments were carried out to determine its validity. On obtaining such curves as shown in fig. 7, in which the apparent intensity decreased with increasing field, it was obvious that there was a fundamental flaw in the method. Moreover the measured intensities were not independent of the magnitude of the transverse field.

The transverse field method tacitly assumes that the magnetization vector remains fixed relative to the specimen. However, Sucksmith, Potter and Broadway (1928) in a criticism of a similar technique for the determination of the parallel component of magnetization of a single crystal of nickel pointed out that the effective field on the specimen is the resultant of the applied fields and the demagnetizing fields. For an inhomogeneous alloy in which the ferromagnetic regions are isolated, a complete interpretation of the results requires the consideration of the demagnetizing field of each individual region. In the dispersed systems of aggregates whose shape and distribution is random the above method would appear to be inapplicable and was therefore abandoned, and all measurements carried out by the method described earlier in which the translational force between field and moment are collinear. Figure 7 shows curves obtained by both methods on the same specimen.

REFERENCES

Bitter, J., and Kaufmann, A. R., 1939, *Phys. Rev.*, **56,** 1044.
Bitter, J., Kaufmann, A. R., Starr, C., and Pann, S. T., 1941, *Phys. Rev.*, **60,** 134.
Constant, F. W., Faires, R. E., and Lenander, H. E., 1943, *Phys. Rev.*, **63,** 441.
Constant, F. W., and Formwalt, J. M., 1939, *Phys. Rev.*, **56,** 373.
Edwards, O. S., and Lipson, H., 1943, *J. Inst. Metals*, **69,** 177.
Frenkel, J., and Dorfman, J., 1930, *Nature, Lond.*, **126,** 274.
Kittel, C., 1949, *Rev. Mod. Phys.*, **21,** 541.
Néel, L., 1947 a, *C.R. Acad. Sci., Paris*, **224,** 1488 ; 1947 b, *Ibid.*, **224,** 1550.
Smith, C. S., 1940, *Phys. Rev.*, **57,** 337.
Stoner, E. C., and Wohlfarth, E. D., 1948, *Phil. Trans.* A, **240,** 599.
Sucksmith, W., 1952, *B.E.A.I.R.A. Report* Ref. N/T 61.
Sucksmith, W., Potter, H. H., and Broadway, L., 1928, *Proc. Roy. Soc.* A, **117,** 471.
Troiano, A. R., and Tokisch, J. L., 1948, *A.I.M. and Met. E. Tech. Publ.* No. 2348.
Weil, L., 1951, *J. de Phys.*, **12,** 437.

LXXI. *The Multiple Scattering of Positrons and Electrons by Nitrogen and Argon*

By N. Cusack and P. Stott
Birkbeck College, London*

[Received February 16, 1955]

Summary

A combination of lens spectrometer and cloud chamber was used to measure and compare the multiple scattering of positrons and electrons at energies in the neighbourhood of 0·4 Mev. The ratio of observed to theoretical mean absolute scattering angle was 0·99 for N_2 and 0·92 for A, with a standard error of 3%. Comparable results by other workers are discussed. In contrast with the conclusions of other workers, no significant difference in the behaviour of positrons and electrons could be detected.

§ 1. Introduction

The multiple scattering of charged particles has been the subject of much theoretical and practical study. A method of calculating the multiple scattering distribution function has been described by Bethe (1953) in a paper which contains also a discussion of the relation between the various derivations and formulae. Most multiple scattering investigations are now based on the cross section for single scattering by a Thomas–Fermi field first given by Moliere (1947). Simple formulae for mean value quantities of practical utility have been given by Scott (1952) and Scott's formulae reproduce the numerical values given by Moliere's multiple scattering theory (1948) with an error of 1%.

The experiments fall into three main classes : (i) scattering of collimated electron beams by foils with a counter or ionization chamber as detector ; (ii) application of Fowler's or a similar method to individual tracks in nuclear emulsions ; (iii) measurement of the scattering produced by the gas filling of cloud chambers (Groetzinger *et al.* 1950). Some of these experiments are reviewed by Corson and Hanson (1953) and on the whole there is agreement with the theory to within a few per cent. There are however several experimental results not fully explained, e.g. (i) the accurate experiment by Hanson *et al.* (1951) on 15·7 Mev electrons shows scattering larger than that predicted at the larger angles (Spencer and Blanchard 1954) ; (ii) an unexpectedly large difference between the scattering of electrons and positrons of about 1 Mev has been reported by Groetzinger *et al.* (1952) and discussed by Mohr (1954) ; (iii) electrons of 0·59 Mev in nuclear emulsion show abnormally low scattering according to Hisdal (1952) .

---

* Communicated by the Authors.

The mean multiple scattering angle is inversely proportional to the product, *pv*, of the momentum and velocity of the scattered particles. The discrepancies just mentioned, having occurred with light particles of comparatively low energy involve low values of *pv*. The present paper describes an experiment with both positrons and electrons of the same low energy. An improvement in accuracy on previous cloud chamber work has been made by (i) avoiding the difficulties of magnetic curvature measurement by selecting and measuring the particle energy before entry into the chamber ; (ii) investigating in a subsidiary experiment the effect of track distortion due to turbulence ; (iii) decreasing the statistical errors, and (iv) taking special precautions in respect of comparative measurements on electrons and positrons.

§ 2. APPARATUS

The scattering medium was the gas of a conventional horizontal expansion chamber, 20 cm in diameter, operated at atmospheric pressure.

The particle beam was provided by an iron-free solenoidal lens spectrometer in which the emitting object was a disc, 3 mm in diameter, of Cu^{64} which radiates both electrons and positrons. At the image position was an aperture through which the focussed beam passed to the cloud chamber along a brass tube, 16 cm long, containing collimating slits and anti-scattering baffles. The spectrometer vacuum was separated from the cloud chamber by a 1·5 mg/cm^2 distrene foil window supported on a brass grid flush with the chamber wall. The beam entered in the plane of the illuminated region of the chamber and was photographed with normal technique.

The Cu^{64} source was mounted 6 mm from the lens axis and, on account of the opposite rotation of 90° given to the positron and electron beams by the lens field, it produced separate positron and electron images 12 mm apart. By rotating the source about the lens axis with the help of a Wilson seal either of the images could be brought over the exit hole and either of the beams sent into the chamber without altering any other part of the apparatus. This enabled alternate batches of ten pictures to be taken with electrons and positrons under identical conditions.

The resolving power of the spectrometer, determined from the shape of the Thorium F-line, was such that the beams entering the chamber from the Cu^{64} had a roughly triangular $H\rho$-spectrum with $\Delta H\rho/H\rho=4\%$, where $\Delta H\rho$ is the width at half-height. The value of $H\rho$ was measured by reference to the F-line using for the latter the value 1388 gauss-cm given by Craig (1952). The momentum of the beams was kept constant through the experiment to about 1 in 10 000.

To make sure that all the tracks measured actually came from the source, every tenth photograph was taken with the source covered with a shutter. 100 such pictures showed no tracks that would have been included in the measurements. Further details of the apparatus are given elsewhere (Stott, 1955).

It was necessary to show to what extent the distortion of the tracks would influence the measurement of multiple scattering. On the basis of distortion measurements, made by a new method, of which the description and results are given elsewhere (Cusack and Stott 1955), it was concluded that distortion had a negligible effect on the measured mean scattering angle. Additional evidence for the absence of systematic chamber produced distortions is the fact that equal numbers of particles were scattered to the left and right and the algebraic means of the positron and electron scattering angles were very close to zero.

Fig. 1

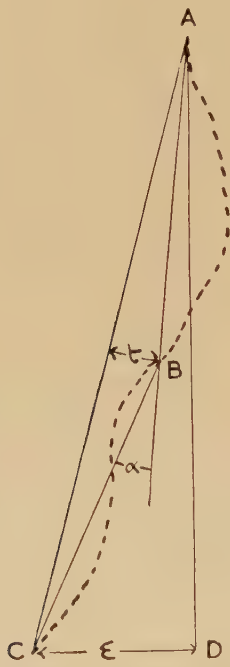

Definition of the measurable quantities t, α, and ϵ. The radius of the circle through ABC could also be measured.

§ 3. TRACK SELECTION AND MEASUREMENT

Figure 1 indicates the definition of several measurable quantities. After trials it was decided that the most accurate procedure was to measure t on the film, using a microscope with a calibrated eyepiece scale consisting of a line representing AC and graduations perpendicular to it at the mid-point. The magnification was chosen so that AC was equivalent to a $10{\cdot}0 \pm 0{\cdot}01$ cm chord in the chamber. The values of t were converted to α's for comparison with theory.

Every track containing a 10 cm chord was measured unless (i) it gave rise to a secondary electron of range $\geqslant 3$ mm or (ii) it did not come from the beam entry window. As only one chord per track was used, all the scattering angles were independent and, as no movement of the microscope was involved, there was no 'stage noise'. Many tracks were, of course, longer than 10 cm and the rule was adopted that the chord should begin at the nearest clearly identifiable droplet to the entry window. Among the positron tracks in argon there occurred five with very large values of α between 50° and 70° resulting from single scattering events with projected angles between 50° and 90°. Five such large single scatters is about the number to be expected in 4200 cm of track in argon, according to the projected Massey formula for positron scattering, and they may therefore be regarded as part of the single scattering tail of the distribution. On the other hand, one at least suggested by its appearance that it was a rather low energy track, perhaps a Compton electron. These five tracks are excluded from fig. 2 (*b*) and the tables. If they were included, $\overline{|\alpha|}$, for positrons only, would be 10·6, and, for all tracks, 10·4. The figure 0·92 for argon in table 2 would become 0·945. This would not affect the conclusions to be drawn either for the absolute or the comparative measurements.

§ 4. CALCULATION OF EXPECTED SCATTERING

The momentum at the mid-point of the tracks was derived from the $H\rho$ focussed by the lens less a 3% correction for loss in the distrene window and chamber gas. The error in the corrected value should not exceed 0·5%. The momentum thus found is the peak momentum of the triangular spectrum referred to above. ΣNZ^2 was computed from the observed temperature and pressure allowing for the water and alcohol condensant which contributed about 5% to the sum for nitrogen and 2% for argon.

Using the formulae and notation of Scott (1952), the value of $\overline{|\alpha|}$ was calculated from the equation

$$(\overline{|\alpha|})^2 = \chi_\gamma{}^2 \Omega\ (0{\cdot}299 + 0{\cdot}269 \log_{10} \Omega).$$

To allow for electron–electron scattering it is usual to increase Z^2 by a factor $(1+1/Z)$. U. Fano (1954) has recently given a more exact treatment of this correction and in the present case his formulae increase the value of $\overline{|\alpha|}$ by an additional 2% for N_2 and 0·6% for A.

The mean scattering angle also requires correction for the 'flat-chamber effect' (Moliere 1948). The literature does not contain projected multiple scattering distributions for scattering media of finite depth, but it is clear that the effect of excluding tracks that reach large distances perpendicular to the observation plane will be to sharpen the distribution by reducing the large angle tail. Moliere gives the mean scattering angle for the limiting case of an infinitesimally thin chamber. The conditions of the present experiment were chosen to approximate to the latter condition as closely as practicable. A comparatively thin illuminated layer of 1 cm was used and long tracks, i.e. >10 cm, were selected. An elementary calculation shows that only some 5% of the incident particles survive to the end of the observation length without being scattered out of the light beam. It is believed therefore that Moliere's 'flat chamber' scattering angle is the appropriate one for comparison, though it may slightly underestimate the scattering, since the extreme case is obviously not completely realized. Equations 10.4 and 10.4′ of Moliere (1948) give

$$\overline{|\alpha|}\text{ (flat chamber)}=0{\cdot}87\ \overline{|\alpha|}\text{ (infinite chamber)}.$$

All the relevant numerical quantities are given in table 1.

Table 1

	Nitrogen	Argon
$H\rho$ (gauss-cm)	1929	2496
Number of positrons	336	418
Number of electrons	335	220
$\overline{\|\alpha\|}$ (pos.)	8·3	10·1
$\overline{\|\alpha\|}$ (elec.)	9·0	10·0
Total number of tracks	671	638
$\overline{\|\alpha\|}$ (all tracks)	8·6	10·1
ΣNZ^2	$2{\cdot}56\times10^{21}$	$7{\cdot}82\times10^{21}$
Ω	155	198
χ_ν	0·85	0·93
$\overline{\|\alpha\|}$ (theor., flat ch.)	8·9	11·0

The angles are in degrees ; Ω is the number of scatters in 10 cm of track ; Ω and χ_ν are computed from eqns. (2) and (3) of Scott (1952).

§ 5. Results and Comparison with Theory

The theories based on Moliere's single scattering law do not differentiate between positrons and electrons because they neglect the spin–orbit effect, and the calculated value should therefore be compared with the results for positrons and electrons taken together. Fig. 2 shows the distribution of observed scattering angles and a gaussian curve of the same area and standard deviation as the sample. The gaussian fits satisfactorily for both nitrogen and argon and the deviations from it are such that the fit would be improved if higher terms of the Moliere distribution were used ; however, experiments of this sort are not capable of demonstrating the finer points of the distribution shape. A better test is the value of $\overline{|\alpha|}$ (see table 1). The main error in $\overline{|\alpha|}$ (obs.) is the statistical one of 3%. Microscope setting errors are present in each reading but exert a negligible effect on the mean value, and 671 tracks in nitrogen, when measured independently by two observers, gave mean values agreeing to better than

$0{\cdot}5\%$. The main error in $\overline{|\alpha|}$ (theor.) is probably due to the small departure from the infinitesimal chamber mentioned above. In addition the value of the screening angle may have some slight inaccuracy because the field of the nitrogen molecule will not be represented exactly by the Thomas–Fermi field. The error arising from temperature and pressure measurements is unlikely to exceed $0{\cdot}5\%$.

Fig. 2

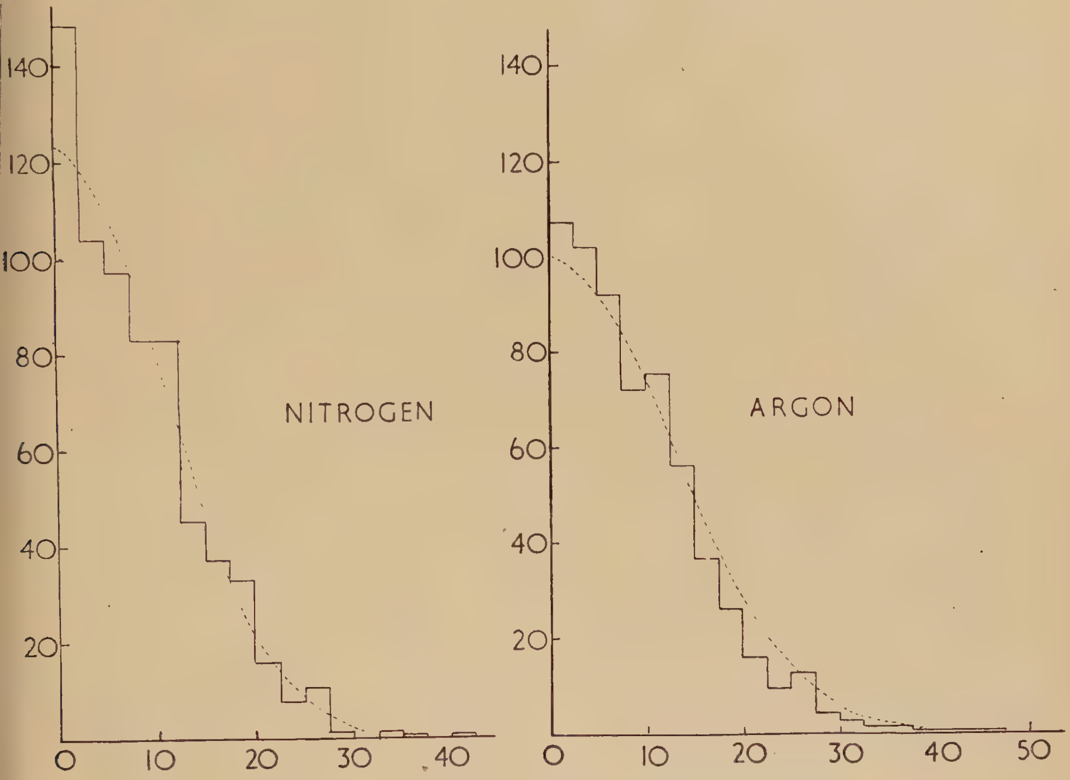

The measured distribution of $|\alpha|$. $|\alpha|$ is in degrees.

For nitrogen, therefore, the agreement with Moliere's and the equivalent theories, supplemented by Fano, is good. Taken by itself the argon result could also be called satisfactory agreement but table 2 shows that it goes some way towards confirming Hisdal's result and suggests that the deficiency in scattering may be a real effect increasing with Z. As Hisdal has pointed out, most though not all experimental values of electron scattering are lower than the theoretical value. The most likely place to introduce small corrections into the theory is in the value of the screening angle. A recent paper by Lenz (1954) gives support to this and shows that the single scattering cross section for small scattering angles is considerably overestimated by the use of the Thomas–Fermi field because the latter does not give a good representation of the falling off of the outer parts of the field. By choosing a more suitable representation, Lenz gave another cross section which accorded much better with the otherwise unexplained results of Bibermann *et al.* (1949). However, these results refer to very small angles ($\sim 10^{-2}$ to 10^{-3} radians) and the energies are only 50 to 100 kev. It seems therefore that such deficiencies of scattering, of the order of a few per cent, that cannot certainly be ascribed to experimental errors, can be qualitatively explained by the imperfection of the Thomas–Fermi field. Discrepancies in the scattering of electrons by beryllium have been attributed to this cause by Hanson *et al.* (*loc. cit.*).

Table 2

	Nitrogen	Argon	G5 emulsion*
Energy (MEV)	0·26	0·40	0·59
$\overline{\lvert\alpha\rvert}$ (obs.)/$\overline{\lvert\alpha\rvert}$ (theor.)	0·97	0·92	0·62
Standard error	3%	3%	10%

* Hisdal (1952).

To compare positron and electron scattering, certain additional precautions were taken to ensure that no conditions were changed other than the sign of the particles. This gave a reasonable chance of detecting the difference if it existed to the extent of 10% as reported by Groetzinger *et al.* These precautions were : (i) positron and electron pictures were taken in alternate batches of 10, taking advantage of the Cu^{64} source which emits both. The lens field was kept constant and any long period changes in the cloud chamber operation would affect both particles equally; (ii) the energy was such that the energy losses suffered in the window and chamber gas were the same for both beams according to Rohrlich and Carlson (1954) ; (iii) measurements were made by observers who did not know the sign of the particles. Scattering was slightly greater for positrons than for electrons in argon and, in nitrogen, $\overline{|\alpha|}$ was 8% less for positrons than electrons. The significance of the latter difference may conveniently be estimated by applying the variance ratio test (F-test) which compares the widths of the α distributions. It shows that the probability of obtaining the observed positron and electron samples from the same distribution is greater than 12%. These results are at variance with the conclusions of Groetzinger *et al.*, but the opportunities for statistical and systematic errors seem less in the present experiment and the best conclusion seems to be that the results are quite consistent with Mohr's theory which states that at low Z the spin–orbit effect makes the positron r.m.s. scattering angle only 1% less than the electron one. To verify this accurately would require a considerable development of technique.

ACKNOWLEDGMENTS

The authors wish to thank Prof. J. D. Bernal for facilities in his department; the Central Research Fund of the University of London for financial assistance; Mr. F. Roberts and Mr. V. Hallewell for making apparatus; and Dr. D. K. Butt for invaluable advice on the electron optical part of the work.

REFERENCES

BETHE, H. A., 1953, *Phys. Rev.*, **89,** 1256.
BIBERMAN, *et al.*, 1949, *Doklady Akad. Nauk. U.S.S.R.*, **69,** 519.
CORSON, D., and HANSON, A., 1953, *Annual Review of Nuclear Science.*
CRAIG, H., 1952, *Phys. Rev.*, **85,** 688.
CUSACK, N., and STOTT, P., 1955, *J. Sci. Instrum.*, **32,** 34.
FANO, U., 1954, *Phys. Rev.*, **93,** 117.
GROETZINGER *et al.*, 1950, *Phys. Rev.*, **77,** 584; 1952, *Ibid.*, **85,** 78.
HANSON *et al.*, 1951, *Phys. Rev.*, **84,** 634.
HISDAL, E., 1952, *Phil. Mag.*, **43,** 790.
LENZ, F., 1954, *Z. Naturforsch.*, **9*a*,** 185.
MOLIERE, G., 1947, *Z. Naturforsch.*, **2*a*,** 113; 1948, *Ibid.*, **3*a*,** 78.
ROHRLICH, F., and CARSON, B., 1954, *Phys. Rev.*, **93,** 38.
SCOTT, W. T., 1952, *Phys. Rev.*, **85,** 245.
SPENCER, and BLANCHARD, C., 1954, *Phys. Rev.*, **93,** 114.
STOTT, P., 1955, *M.Sc. Thesis*, University of London, 1955.

LXXII. *The Production of Neutrons and Protons by the Bombardment of Boron by Low Energy Alpha-Particles*

By E. S. Shire and R. D. Edge*
Cavendish Laboratory, Cambridge†

[Received January 20, 1955]

Summary

The numbers of neutrons and protons produced in the reactions $^{10}B(\alpha n)^{13}N$ and $^{10}B(\alpha p)^{13}C$ at 1·51 Mev bombarding energy have been compared and the ratio of the reduced widths, γ_n^2/γ_p^2, found to be $5{\cdot}7 \pm 0{\cdot}5$. Between 1·4 and 2·4 Mev bombarding energy, the emission of protons is closely similar to that of neutrons, but γ_n^2/γ_p^2 has fallen to a value nearer unity at a resonance at 2·16 Mev.

The resonance previously reported when ^{11}B is bombarded by alpha-particles of 1·58 Mev energy has been shown to be a doublet and a further resonance for neutron emission, but not proton emission, has been found at 2·05 Mev.

§ 1. Introduction

From experiments described in a recent paper (Shire, Wormald, Lindsay-Jones, Lunden and Stanley 1953) we found that the reduced width, γ_n^2, from the reaction $^{10}B(\alpha n)^{13}N$ at an alpha-particle energy of 1·51 Mev was about 15 times larger than the corresponding reduced width, γ_p^2, for the production of protons from the mirror reaction $^{10}B(\alpha p_0)^{13}C$. In the same experiments we showed that the yield of neutrons varied with alpha-particle bombarding energy in a way closely similar to that of protons giving the ground state of ^{13}C, except that a resonance for neutron production at 2·05 Mev bombarding energy was absent in the proton yield curve.

We describe in the present paper a more careful determination of the ratio of the reduced widths γ_n^2 and γ_p^2 and an examination of the neutron and proton yields to higher bombarding energies than were possible at the time the previous paper was written. We have also obtained the $^{11}B(\alpha n)^{14}N$ and $^{11}B(\alpha p)^{14}C$ yield curves between 1·4 and 2·4 Mev bombarding energy.

References to earlier work on the bombardment of boron by alpha-particles are given in our previous paper and in Ajzenberg and Lauritsen (1955).

---

* Communicated by the Authors.

† Now at Australian National University, Canberra, A.C.T., Australia.

§ 2. Comparison of Proton and Neutron Yields at 1·51 Mev Alpha-Particle Energy

2.1. *Experimental Method and Apparatus*

We used a beam of a few microamps of singly charged helium ions from our electrostatic generator and the separated isotope ^{10}B on thick aluminium backings. Since ^{11}B was found to be a copious emitter of neutrons near 1·5 and 2·0 Mev we carefully examined the ^{10}B targets for ^{11}B contamination and measured the amount of this isotope present.

In our previous experiments the yield of protons was determined by one experiment and the yield of neutrons by another separate one. Substantial errors were possible in the measurement of the bombarding current, due to electron emission from the target and its surroundings, and to differences in the two targets. Even when the same target was used for both experiments there was no certainty that the target was uniform and unchanged or that exactly the same portions of a non-uniform target were employed in the two experiments. We have avoided these sources of error in the present experiments by measuring the protons and neutrons simultaneously. The apparatus we used is shown diagrammatically in fig. 1. We supported the target T at the end of a long thin-walled brass tube A and, to avoid carbon deposits, heated it to a suitable temperature by the heater H before the beginning of an experiment. Alpha-particles entered through a defining aperture B and protons from the target were counted by the gridded ionization chamber C. This we filled with argon at about one atmosphere pressure, at which pressure the ground state protons gave output pulses at least ten times the amplifier noise. Low energy protons arising from reactions leaving ^{13}C in an excited state or from the ^{11}B(αp)^{14}C reaction were excluded by the thin copper foil window W, which we soldered to the ionization chamber. Bevelled apertures E were placed at 5 cm intervals between the target and the ionization chamber to prevent protons from being scattered into the ionization chamber from the tube A.

Fig. 1

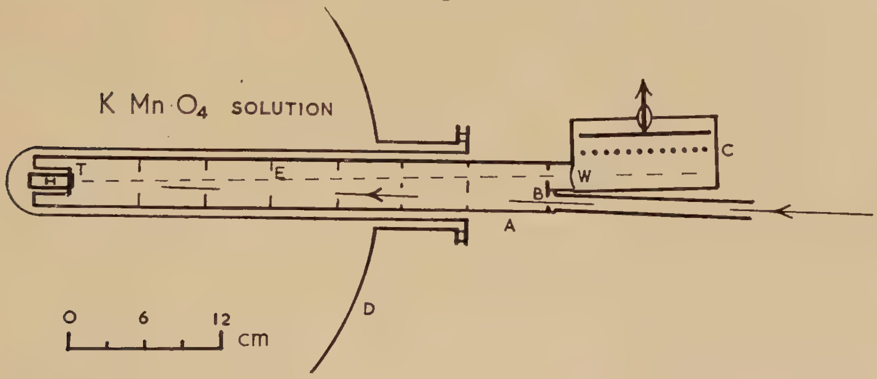

Apparatus for comparing neutron and proton yields. For details see text.

We measured the neutrons by means of the Szilard–Chalmers reaction (Szilard and Chalmers 1934) produced in potassium permanganate solution contained in the spherical glass vessel, D (an acid carboy), surrounding the target. We used 48·7 litres of a solution of 40 grams of potassium permanganate per litre. This volume was large enough to make the correction for loss of neutrons from the surface reasonably small without making the apparatus, when full of solution, too difficult to handle. After a bombardment of the target, which took from 10 to 30 minutes, we recovered the radioactive $^{56}MnO_2$ produced by filtering the irradiated solution, and suitable washings of the vessel, through Whatman 54 filter paper, that had previously been impregnated with inactive MnO_2. We then carefully dried the filter paper, encased it in cellophane, wrapped it round a thin-walled Geiger counter and measured the number of counts under standard conditions at a known time after the irradiation. We calibrated this detecting system by means of a standard $RaBeF_4$ source. (See § 2.2 (ii).)

Corrections were made to the raw data to allow for the escape of neutrons from the potassium permanganate solution, for the dead time and secular variation of sensitivity of the Geiger counter, and for decay of the ^{56}Mn during and after bombardment. We discuss these corrections and the accuracy of our measurements in the next section.

2.2. *Errors and Corrections*

(i) *Proton measurements*

The solid angle over which protons entered the ionization chamber was defined to better than $\frac{1}{2}\%$ by one of two alternative apertures (0·998 cm and 0·674 cm diameter) placed just in front of the window W (fig. 1), and the mean angle between incident alpha-particle beam and counted protons was known to better than one degree. The total number of protons counted was more than 10 000, so that the statistical error was less than 1%. We assumed that the angular distribution of the p_0 protons was exactly $N_\theta = N_{90}(1-0{\cdot}9\cos\theta)$ in centre-of-mass space, a distribution in close agreement with the experimental results given in our earlier paper and with a more recent measurement made with somewhat improved apparatus. With this assumption the only significant error arises from the measurement of the number of protons actually entering the ionization chamber.

Figure 2 shows a typical pulse-height distribution obtained with a Hutchinson–Scarrott pulse-height analyser (Hutchinson and Scarrott 1951). The ' tail ' on the small-pulse side of the peak raises the question as to how much of it, if any, should be included in the proton count. These small pulses (about 10% of the total in number) were not mainly due to protons scattered into the ionization chamber from defining apertures or other material outside it, for such scattered particles would have had less energy than unscattered protons and so would in many cases have produced more ionization and larger pulses than unscattered protons. The energy of the unscattered protons was 4·1 MeV with a range in air or argon of about 24 cm. The copper windows (two alternative thicknesses were used) were equivalent to about 4 and 6 cm of air, so that unscattered protons after passing through the window had a residual range of 18 to 20 cm, of which only about 10 cm was lost in passing through the chamber. Thus all scattered protons with energies between about 2 MeV and 4·1 MeV would have given larger pulses than the unscattered protons, and the number of such pulses was well below 1% of the number in the main peak. An experiment, in which we used a circular stop to prevent protons reaching the ionization chamber direct from the target, but which allowed protons scattered from the baffles E (fig. 1) to be counted, showed that the number of protons scattered into the ionization was less than 1%.

Fig. 2

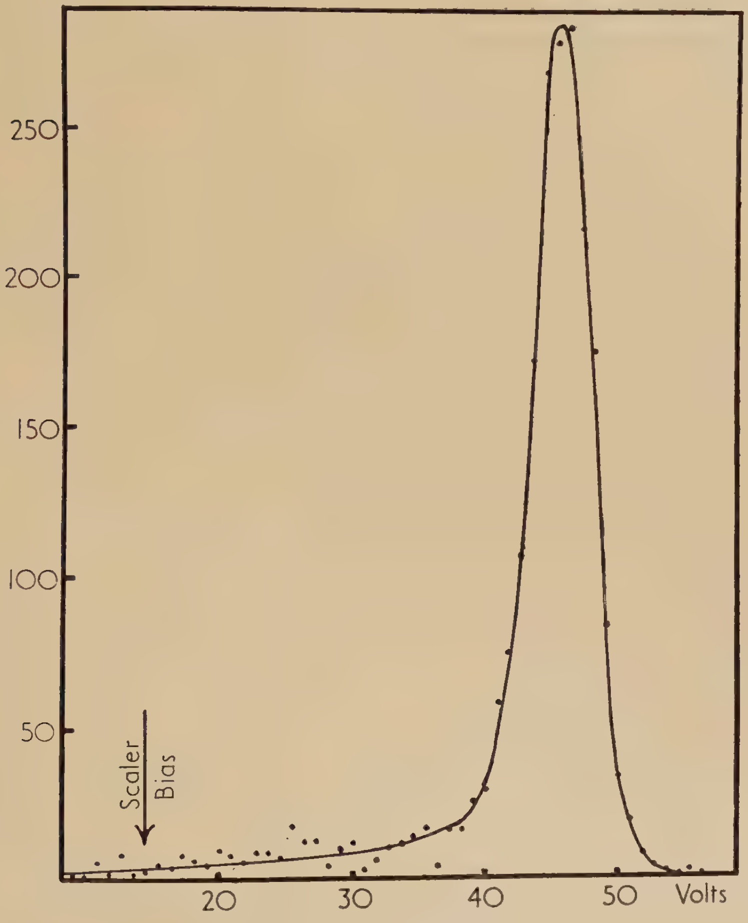

Proton pulse-height distribution.

We can account for the tail by assuming that it was due to protons scattered by the copper window which had hit the walls of the ionization chamber without traversing the full 10 cm path necessary to give a pulse of normal size. A rough calculation showed that this explanation gave the right number of small pulses within a factor of two or three. We have therefore taken the numbers indicated by our counting equipment as the true number of protons and made no correction for the tail. We have not, however, included the portion of the tail consisting of pulses smaller than the setting of our scaler discriminator. The correction would be only 1 or 2% at most and its omission will tend to compensate for the small number of protons which may in fact be scattered into the ionization chamber by the apertures E.

(ii) *Neutrons*

The corrections applied for the dead time of the Geiger counter and for the decay of the radioactive manganese during and after irradiation were straightforward and need not be discussed in detail. We checked the sensitivity of the Geiger counter before and after each run by means of a standard γ-ray source. Errors arising from these corrections appear with other random errors in the neutron–proton plot in fig. 4. In an experiment carried out with a blank aluminium target we found no neutrons, so that no errors arose due to neutrons from the target backing or from the apparatus. A comparison of our neutron yield curve with that of Jones and Wilkinson (1953) for the $^{13}C(\alpha n)^{16}O$ reaction showed that our results are not significantly affected by carbon contamination.

The three possible sources of substantial systematic error arise from the estimation of the correction to be applied to neutrons escaping from the permanganate solution, from the uncertainty in the value of the standard $RaBeF_4$ neutron source, and from the presence of ^{11}B in the ^{10}B target.

In fig. 3 we plot the fraction of neutrons captured against mean neutron energy, calculated by using Wallace's elementary diffusion theory (Wallace 1949) and Marshak's values for the slowing down length (Marshak 1947). This theory, which is only approximate, predicts too great a loss of neutrons. We have, therefore, compared experimentally the loss of neutrons from a $RaBeF_4$ source and from a ^{24}Na–D source to obtain a value of $0{\cdot}78 \pm 0{\cdot}05$ (A, fig. 3) for the fraction of neutrons of 4·5 MeV mean energy captured in our experimental vessel. The fractions of neutrons captured from the $^{10}B(\alpha n)^{13}N$ and the $^{11}B(\alpha n)^{14}N$ reactions must then be close to the values shown at B and C, fig. 3. We adopt values of $0{\cdot}89 \pm 0{\cdot}05$ and $0{\cdot}96 \pm 0{\cdot}04$ where the errors allow for both the estimated error of the determination of point A and the errors of interpolation.

The preparation and calibration of our standard $RaBeF_4$ source has been described by Bretscher, Cook, Martin and Wilkinson (1949). It has recently been recalibrated in terms of the ^{24}Na γ-ray photo-disintegration cross section of deuterium and found to give $7{\cdot}75\times10^4\pm4\%$ neutrons per second.*

The yield of neutrons from the $^{11}B(\alpha n)^{14}N$ reaction is substantial at 1·51 Mev alpha-particle energy (see fig. 5(*d*)). We measured the amount of ^{11}B present in our ^{10}B target by three methods: (*a*) the $^{11}B(p\alpha)^{8}Be$ reaction at 0·7 Mev bombarding energy, (*b*) the $^{11}B(\alpha p)^{14}C$ reaction at 1·58 Mev, and (*c*) the $^{11}B(\alpha n)^{14}N$ reaction at 2·05 Mev. We used a magnet to analyse the alpha-particles emitted in (*a*) and to separate the protons from ^{11}B from those of ^{10}B in (*b*). Method (*c*) assumes that the peak observed in the ^{10}B target at a bombarding energy of 2·05 Mev is in fact due entirely to the presence of ^{11}B. Our reasons for this assumption are given in § 3.2 (i). The three methods gave values of $0{\cdot}07\pm0{\cdot}02$, $0{\cdot}06\pm0{\cdot}02$ and $0{\cdot}08\pm0{\cdot}02$ for the number of ^{11}B atoms in the ^{10}B target relative to the number of ^{11}B atoms in the ^{11}B target. We have used the mean value $0{\cdot}07\pm0{\cdot}01$ for this ratio. We measured the ratio of the number of neutrons from the same ^{10}B and ^{11}B targets at 1·51 Mev bombarding energy and also the angular distributions of the neutrons (see § 3). From these results we calculated that the number of $^{11}B(\alpha n)^{14}N$ neutrons of 1·23 Mev energy entering our permanganate solution was $3{\cdot}6\pm1{\cdot}2\%$ of the number of $^{10}B(\alpha n)^{13}N$ neutrons. If we ignore, as we reasonably may for a correction term, the difference in the capture fractions for the two groups of neutrons, the number of neutrons measured by means of the permanganate solution must be multiplied by $1-0{\cdot}036$, or $0{\cdot}964\pm0{\cdot}012$, to allow for the presence of ^{11}B atoms in the ^{10}B target.

Fig. 3

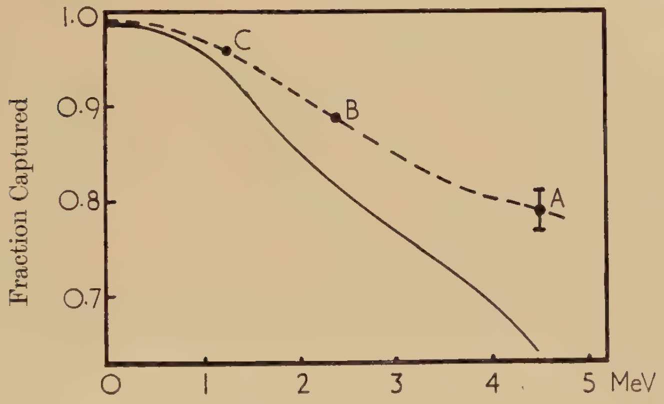

Loss of neutrons from tank.

——— Theoretical curve for tank radius 23 cm.

– – – – – Curve assumed for calculating corrections.

A, experimental point for neutrons from $RaBeF_4$ source.

B, C, points assumed for neutrons from $^{10}B(\alpha n)^{13}N$ and $^{11}B(\alpha n)^{14}N$ reactions.

---

* D. H. Wilkinson. Private communication.

2.3. *Experimental Results*

The results of six measurements of the protons and neutrons from ^{10}B are shown in fig. 4, before corrections have been applied for the loss of neutrons from the permanganate solution or the presence of ^{11}B. The mean value of the ratio of neutrons to protons is $2{\cdot}71 \pm 0{\cdot}05$ where the results have been weighted in proportion to the number of proton counts and the errors shown do not include the errors discussed in § 2.2 (ii). Applying now the corrections for these errors we obtain the final corrected value of $2{\cdot}27 \pm 0{\cdot}21$ for the ratio of the number of protons from the reaction $^{10}\mathrm{B}(\alpha p_0)^{13}\mathrm{C}$ at $E_\alpha = 1{\cdot}51$ Mev to the number of neutrons from the reaction $^{10}\mathrm{B}(\alpha n)^{13}\mathrm{N}$ at the same bombarding energy. If we use for the reaction radii the value $1{\cdot}45(13^{1/3}+1^{1/3}) \times 10^{-13}$ cm, i.e. $4{\cdot}86 \times 10^{-13}$ cm, we obtain for $\gamma_n{}^2/\gamma_{p_0}{}^2$ the value $5{\cdot}7 \pm 0{\cdot}5$.

Fig. 4

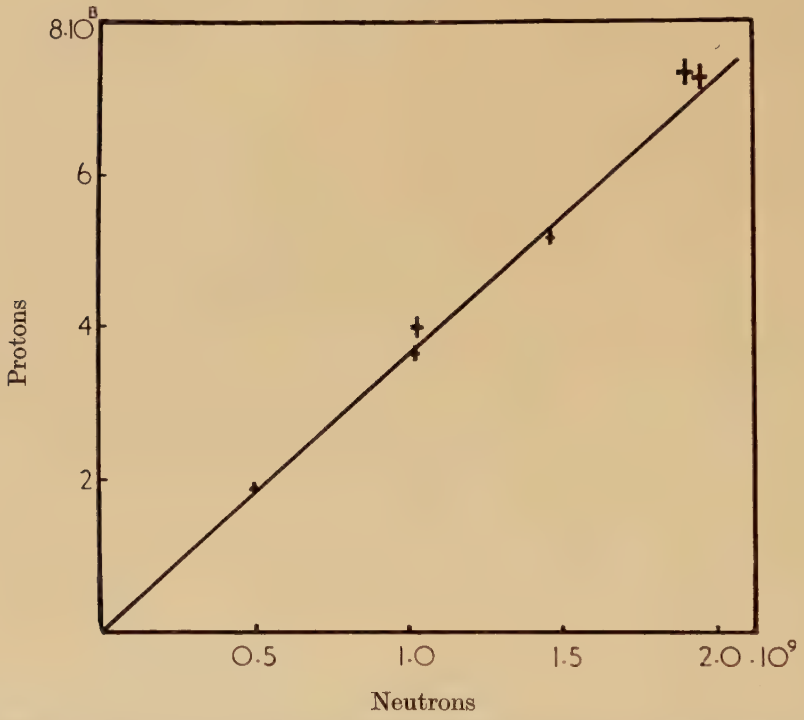

Total number of protons and neutrons emitted at 1·51 Mev alpha-particle energy. The errors shown are the statistical errors arising from the number of particles counted.

§ 3. Resonances, Yield Curves and Angular Distributions

3.1. *Experimental Method and Apparatus*

To count protons we used two ionization chambers of the kind described in § 2.1. One was usually left fixed at approximately 90° to the alpha-particle beam and the other could be moved to any angle between 9°

and 171° to the beam without disturbing the vacuum. By choosing a suitable thickness for the copper windows we excluded scattered alpha-particles and, in the case of the $^{10}B(\alpha p)^{13}C$ reaction, protons other than those leaving the residual ^{13}C nucleus unexcited.

Fig. 5

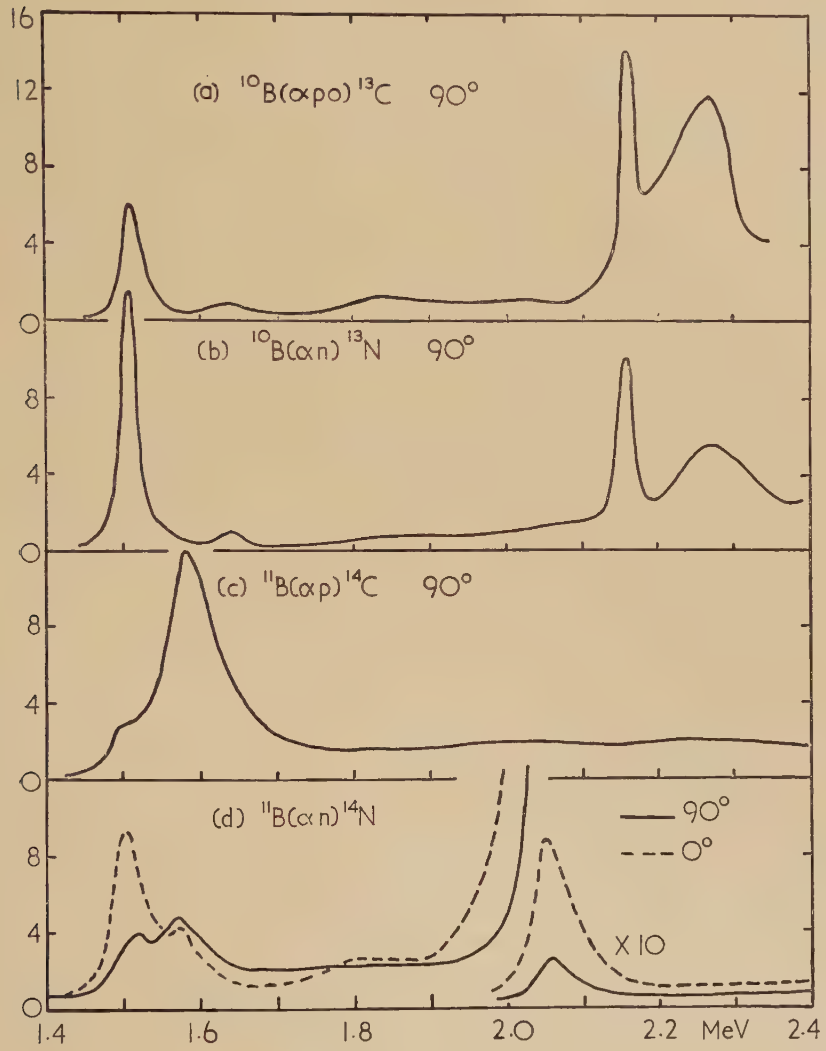

Proton and neutron yields.

The vertical scales of (*a*) and (*b*) have been adjusted to make the ratio of neutrons to protons at 1·51 MeV bombarding energy equal to 2·27. (See § 2.3.)

Neutrons were measured by a ZnS-plastic scintillator and photomultiplier of the type described by Hornyak (1952). The data given by Hornyak show that the number of counts for a given discriminator setting is fairly closely proportional to the energy of the neutrons. We have assumed exact proportionality in estimating the number of neutrons from our observed counts. For angular distribution measurements we used two scintillators, one fixed near 90° to the incident beam, the other movable between 0° and 135°. To obtain a reasonable counting rate we placed the scintillators close to the boron targets, and we have applied corrections for the finite solid angle of the movable scintillator in the angular distribution experiments. To compare the angular distribution of the neutrons from the $^{10}B(\alpha n)^{13}N$ reaction with theory, we first computed the angular distribution to be expected in laboratory space for an assumed centre-of-mass distribution and then applied a finite-counter correction by the method proposed by Breitenberger (1953), using the tables given by Price (1954) to express the point-counter laboratory distribution in terms of Legendre polynomials. For other distributions we corrected for finite counter size by the method given by Deutsch (1951).

3.2. *Experimental Results*

(i) *Yield Curves*

We give in figs. 5(*a*), 5(*b*), 5(*c*) and 5(*d*) our yield curves for the reactions $^{10}B(\alpha p_0)^{13}C$, $^{10}B(\alpha n)^{13}N$, $^{11}B(\alpha p)^{14}C$ and $^{11}B(\alpha n)^{14}N$. The ^{10}B results at 2·16 Mev bombarding energy lead to values of γ_n^2/γ_p^2 of 1·1 or 1·6 according as l for the outgoing particle is taken to be 1 or 2. The γ-ray yield which we obtained (not shown) for the $^{10}B(\alpha, p, \gamma)^{13}C$ reaction agreed with the results of Talbott and Heydenburg (1953).

A neutron resonance at 2·05 Mev for the $^{10}B(\alpha n)^{13}C$ reaction, reported in our previous paper, is almost certainly due to the $^{11}B(\alpha n)^{14}N$ reaction for which there is a very strong peak at 2·05 Mev. We used three different targets of ^{10}B and found the height of the 2·05 Mev peak proportional to the amount of ^{11}B contamination present. The resonance which we previously reported at 1·58 Mev for the $^{11}B(\alpha p)^{14}C$ reaction consists of two resonances at 1·51 and 1·58 Mev. These can be more clearly seen in the results of the $^{11}B(\alpha n)^{14}N$ reaction (figs. 5(*c*) and 5(*d*)). The resonances observed for bombarding energies of 1·51, 1·58 and 2·05 Mev correspond to levels in ^{15}N at 12·096, 12·147 and 12·491 Mev previously found by Roseborough, McCue, Preston and Goodman (1951) by means of the $^{14}C(pn)^{14}N$ reaction.

(ii) *The Angular Distribution of the Neutrons from the Reaction* $^{10}B(\alpha n)^{13}N$

We show in fig. 6 the experimental points found at 1·51 Mev bombarding energy together with a theoretical curve obtained from an assumed distribution $1-0{\cdot}9\cos^2\theta$ in centre-of-mass space, converted to laboratory space and adjusted for the finite detector used.

(iii) *Other Angular Distributions*

At 2·16 Mev the protons from $^{10}B(\alpha p_0)^{13}C$ and the neutrons from $^{10}B(\alpha n)^{13}N$ have similar distributions. Both could be fitted in centre-of-mass space to $1-(0{\cdot}5\pm0{\cdot}1)\cos^2\theta$.

We measured the neutron distribution for the $^{11}B(\alpha n)^{14}N$ reaction at 1·51 MEV bombarding energy, as part of the determination of the correction for contamination of our ^{10}B targets by ^{11}B, and in a preliminary way at 1·58 MEV and 2·05 MEV. The strong forward and backward intensities observed at 1·51 MEV suggest that the 12·096 MEV level in ^{15}N has spin 5/2 and even parity, an assignment tentatively made by Hinchey, Stelson and Preston (1952) from measurements of the total neutron cross section of nitrogen. The distribution at 1·58 MEV bombarding energy is nearly isotropic, which suggests that the ^{15}N level at 12·147 MEV has spin 3/2 and odd parity, but our present results could be fitted by other assignments if suitable choices of spin-channel intensities are made. The strong forward intensity at 2·05 MEV suggests that the ^{15}N level at 12·495 MEV has spin 5/2 and even parity, but our measurements indicate

Fig. 6

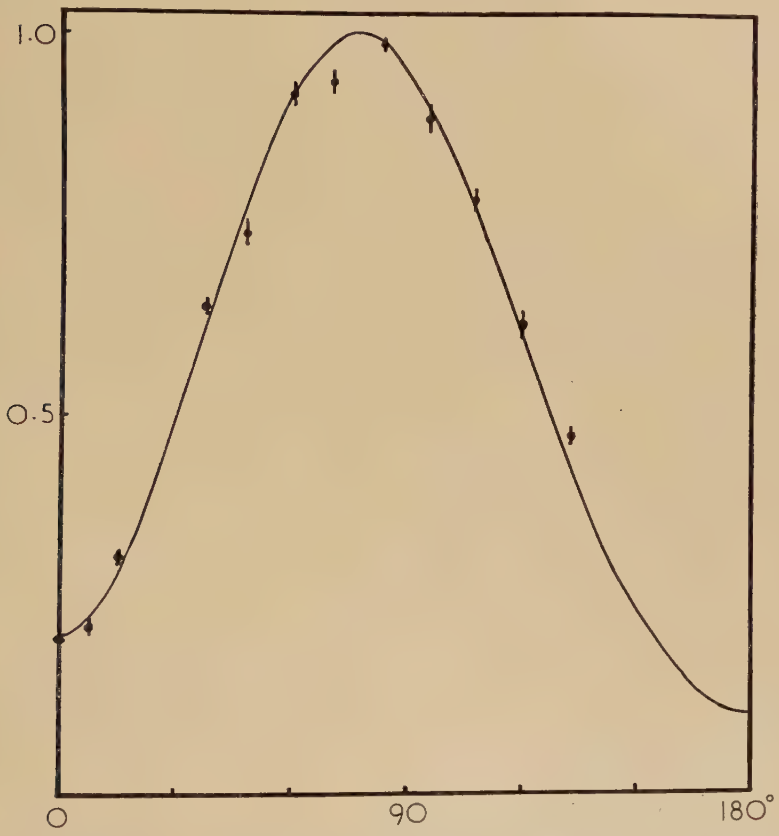

Angular distribution of neutrons from ^{10}B at 1·51 MEV alpha-particle energy. The curve gives the theoretical angular distribution corresponding to $1-0{\cdot}9\cos^2\theta$ in centre-of-mass space.

that the backward and forward intensities (in centre-of-mass space) are not equal, so that interference effects may be occurring. We intend to the measure proton angular distributions from the $^{11}B(\alpha p)^{14}C$ reaction for these levels, since these distributions should determine the spins and parities concerned unambiguously.

§ 4. Discussion and Conclusion

The main conclusion that we may draw from our results is that the emission of protons in the $^{10}B(\alpha p_0)^{13}C$ reaction and the emission of neutrons in the mirror reaction $^{10}B(\alpha n)^{13}N$ are strikingly similar. The yield curves for the two reactions (figs. 5(*a*) and 5(*b*)) show similar resonances for all bombarding energies between 1·4 and 2·4 Mev ; the angular distributions of protons and neutrons fit with a high degree of accuracy in centre-of-mass space the relation $I_\theta = I_0(1-0{\cdot}9\cos^2\theta)$ for a bombarding energy of 1·51 Mev and are similar and perhaps identical at higher energies. Nevertheless, the ratio of the reduced widths γ_n^2/γ_p^2 obtained from our results at 1·51 Mev bombarding energy, though lower than the estimate given in our earlier paper (Shire *et al.* 1953), is substantially greater than the value of unity which might be expected, if charge independence holds, for mirror reactions. The discrepancy appears to be greater than can easily be accounted for by modification of the usually accepted formulae for barrier penetration (Bloch *et al.* 1951, Blatt and Weisskopf 1952), for instance along the lines proposed by Scott (1954). Nor can the difference be accounted for by taking into consideration values of l for the outgoing particles greater than the minimum value of two ; higher values make a change of only a few per cent in the value of γ_n^2/γ_p^2.

The inequality of γ_n^2 and γ_p^2 is, however, not surprising if the compound nucleus is not in a pure isotopic spin state. Isotopic spin mixing is to be expected when states of the same spin and parity are near to one another and this is likely to be so in the present case where many levels come close together.

The behaviour of ^{11}B is quite different from that of ^{10}B. Though the double resonance near 1·58 Mev bombarding energy appears for both protons and neutrons, protons are almost completely absent for the very strong neutron resonance at 2·05 Mev. Such difference is, of course, not surprising, as the reactions $^{11}B(\alpha p)^{14}C$ and $^{11}B(\alpha n)^{14}N$ are in no sense mirror reactions.

Acknowledgments

We wish to thank Mr. J. M. C. Scott, Dr. B. M. Flowers and Dr. A. M. Lane for a number of helpful discussions, Mr. J. Simao for help in making many of the readings and the Atomic Energy Research Establishment, Harwell, for preparing separated isotope targets for us. One of us (R. D. E.) wishes to thank the Department of Scientific and Industrial Research for financial assistance while this work was in progress.

References

AJZENBERG, F., and LAURITSEN, T., 1955, *Rev. Mod. Phys.*, **27,** 77.

BLATT, J. M., and WEISSKOPF, V. F., 1952, *Theoretical Nuclear Physics* (New York : Wiley).

BLOCH, I., HULL, M. M., Jr., BROYLES, A. A., BOURICIUS, W. G., FREEMAN, B. E., and BRIET, G., 1951, *Rev. Mod. Phys.*, **23,** 147.

BREITENBERGER, E., 1953, *Proc. Phys. Soc.* A, **66,** 846.

BRETSCHER, E., COOK, G. B., MARTIN, G. R., and WILKINSON, D. H., 1949, *Proc. Roy. Soc.* A, **196,** 436.

DEUTSCH, M., 1951, *Rep. Prog. Phys.*, **14,** 209 (London : Physical Society).

HINCHEY, J. J., STELSON, P. H., and PRESTON, W. M., 1952, *Phys. Rev.*, **86,** 483.

HUTCHINSON, G. W., and SCARROTT, G. G., 1951, *Phil. Mag.*, **42,** 792.

JONES, G. A., and WILKINSON, D. H., 1953, *Proc. Phys. Soc.* A, **66,** 1176.

MARSHAK, R. E., 1947, *Rev. Mod. Phys.*, **19,** 185.

PRICE, P. C., 1954, *Phil. Mag.*, **45,** 237.

ROSEBOROUGH, W. D., MCCUE, J. J. G., PRESTON, W. M., and GOODMAN, C., 1951, *Phys. Rev.*, **83,** 1133.

SCOTT, J. M. C., 1954, *Phil. Mag.*, **45,** 441.

SHIRE, E. S., WORMALD, J. R., LINDSAY-JONES, G., LUNDEN, A., and STANLEY, A. G., 1953, *Phil. Mag.*, **44,** 1197.

SZILARD, L., and CHALMERS, T. A., 1934, *Nature, Lond.*, **134,** 462, 494.

TALBOTT, F. L., and HEYDENBURG, N. P., 1953, *Phys. Rev.*, **90,** 186.

WALLACE, P. R., 1949, *Nucleonics*, **4,** No. 2, p. 30 ; No. 3, p. 48.

LXXIV. *The Nuclear Interactions produced in Carbon, Nitrogen and Oxygen by* 140 MeV *Protons*

By H. Muirhead and W. G. V. Rosser
Department of Natural Philosophy, University of Glasgow*

[Received January 25, 1955]

Summary

A comparison is made between the nuclear disintegrations produced in carbon, nitrogen and oxygen by 140 MeV protons, and the nature of the disintegrations expected from the Goldberger model (1948).

§ 1. Introduction

There have been two previous communications from this laboratory relating to the nuclear interactions produced in photographic emulsions by 140 MeV protons. Lees *et al.* (1953), referred to as I, reported on measurements of the cross sections for the production of nuclear disintegrations by protons with an average kinetic energy of 130 MeV in both the heavy (silver and bromine) and light (carbon, nitrogen and oxygen) constituents of nuclear emulsions. The results were shown to be in agreement with the 'optical model' of Fernbach, Serber and Taylor (1949).

Morrison, Muirhead and Rosser (1953), referred to as II, reported on an experimental study of the nuclear disintegrations produced in silver and bromine by protons with an average kinetic energy of 140 MeV. The results obtained were shown to be consistent with the assumption that the disintegrations proceeded in two main stages. During the first stage the incident proton initiated a nucleon cascade leading to the direct emission of energetic nucleons (Goldberger 1948). The nucleus was then left in an excited state and nuclear particles were subsequently evaporated from it (Weisskopf 1937) until the residual nucleus reached its ground state.

In this paper a description will be given of the disintegrations observed in nuclear emulsions when protons with an average kinetic energy of 140 MeV strike the light nuclei carbon, nitrogen and oxygen. The experimental results will be compared with a theoretical model similar to that used in paper II.

---

* Communicated by Professor P. I. Dee, F.R.S.

§ 2. EXPERIMENTAL CRITERION FOR THE SELECTION OF STARS PRODUCED IN LIGHT NUCLEI

The stars were found by ‘ area scanning ’ in Ilford G5 emulsions which had been exposed to the external beam of the Harwell cyclotron. The protons entering the emulsions possessed a kinetic energy of 146 MEV.

The stars selected for analysis, as representing the disintegration of a light nucleus, were those in which an α-particle with a kinetic energy of less than 9 MEV had been emitted (Menon *et al.* 1950, Hodgson 1954). It will be shown in § 4, that the stars selected using this criterion do not represent all the modes of disintegration of a light nucleus.

§ 3. THE THEORETICAL MODEL

3.1. *Procedure*

Our theoretical model assumed that the incident protons possessed a kinetic energy of 140 MEV and that they initiated nucleon cascades in the light nuclei leading to the direct emission of knock-on nucleons. The residual nuclei were then left in excited states, and at a later stage de-excitation occurred.

The procedure for obtaining numerical data on the products of a nucleon cascade, and on the excitation energy of the residual nucleus was the same as that outlined for the heavy nucleus in paper II. This procedure will be referred to as the Goldberger method.

The struck nucleus was assumed to consist of 7 protons and 7 neutrons and to possess a radius of $3{\cdot}4\times10^{-13}$ cm ; it was also assumed that the nucleus possessed an effective coulomb barrier of 2 MEV.

3.2. *Limits of Application*

In carrying out the calculations we assumed that only single nucleon–nucleon collisions took place at all energies. However, evidence will be offered in § 6, from which it is necessary to conclude that the knock-on nucleons may occasionally collide with nuclear subgroups, such as α-particles, inside light nuclei. It will be shown that the effect is a small one, so that the use of single nucleon–nucleon collisions for the Goldberger method is not likely to be grossly incorrect.

In performing the calculations the possible effects of the wide spacing of the energy levels in light nuclei were neglected initially. However, the results of Titus and Strauch (1954) have shown that the wide spacings of nuclear energy levels in light nuclei play an important role when protons of 96 MEV are inelastically scattered by light nuclei. This feature will be discussed more fully in § 7.

Despite these inadequacies it will be shown in subsequent sections that the model gives a satisfactory explanation of many of the modes of disintegration of a light nucleus when struck by a proton with an energy of 140 MEV.

§ 4. The Cross Section for Nuclear Interaction

The total cross section, calculated by us, for the production of nuclear interactions in light nuclei (referred to henceforth as ‘ stars ’) was $(21\pm3)10^{-26}$ cm^2. This is in very good agreement with the experimental value of $(16\pm7)10^{-26}$ cm^2, presented in paper I, and with the value of $(22\pm2)10^{-26}$ cm^2 obtained by Cassels and Lawson (1954), using counter techniques and 134 Mev protons incident on carbon.

The size–frequency distribution for stars produced in light nuclei, presented in paper I, is reproduced in table 1, column 2. This was obtained experimentally from a comparison of stars produced in normal and diluted Ilford G5 emulsions. Unfortunately this method does not allow us to decide whether any individual star was produced in a heavy or light nucleus.

Table 1

Type of star	Cross section × 10^{26} cm^{-2}				
	Experimental				Theoretical
	Paper I		Stars with α-particle<9 Mev		
0p	2±1·5	7±4	—	3·4	~ 9
1p	5±5		0·1		
2p	−3±4		0·3		
3p	3±2		3·0		
4p	4 ±1·5	9±4	6·0	11·6	~ 12
5p	3·5±1		4·0		
6p	1·5±0·5		1·6		
Total	16±7		15±2		21±3

In the present work if an α-particle with an energy less than 9 Mev was observed to be emitted from a star, then that star was attributed to the disintegration of a light nucleus. The size-frequency distribution obtained with this criterion is also shown in table 1, column 3. The value of 32·5±2·5 cm obtained in paper I for the mean free path for star production in Ilford G5 emulsions, was used to determine the absolute cross sections. It can be seen that with our criterion we select most of the 3, 4, 5 and 6 prong stars produced in the light nuclei, but that many of the 0, 1 and 2 prong stars are not selected.

As there is no reliable statistical theory available for the processes following the nucleon cascade in light nuclei, it is not possible to calculate the size–frequency distribution from the Goldberger model, but it is possible to make a qualitative estimate.

The distribution of the excitation energy of the residual nucleus obtained by the Goldberger method is shown in fig. 1; the average value for this quantity was 23 Mev. For high excitation energies the nucleus is expected to break up completely, but at low excitation energies the residual nucleus need emit only one charged particle or possibly a γ-ray before losing its excitation energy. The thresholds for the nuclear reactions $^{12}\mathrm{C}(\mathrm{p}\,;\,\mathrm{p}, 3\alpha)$, $^{14}\mathrm{N}(\mathrm{p}\,;\,\mathrm{n}, 2\mathrm{p}, 3\alpha)$ and $^{16}\mathrm{O}(\mathrm{p}\,;\,\mathrm{p}, 4\alpha)$ are 7·3, 19·8 and 14·5 Mev respectively. Therefore at excitation energies below about 15 Mev very few nuclei will break up completely whereas at higher energies the probability for these processes is high. If it were assumed arbitrarily that for excitation energies greater than 15 Mev the light nucleus broke up completely, giving a 4p, 5p or 6p star and that for lower excitation energies it did not, then we would expect the cross section for stars of $(0+1+2+3)$ prongs to be about $9\times10^{-26}\,\mathrm{cm}^2$, and about $12\times10^{-26}\,\mathrm{cm}^2$ for stars of $(4+5+6)$ prongs. These values are in satisfactory agreement with those shown in column 2 of table 1. The Goldberger model can, therefore, account qualitatively for the number of small and large stars observed experimentally.

Fig. 1

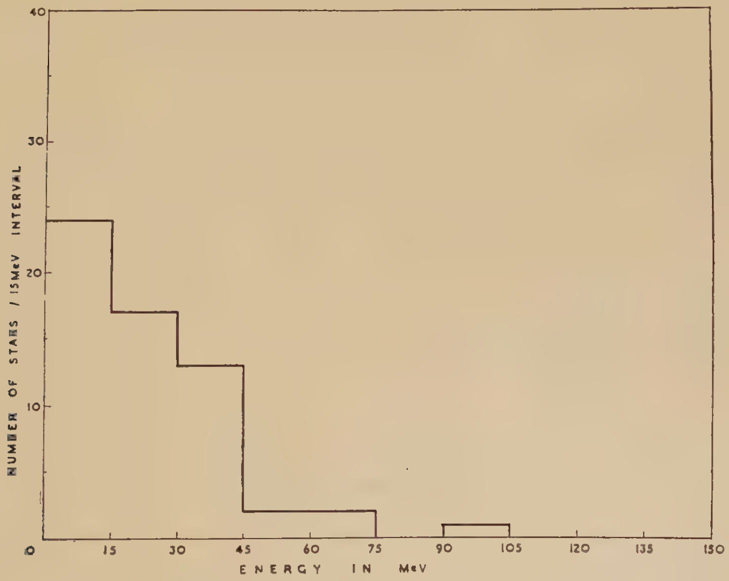

Calculated distribution of excitation energy in residual nucleus following the passage of the nucleon cascade.

A comparison of columns 3 and 4 of table 1 also suggests that the application of the criterion discussed in § 2 favours the selection of stars with excitation energy greater than ~15 Mev. Further evidence in support of this conclusion will be offered in the next section.

§ 5. COMPARISON OF THE CALCULATED AND EXPERIMENTAL DATA FOR PROTONS EMITTED WITH ENERGIES GREATER THAN 30 MEV

In table 2 the experimental energy distribution of protons emitted with energies >30 MeV is compared with the predictions of the Goldberger model. The energies of the primary and secondary protons were determined by grain counting. The experimental results are based on 71 stars, all of which had primary protons with energy greater than 130 MeV, their mean energy being close to 140 MeV; they also had at least one α-particle <9 MeV.

Table 2

Energy in MeV	30–55	55–75	75–95	95–115	>115
No. of protons :— experimental	19	15	10	8	1
Goldberger model excitation energy >15 MeV	22	14	4	6	4
Goldberger model excitation energy <15 MeV	0	6	6	8	12

Our calculated results are shown in table 2, and are based on 118 'stars', the data for 59 'stars' being doubled. Of these 68 had excitation energies greater than 15 MeV. An examination of table 2 shows satisfactory agreement between the experimental data, and the energy spectrum calculated for nuclei which are left with excitation energy greater than 15 MeV. This agreement lends further support to the suggestion made at the end of § 4 that the stars selected experimentally by the presence of an α-particle with energy <9 MeV are produced by a nuclear excitation greater than ~15 MeV.

Table 3

Angle in degrees	0–20	20–40	40–60	60–80	80–100	100–120	>120
No. of protons :— experimental	11	22	7	8	3	1	1
Goldberger model excitation energy >15 MeV	12	24	8	2	—	2	2
Goldberger model excitation energy <15 MeV	12	12	4	4			

It was suggested in paper II that the angular distribution obtained by the Goldberger method should be compared with the distribution of the actual angle in space between the primary and secondary protons. The calculated angular distribution is compared with the experimental results in table 3. It can be seen that the agreement is satisfactory.

§ 6. Comparison of the Calculated and Experimental Data for the Charged Particles Emitted with Energies less than 30 Mev

The majority of the tracks of particles with energy less than 30 Mev are emitted in the processes following the nucleon cascade. There is at present no reliable statistical theory for the processes occurring in light nuclei during the second stage of the disintegration so that no exact comparison can be made between the calculated and experimental results. The experimental results will be discussed in the light of the predictions of the Goldberger type calculations.

It was found experimentally that there was little variation in either the average star size or in the characteristics of the stars produced in light nuclei when the energy of the primary protons varied within reasonable limits. In this section results are included from all stars from which an α-particle <9 Mev had been emitted, and whose primary protons had energies greater than 110 Mev. The total number of stars examined was 176.

6.1. *Results for α-particles*

The experimental value for the ratio of the number of α-particles to the total number of prongs in a star was $0\cdot48 \pm 0\cdot03$ for the 176 stars produced in light nuclei. This high value reflects the ease with which light nuclei break up into α-particles at comparatively low excitation energies. The value obtained is consistent with the results obtained from stars produced by π-mesons and the cosmic radiation (Menon *et al.* 1950, Harding 1949).

The measured energy spectrum for the α-particles emitted from stars produced in light nuclei is shown in fig. 2.

The experimental ratio of the number of α-particles emitted in the forward direction in the laboratory system to the number emitted in the backward direction is shown in table 4 as a function of energy.

Table 4

Energy in Mev		0–2	2–4	4–6	6–8	8–10	>10	Total
Forward to backward ratio for α-particles	Experimental	1·9 ±0·6	2·3 ±0·5	2·5 ±0·6	2·3 ±0·7	3·6 ±1·4	2·9 ±1·2	2·4 ±0·3
	Calculated	2·1	2·4	1·9	1·6	1·5	1·35	—

The forward excess observed may be attributed mainly to the forward momentum the nucleus normally possesses after the residual nucleon cascade is over. The average forward velocity of the nucleus calculated by the Goldberger method for ‘ stars ’ with excitation energies greater than 15 Mev was 4×10^8 cm/sec. Using this value the forward to the backward ratio was calculated assuming that all the α-particles were emitted isotropically in the coordinate system of the recoiling nucleus during the process following the nucleon cascade. The calculated results are also shown in table 4. It can be seen that the forward excess for low energy α-particles can be accounted for in this manner, but it is difficult to explain the forward excess at higher energies in a similar fashion. For example, the forward to backward ratio for all α-particles greater than 8 Mev is observed to be $3{\cdot}2\pm0{\cdot}9$, whereas the calculated value is 1·4. There is some uncertainty in the model used in the Goldberger type calculations, but the number and angular distribution of high energy protons experimentally observed to leave the nucleus show that, after the nucleon cascade is over, the velocity of the recoiling nucleus cannot be considerably greater than the calculated value.

Fig. 2

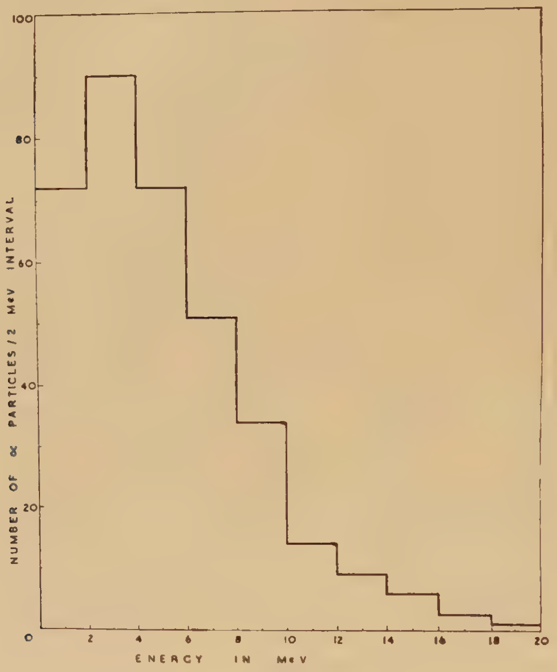

Measured energy spectrum for α-particles.

The forward excess could be explained if either the α-particles were emitted preferentially in the forward direction relative to the recoiling nucleus during the processes following the nucleon cascade, or if some α-particles were emitted in direct collision processes during the nucleon cascade. The latter view is supported by the occasional observation of α-particles ejected with energies >30 Mev in identified disintegrations of light nuclei. These α-particles could arise either from a direct collision between a nucleon and an α-particle inside the nucleus, or a 'pick-up' process during the nucleon cascade (Chew and Goldberger 1950).

One of these two events was of particular interest in that an α-particle of energy 43 Mev was emitted at an angle of 26° with respect to a primary proton of measured energy 140 Mev, and a proton of energy 65 ± 20 Mev was emitted at an angle of 134° with respect to the primary particle. The three tracks were coplanar, the angle between the high energy α-particle and the secondary proton being 160°. The only other charged particle emitted was an α-particle of energy 2·5 Mev which was probably due to the decay of the residual nucleus. The dynamics of the problem suggest that the 65 ± 20 Mev proton represents the primary particle recoiling after colliding with an α-particle subgroup inside the nucleus. If the high energy α-particle were due to a 'pick-up' process, then the dynamics of the collision should correspond to a single nucleon–nucleon collision, which would be unlikely to give a proton of energy 65 Mev in the backward direction even after allowing for possible double scattering. One other similar event was observed in which an α-particle of energy 26 Mev was emitted at an angle of 38° with respect to a primary proton of energy 140 Mev. A proton of energy 55 ± 10 Mev was emitted at an angle of 99° with respect to the primary. As no other tracks were emitted, this event was classified as a disintegration of a heavy nucleus.

We, therefore, conclude tentatively that the primary protons and knock-on nucleons sometimes collide with α-particle sub-groups inside light nuclei, although part of the forward excess may be due to a 'pick-up' process. An average of $\sim 0 \cdot 25$ α-particles per star, emitted in the forward direction during the nucleon cascade, is adequate to account for our experimental results. This number is much lower than the average of one knock-on proton and one knock-on neutron per star emitted during the nucleon cascade. We need, therefore, assume that only a small proportion of the collisions inside light nuclei involve α-particles and the use of only single nucleon–nucleon collisions in the Goldberger type calculations is not likely to be grossly incorrect.

6.2. *Results for Protons of Energies less than* 30 Mev

The measured energy distribution of protons emerging from 176 stars produced in the light nuclei is shown in fig. 3. The shaded area represents the calculated number of knock-on protons expected on the Goldberger model. These results were obtained from 'stars' with calculated excitation energies greater than 15 Mev; the results were normalized to a total of 176 stars. It can be seen that the broad tail in the energy spectrum can be accounted for as due mainly to knock-on protons emitted during the nucleon cascade. The statistical errors on the number of protons having energies between 20 and 30 MeV and ending in the emulsion are large, but the existence of these protons was confirmed by the observation of protons in this energy range by grain counting in underdeveloped plates.

Fig. 3

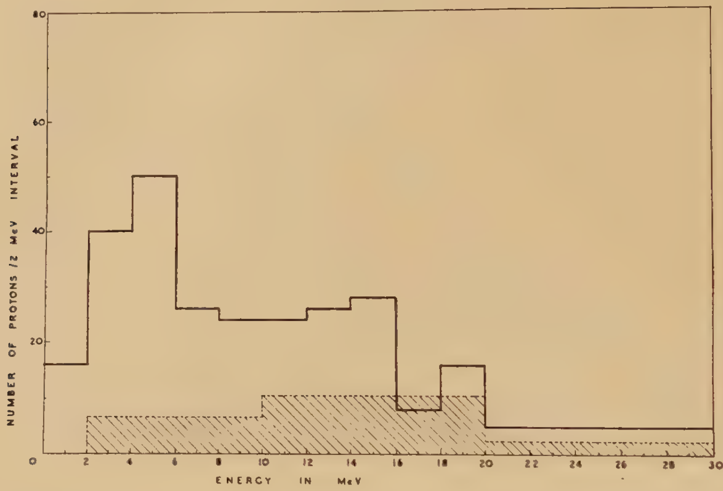

Measured energy spectrum for protons. Shaded area represents the calculated contribution to the spectrum from knock-on protons.

The experimental forward to backward ratio for all identified protons of energies less than 30 MeV was $2{\cdot}3 \pm 0{\cdot}3$. If we assumed that there were no knock-on protons with energies less than 30 MeV the velocity of the residual nucleus after the passage of the nucleon cascade would be increased from 4×10^8 cm/sec to $5{\cdot}2 \times 10^8$ cm/sec, using the Goldberger model. The forward to backward ratio calculated assuming that all protons of energy below 30 MeV were emitted isotropically relative to a residual nucleus which had a velocity of $5{\cdot}2 \times 10^8$ cm/sec was 1·4. It can be seen that the forward excess observed experimentally cannot be due only to the motion of the recoiling nucleus. If, on the other hand, it were assumed that the number of knock-on protons emitted in the 176 stars produced in the light nucleus is as shown in fig. 3 and that they had the angular distribution given by the Goldberger model, and that all the other protons were emitted isotropically relative to a residual nucleus which had a velocity of 4×10^8 cm/sec, then the forward to backward ratio should be 2·4. This value is in good agreement with the experimental figure of $2{\cdot}3 \pm 0{\cdot}3$, showing that the Goldberger model can account satisfactorily for the forward excess of protons <30 MeV observed experimentally.

§ 7. Discussion

The results obtained in this paper lend further support to the suggestion made in paper II that nucleons of low energy (<30 MeV) do emerge from nuclei during a nucleon cascade, and that they must, therefore, have a finite mean free path in nuclear matter before being incorporated in a compound nucleus. The work of Bernardini, Booth and Lindenbaum (1952) and of Hodgson (1954) also supports this assumption.

Our theoretical model is able to account satisfactorily for the total cross section for nuclear interaction in the light nuclei, and qualitatively for the size-frequency distribution (§ 4). The model also gives an adequate description of the modes of disintegration of the light nuclei when the nuclear excitation is greater than ~15 MeV (§§ 5 and 6).

When small quantities of energy are transferred to the nuclei by the primary protons, however, the subsequent de-excitation is frequently realized by γ-emission or by the ejection of a single nucleon. Interactions of this type cannot be attributed to the light nuclei when observed in a nuclear emulsion. Interactions involving low nuclear excitation may be examined, however, in experiments using other techniques, and the results obtained show that in this region our theoretical model is inadequate.

The theoretical model is based on the assumption that the nucleon cascade proceeds through a series of nucleon–nucleon collisions. We have also assumed that, with the exception of the operation of the Pauli exclusion principle, these collisions take place in the same manner as those between free nucleons. Using these parameters our model cannot account for the experimental results of Titus and Strauch (1954), who have shown that when 96 MeV protons are incident upon light nuclei there are peaks in the energy spectrum of the inelastically scattered protons. These peaks occur at energies equal to the primary energy minus the excitation energies of known nuclear levels. For example, peaks were observed at 4·3, 10·0 and 20·9 MeV below the elastic peak with carbon. Our theoretical model would predict that the energy of the knock-on protons should be continuous.

It might be expected that the effect of the discrete spacing of energy levels in light nuclei would be to forbid all the collisions of the primary proton, except when the energy transferred in the collision corresponded to the excitation of a nuclear energy level. On our model this would reduce the number of allowed collisions for the primary proton, and therefore the calculated cross section for star production. The widths of the nuclear levels of low excitation energy in light nuclei are generally much narrower than the average distance between levels, and the density of levels only becomes appreciable at excitation energies of about 25 MeV. The Goldberger type calculations were, therefore, repeated assuming that all collisions for which the energy transferred from the primary proton was less than 25 or greater than 115 MeV were forbidden. It was found that the calculated cross section for star production was reduced from $(21 \pm 3)10^{-26}$ cm² to $(10 \pm 2)10^{-26}$ cm². This value is significantly smaller than the figure of $(22\pm2)10^{-26}$ cm^2 determined experimentally by Cassels and Lawson (1954) for carbon. Furthermore, with this model the number of collisions with the correct energy transfers is not enough to account for the number of protons present in the peaks observed by Titus and Strauch. We are, therefore, forced to conclude that the assumption of single nucleon–nucleon collisions using the parameters observed for free collisions does not hold exactly for light nuclei. It is possible that the distribution of scattering angles in the centre of momentum system of the colliding nucleons may be modified in the presence of the potential well in light nuclei such that energy transfers corresponding to excited levels of the nucleus are preferred, whilst the total cross section for collision remains about the same as that expected using our original model. If, on the other hand, the use of the parameters for free collisions were correct as a first approximation and collisions leading to energy transfers between levels were allowed, then the peaks observed by Titus and Strauch would have to be due to a different type of collision that occurred occasionally, possibly involving the collision of the primary proton with a nuclear subgroup or possibly even the nucleus as a whole.

The present work does not allow us to decide whether the excited nucleus, left after the passage of the nucleon cascade, sometimes breaks up completely in one act, or always emits single particles or photons successively until it has either lost all its excitation energy, or broken up completely into its constituents. The work of Livesey and Smith (1953) and Goward and Wilkins (1953) on the photodisintegration of carbon and oxygen at γ-ray energies below 25 MEV suggests that the latter view is probably the correct one.

REFERENCES

BERNARDINI, BOOTH, and LINDENBAUM, 1952, *Phys. Rev.*, **88,** 1017.
CASSELS, and LAWSON, 1954, *Proc. Phys. Soc.* A, **67,** 125.
CHEW, and GOLDBERGER, 1950, *Phys. Rev.*, **77,** 470.
FERNBACH, SERBER, and TAYLOR, 1949, *Phys. Rev.*, **75,** 1352.
GOLDBERGER, 1948, *Phys. Rev.*, **74,** 1269.
HARDING, 1949, *Nature, Lond.*, **163,** 440.
HODGSON, 1954, *Phil. Mag.*, **45,** 190.
LEES, MORRISON, MUIRHEAD, and ROSSER, 1953, *Phil. Mag.*, **44,** 304.
LIVESEY, and SMITH, 1953, *Proc. Phys. Soc.* A, **66,** 689.
MENON, MUIRHEAD, and ROCHAT, 1950, *Phil. Mag.*, **41,** 583.
MORRISON, MUIRHEAD, and ROSSER, 1953, *Phil. Mag.*, **44,** 1326.
PEASLEE, 1952, *Phys. Rev.*, **86,** 269.
TITUS, and STRAUCH, 1954, *Phys. Rev.*, **94,** 785.
WEISSKOPF, 1937, *Phys. Rev.*, **52,** 295.
WILKINS, and GOWARD, 1953, *Proc. Phys. Soc.* A, **66,** 661.

LXXV. *Positrons from* ^{25}Al *and* ^{26m}Al

By B. Elbek, B. S. Madsen and O. Nathan
Institute for Theoretical Physics, University of Copenhagen *

[Received February 3, 1955]

ABSTRACT

The positron emitters 7·4 sec ^{25}Al and 6·6 sec ^{26m}Al have been produced by proton capture in ^{24}Mg and ^{25}Mg. Their subsequent decays have been investigated by means of a magnetic lens spectrometer. The maximum energies were measured as 3·24±0·03 mev for ^{25}Al and 3·21±0·03 mev for ^{26m}Al. The spectra show no complexities and yield straight Fermi plots down to about 1300 kev. The deviations from linearity at lower energies are probably due to scattering in the spectrometer. No gamma-rays except annihilation radiation was found.

§ 1. EXPERIMENTAL

THE maximum energies of the positron emitters 7·4 sec ^{25}Al and 6·6 sec ^{26m}Al have earlier been determined by absorption and cloud chamber methods (Hunt, Jones and Churchill 1954 ; see also Endt and Kluyver 1954). In the present investigation the positrons have been studied by means of a magnetic lens spectrometer, while gamma-rays associated with the beta-decays were searched for with a NaI crystal.

In the study of ^{25}Al, thin targets of natural magnesium were bombarded with 225 kev protons corresponding to the lowest ^{24}Mg (p, γ)^{25}Al resonance. At this energy the yield of ^{26m}Al is negligible (Hunt, Jones, Churchill and Hancock 1954). ^{26m}Al was investigated by bombarding separated ^{25}Mg targets and utilizing the 391 kev capture resonance in ^{25}Mg. The protons were accelerated in a Greinacher coupled, high tension generator and deflected through 90° by an analysing magnet. Several circular slits, 5 mm in diameter, between the analysing magnet and the spectrometer defined the position of the beam before it hit the magnesium target, which was supported by a 2·5 mg/cm^2 Al foil. The target arrangement is shown in fig. 1. The Al foil was placed at the source position of the lens spectrometer, and a Geiger counter, which was situated behind the foil in the spectrometer axis, was used as a beta-monitor. A tungsten foil in front of the monitor absorbed x-rays from the target.

In the case of natural magnesium, the targets were prepared by evaporation *in vacuo* with subsequent oxidation in air at 450°c, and in the case of ^{25}Mg, by spraying a dilute ^{25}Mg(NO$_3$)$_2$ solution on to a hot Al foil. ^{25}Mg was obtained from Harwell as ^{25}MgO containing 3·8% ^{24}Mg, and very pure ^{25}Mg targets were also prepared in the isotope separator of the Institute. In all cases rather stable targets were obtained, which were able to withstand proton beams of 10–15 μamp for many hours.

---

*Communicated by Professor Niels Bohr.

The spectrometer used was of the Siegbahn–Slätis type (Slätis and Siegbahn 1950), which utilizes the focusing properties of a U-shaped field. The baffle system consisted of a central baffle, which formed a ring aperture 8 mm wide and 20 cm in diameter, and two identical ring apertures near the source end and the detector, respectively. The resolving power of the instrument was 3·3% for a point source and 3·7% for a source spot 5 mm in diameter. The transmission was about 7%.

Fig. 1

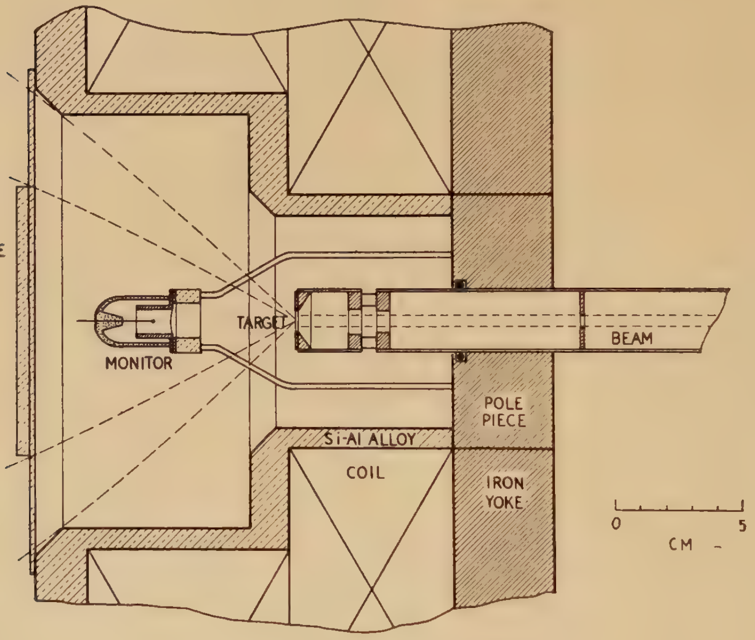

Source end of lens spectrometer.

The beta-particle detector was an anthracene crystal, which was 3 mm thick and 15 mm in diameter. It was mounted on the end of a 25 cm long lucite rod in optical contact with the photo-cathode of an EMI 5311 photomultiplier. The multiplier was shielded from the stray magnetic field by means of an iron tube, and it was verified that the counting rate of the detector was independent of the magnetic field when a gamma-ray source was placed outside the spectrometer.

The iron yoke of the spectrometer made it necessary to check the linearity of the current-momentum relationship. Measurements were made on several of the conversion lines of Th(B+C′+C″) including the

2·53 Mev x-line and on the 624 kev ^{137}Cs line. Furthermore the beta-rays from ^{42}K were studied and the calibration yielded for this case a maximum energy of 3·56±0·05 Mev, which is in excellent agreement with the accepted value 3·56 Mev (Koerts *et al.* 1954).

The counting rate of the Geiger monitor showed some dependence on the magnetic field strength, and correction curves were, therefore, determined by measuring the beta-rays from 1·7 Mev ^{32}P and from 3·6 Mev ^{42}K. The curves for the counting rate as function of $p/p_{\max}$ were nearly identical in the two cases.

The amount of scattering present in the spectrometer was studied by means of the beta-rays from ^{32}P. For this purpose a thin source was mounted on a 100 μg/cm^2 Zapon film. The resulting Fermi plot deviated from a straight line below 700 kev. We believe that the scattering took place mainly at the source end of the spectrometer, where the construction was rather compact (see fig. 1). Another ^{32}P source was mounted on a 2·5 mg/cm^2 Al foil, but the corresponding spectrum showed no additional scattering. Backscattering from our target support was thus negligible in this energy region compared with spectrometer scattering.

The technique used in the measurements of the Al spectra was a continuous irradiation and counting over a period long compared with the half-life, generally 10–15 minutes. The beam current to the electrically insulated target was measured by a beam integrator, by means of which the target yield versus beam current was controlled.

§ 2. Results

Figure 2 shows the obtained spectrum of ^{25}Al, representing the average of 11 runs with a total of 45 000 counts. Owing to the low accelerator voltage used, only a machine-independent background of 3 cpm was observed when the detector bias corresponded to 200 kev positron energy. Figure 3 represents the corresponding Fermi plot from which the maximum energy was determined by the method of least squares to be 3·24±0·03 Mev. This figure includes a 4 kev correction for energy loss in the target support.

In the investigation of ^{26m}Al at the 391 kev resonance, we found a small background at lower positron energies. This was caused by 10 min ^{13}N formed by proton capture in carbon which deposited on the target even though a liquid air trap was placed immediately in front of the spectrometer. Figure 4 shows the spectrum after correction for ^{13}N. It represents the average of 11 runs with a total of 40 000 counts. Both sprayed ^{25}Mg targets and targets prepared in the isotope separator were used for the measurements, but they showed no differences, except in the positron yield per μcoul. The small field-independent background present at higher positron energies was probably produced by capture gamma-rays from ^{26}Al. A similar background was not seen in the measurements on ^{25}Al, however, this can be explained from the fact that the number of capture gamma rays per positron is much lower at the 225 kev ^{24}Mg resonance than at the 391 kev ^{25}Mg resonance. In addition, fluorine contaminations might have contributed in the case of ^{26}Al. For calculation of the Fermi plot, this background was subtracted as indicated by the dotted line in fig. 4. The resulting Fermi plot is shown in fig. 5 and gives an end-point energy of 3·21±0·03 Mev after correction for the energy loss in the target.

Fig. 2

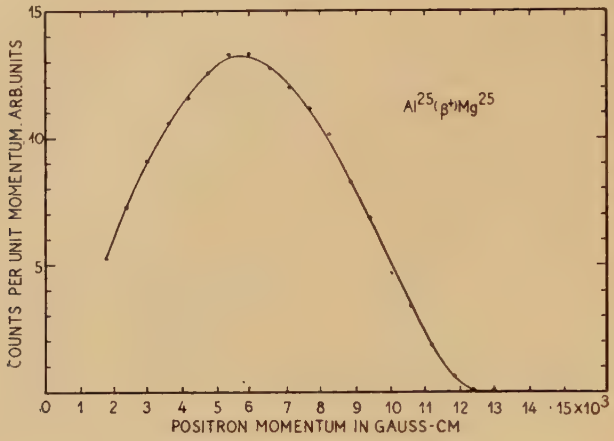

Positron spectrum of ^{25}Al.

Fig. 3

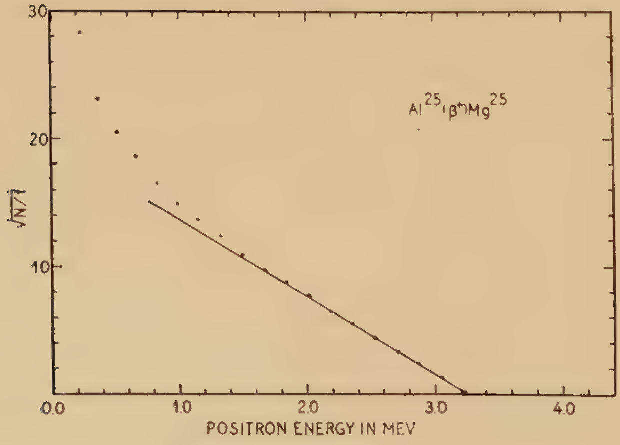

Fermi plot of ^{25}Al.

It can be seen from fig. 2 and fig. 4 that the spectra differ somewhat in shape, but no definite conclusions can be drawn in this respect due to the serious scattering which took place in the spectrometer. It is, however, worth noting that the deviations from the straight line in the Fermi plots are of the same order of magnitude as was observed previously with ^{32}P beta-rays.

With a NaI(Tl) crystal and a single channel pulse-height analyser a search was undertaken for gamma-rays associated with the positron decay. Apart from annihilation radiation, which obscures the region below 500 kev, no gamma-rays were found.

Fig. 4

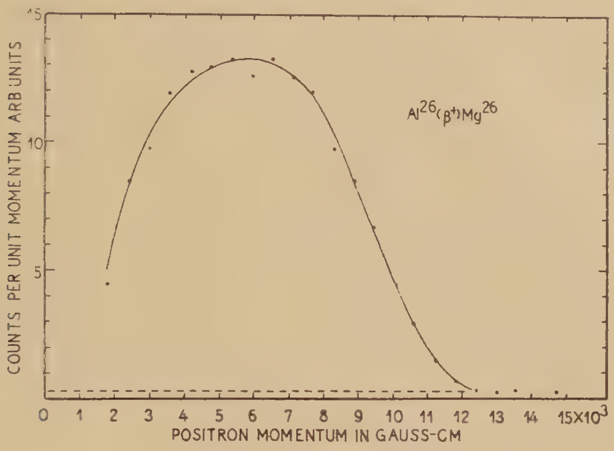

Positron spectrum of ^{26m}Al.

Fig. 5

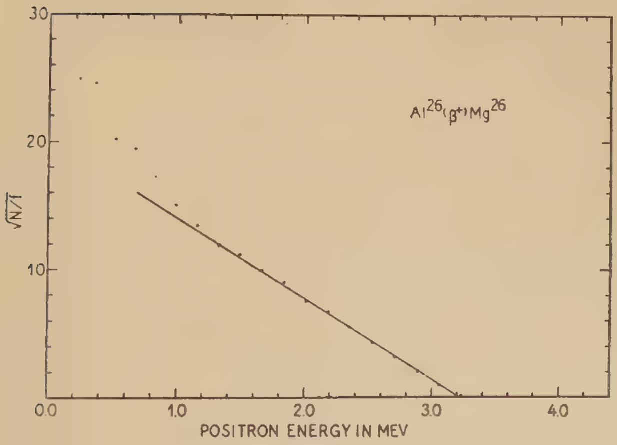

Fermi plot of ^{26m}Al.

§ 3. Discussion

Our observed end-point energy of the positrons from ^{25}Al agrees with the value 3·17±0·15 mev which was obtained by absorption measurements (Hunt, Jones and Churchill 1954). The maximum energy of a beta-transition to the ground state of ^{25}Mg can be derived from the Q values of the ^{24}Mg(d, p)^{25}Mg and the ^{24}Mg(d, n)^{25}Al reactions. The most accurate determinations (Endt *et al.* 1952, Goldberg 1953) give 3·23±0·06 MEV, which is in close agreement with our measurements and, therefore, suggest that the observed transition leads to the ground state of ^{25}Mg. Recent determinations of the half-life (Hunt, Jones, Churchill and Hancock 1954, Green, Harris and Cooper 1954) have given 7·62 sec and 7·20 sec, respectively. If we choose arbitrarily an average value of 7·41±0·21 sec, our determination of the maximum energy yields the *ft* value 3660±200 for this superallowed transition. It is interesting to compare this value with the estimate $ft=3030$, obtained from the unified theory of nuclear structure (Bohr and Mottelson 1953).

There is now both theoretical and experimental evidence for the suggestion that the two lowest lying levels in ^{26}Al undergo independent beta-decay (Moszkowski and Peaslee 1954, Simanton *et al.* 1954). A long-lived activity with a half-life of ~10^6 years originates in the lowest $T=0$ state, which probably has spin 5+ (King and Peaslee 1953), while the 6·6 sec decay is assigned to the lowest $T=1$, $J=0+$ state, leading to the ground state of ^{26}Mg. The latter transition thus belongs to the class of $0\rightarrow0$(no) beta-transitions in $4n+2$ nuclei, for which the theory predicts a common *ft* value directly related to the Fermi coupling constant (cf. e.g. Kofoed-Hansen 1953). The most accurate experimental data in this group of beta-decays have been obtained on the decay of ^{14}O (Gerhart 1954), for which the *ft* value 3275±75 is reported. For a calculation of the ^{26m}Al *ft* value, we take the average 6·56±0·20 sec of the most accurate determinations of the half-life (Hunt *et al.*, *op. cit.* and Green *et al.*, *op. cit.*), which are 6·44 sec and 6·68 sec. By using our value of the maximum energy, one finds $ft=3110\pm200$.

The position of the low-lying $T=0$ levels in ^{26}Al have recently been determined by magnetic analysis of the ^{28}Si(d, α)^{26}Al reaction (Browne 1954). The two lowest of these are located 4·010±0·008 MEV and 4·428±0·008 MEV over the ground state of ^{26}Mg and may be interpreted as the ground state and a 418 kev excited state in ^{26}Al. These levels have also been reported by Kluyver *et al.* (1954). Our measurements locate the (isomeric) level responsible for the 6·6 sec activity, 4·23±0·03 MEV over the ground state of ^{26}Mg, i.e. 220±40 kev over the ground state of ^{26}Al found by the above mentioned authors. This is in accordance with measurements of the ^{27}Al(γ, n) threshold (R. N. H. Haslam, private communication quoted by Browne, *op. cit.*) as this process is unaccompanied by positrons up to 200 kev above the neutron threshold.

We wish to thank Professor Niels Bohr for excellent working conditions at the Institute, and Mr. K. O. Nielsen for having prepared the separated ^{25}Mg targets.

Note added in proof.—Another beta-spectroscopic determination of the maximum energy of ^{26m}Al has recently been published by R. W. Kavanagh, W. R. Mills and R. Sherr (1955, *Phys. Rev.*, **97,** 248). Our work is in excellent agreement with their result, 3·20±0·05 MEV.

REFERENCES

BOHR, A., and MOTTELSON, B. R., 1953, *Dan. Mat. Fys. Medd.*, **27,** No. 16.
BROWNE, C. P., 1954, *Phys. Rev.*, **95,** 860.
ENDT, P. M., ENGE, H. A., HAFFNER, J., and BUECHNER, W. W., 1952, *Phys. Rev.*, **87,** 27.
ENDT, P. M., and KLUYVER, J. C., 1954, *Rev. Mod. Phys.*, **26,** 95.
GERHART, J. B., 1954, *Phys Rev.*, **95,** 288.
GOLDBERG, E., 1953, *Phys. Rev.*, **89,** 760.
GREEN, D. W., HARRIS, J. C., and COOPER, J. N., 1954, *Phys. Rev.*, **96,** 817 (A).
HUNT, S. E., JONES, W. M., CHURCHILL, J. L. W., and HANCOCK, D. A., 1954, *Proc. Phys. Soc.* A, **67,** 443.
HUNT, S. E., JONES, W. M., and CHURCHILL, J. L. W., 1954, *Proc. Phys. Soc.* A, **67,** 479.
KING, R. W., and PEASLEE, D. C., 1953, *Phys. Rev.*, **90,** 1001.
KLUYVER, J. C., VAN DER LEUN, C.,and ENDT, P. M., 1954, *Phys. Rev.*, **94,** 1795.
KOERTS, L., SCHWARZSCHILD, A., GOLD, R., and WU, C. S., 1954, *Phys. Rev.*, **95,** 612 (A).
KOFOED-HANSEN, O., 1953, *Phys. Rev.*, **92,** 1075.
MOSZKOWSKI, S. A., and PEASLEE, D. C., 1954, *Phys. Rev.*, **93,** 455.
SIMANTON, J. R., RIGHTMIRE, R. A., LONG, A. L., and KOHMAN, T. P., 1954, *Phys. Rev.*, **96,** 1711.
SLÄTIS, H., and SIEGBAHN, K., 1950, *Arkiv f. Fysik,* **1,** 339.

LXXVI. *The Bond Lengths of Unsaturated Hydrocarbons*

By HERBERT D. DEAS *
St. Salvator's College, The University of St. Andrews†

[Received December 15, 1954]

SUMMARY

The standard excited state approximation for an unsaturated hydrocarbon molecule is used to determine the equilibrium configuration of the nuclei of the molecule. Each bond length of the molecule is shown to depend, to an approximation, on a scalar quantity, called bond order, which is characteristic of the bond. This concept of bond order is numerically equal to that of π-bond order used by Coulson and others. The quantum mechanical formulation gives the form of the bond order–bond length relation, but its actual shape is determined from the known bond lengths of naphthalene and anthracene.

§ 1. THE EQUILIBRIUM CONFIGURATION OF A MOLECULE

THE quantum mechanical Hamiltonian of a molecule consisting of M nuclei and N electrons, in atomic units, and with spin interactions neglected, is

$$\mathscr{H}=-\tfrac{1}{2}\sum_{\alpha=1}^{M} M_{\alpha}{}^{-1}\Delta_{\alpha}-\tfrac{1}{2}\sum_{i=1}^{N}\Delta_{i}-\tfrac{1}{2}\sum_{\alpha=1}^{M}\sum_{j=1}^{N} r_{\alpha i}^{-1}Z_{\alpha}+\sum_{\alpha>\beta}^{M}\sum^{M} r_{\alpha\beta}^{-1}Z_{\alpha}Z_{\beta}+\sum_{i>j}^{N}\sum^{N} r_{ij}^{-1}. \quad . \quad . \quad . \quad (1.1)$$

M_{α}, Z_{α} are the mass and charge of the αth nucleus ; $r_{\alpha\beta}$, r_{ij} are internuclear and interelectronic distances respectively ; and $r_{i\alpha}$ is the distance between the ith electron and the αth nucleus. $\mathscr{H}$ may be written as the sum, $\mathscr{H}_{e}+\mathscr{H}_{n}$ of electronic and nuclear Hamiltonians,

$$\mathscr{H}_{n}=-\tfrac{1}{2}\sum_{\alpha=1}^{M} M_{\alpha}^{-1}\Delta_{\alpha}+\sum_{\alpha>\beta}^{M}\sum^{M} r_{\alpha\beta}^{-1}Z_{\alpha}Z_{\beta}, \quad . \quad . \quad . \quad . \quad . \quad . \quad . \quad (1.2)$$

$$\mathscr{H}_{e}=\sum_{i=1}^{N} H_{i}+\sum_{i>j}^{N}\sum^{N} r_{ij}^{-1}, \quad . \quad . \quad . \quad . \quad . \quad . \quad . \quad . \quad . \quad . \quad . \quad . \quad (1.3)$$

where

$$H_{i}=-\tfrac{1}{2}\Delta_{i}\ \sum_{\alpha-1}^{M} r_{i\alpha}^{-1}Z_{\alpha}. \quad . \quad . \quad . \quad . \quad . \quad . \quad . \quad . \quad . \quad . \quad (1.4)$$

The wave function of the whole molecule may be written as $\Psi=\Psi_{e}\,.\,\Psi_{n}$, where Ψ_{n} involves only the nuclear co-ordinates, $\mathscr{H}_{e}\Psi_{e}=E\,.\,\Psi_{e}$ and E is an eigenvalue of the electronic energy. Then the Schroedinger equation for the whole molecule,

---

* Now at The University of Sheffield.

† Communicated by the Author.

$$\mathscr{H}\Psi=E_m\Psi,$$

becomes

$$\Psi_e\mathscr{H}_n\Psi_n+E\Psi_e.\Psi_n-\left\{\sum_{\alpha=1}^{M} M_\alpha^{-1}\nabla_\alpha\Psi_e.\nabla_\alpha\Psi_n-\sum_{\alpha=1}^{M} M_\alpha^{-1}\Psi_n\Delta_\alpha\Psi_e\right\}$$
$$=E_m.\Psi_e\Psi_n. \quad . \quad . \quad . \quad . \quad . \quad (1.6)$$

E_m is the total molecular energy. If the terms in the brackets are neglected, because Ψ_e is a slowly varying function of the nuclear co-ordinates (Born–Oppenheimer approximation), (1.6) becomes

$$\left\{-\tfrac{1}{2}\sum_{\alpha=1}^{M} M_\alpha^{-1}\Delta_\alpha+\sum_{\alpha>\beta}^{M}\sum^{M} r_{\alpha\beta}^{-1}Z_\alpha Z_\beta+E\right\}\Psi_n=E_m\,\Psi_n. \quad . \quad . \quad . \quad (1.7)$$

Hence, in the equation of the nuclear motion, the potential term is

$$\mathscr{E}=\sum_{\alpha>\beta}\sum r_{\alpha\beta}^{-1}Z_\alpha Z_\beta+E. \quad . \quad . \quad . \quad . \quad . \quad . \quad . \quad (1.8)$$

$\mathscr{E}$ is a function of the nuclear positions through all its terms. If the molecule is stable there exists a nuclear configuration for which $\mathscr{E}$ is a minimum, and about this configuration nuclear vibrations take place.

In this paper the *standard excited state approximation* to the molecular orbital theory of the electronic structure of an unsaturated hydrocarbon, developed by Hall (1952 a), has been used to determine this equilibrium configuration. Arising out of this formulation, it appears that a bond in an unsaturated hydrocarbon can be characterized by a scalar quantity called *bond order* (so called because it is numerically the same as the π-bond order used previously by Coulson and others), such that the bond lengths are, to an approximation, a function of this parameter alone. The form of the bond order–bond length relation is derived from the quantum mechanical formulation; its actual shape is determined by fitting this curve to the very accurate values of the bond lengths of naphthalene and anthracene, obtained by Ahmed and Cruickshank (1952) by a critical revision of the very accurate X-ray determinations by Robertson and his co-workers (Robertson 1951).

While it is obvious that this treatment of the problem owes much to previous theories, reviewed by Lennard-Jones (1951) and Coulson (1951), it is *logically* independent of them, having a different starting point in the standard excited state approximation for unsaturated hydrocarbons.

§ 2. THE STANDARD EXCITED STATE APPROXIMATION

The molecular orbital theory of molecular structure (Lennard-Jones 1949, Lennard-Jones and Hall 1951 a) assumes that the total electronic wave function of the molecule may be written as a single determinant of the form

$$\Psi_e=(N\,!)^{-1/2}\det\{\phi_1(\boldsymbol{\tau}_1),\phi_2(\boldsymbol{\tau}_2),\phi_3(\boldsymbol{\tau}_3),\ldots\phi_N(\boldsymbol{\tau}_N)\}, \qquad (2.1)$$

where $\boldsymbol{\tau}_1, \boldsymbol{\tau}_2 \ldots \boldsymbol{\tau}_N$ represent the co-ordinates, including spin, of each of N electrons, and $\phi_1, \phi_2 \ldots \phi_N$ are an ortho-normal set of functions, called *spin orbitals*, which are each functions of the co-ordinates of only one electron. Each spin orbital, $\phi_r(\boldsymbol{\tau}_s)$, is assumed to factorize into a space dependent part, the *space orbital*, $\chi_r(\mathbf{x}_s)$, and a spin dependent factor, which can be either of the two possible electron spin functions $\alpha(\sigma_s)$ and $\beta(\sigma_s)$; in a molecule each space orbital, $\chi_r(\mathbf{x}_s)$, may give rise to either one or two of the spin orbitals, $\chi_r(\mathbf{x}_s)\,\alpha(\sigma_s)$ and $\chi_r(\mathbf{x}_s)\,\beta(\sigma_s)$, and accordingly the space orbital is said to be *singly* or *doubly occupied.* The expression (2.1) is a valid wave function only if all the orbitals are doubly occupied, or if all the singly occupied orbitals have the same spin. Further, Ψ_e satisfies the variation equation (e.g. Corson, ch. x),

$$\delta\int \Psi_e\ \mathscr{H}_e \Psi_e\, d\boldsymbol{\tau}=0 \qquad . \quad . \quad . \quad . \quad . \quad . \quad . \qquad (2.2)$$

which gives rise to the integro-differential equations for the orbitals (Hall 1952 a):

$$[H+V+\mathscr{A}'+\mathscr{A}'']\chi_\nu(\mathbf{x})-\sum_{\bar{\mu}}^{d} e_{\bar{\mu}\nu}\chi_{\bar{\mu}}(\mathbf{x})-\sum_{\mu}^{s} e_{\mu\nu}\chi_{\mu}(\mathbf{x})=0, \quad . \quad . \quad . \quad (2.3')$$

$$[H+V+\tfrac{1}{2}\mathscr{A}'+\mathscr{A}'']\chi_{\bar{\nu}}(\mathbf{x})-\sum_{\bar{\mu}}^{d} e_{\bar{\mu}\bar{\nu}}\chi_{\bar{\mu}}(\mathbf{x})-\tfrac{1}{2}\sum_{\mu}^{s} e_{\mu\bar{\nu}}\chi_{\mu}(\mathbf{x})=0. \quad . \quad . \quad (2.3'')$$

In writing these equations the orbitals have been divided into two sets of (i) s singly occupied orbital χ_α, χ_β . . . . and (ii) d doubly occupied orbitals $\chi_{\bar{\alpha}}$, $\chi_{\bar{\beta}}$, ... Greek subscripts are used for singly occupied orbitals; Greek subscripts overscored for doubly occupied orbitals when such a distinction is made; and italic subscripts when no such distinction is intended. A sufficient condition for the consistency of the orbital eqns. (2.3) is that the doubly and singly occupied orbitals belong to different irreducible representations of the symmetry group of the molecule: in the case of flat molecules (which are the only molecules considered here) this is realized if the doubly occupied orbitals are symmetrical (σ-orbitals) and the singly occupied ones are anti-symmetrical (π-orbitals) in the plane of the molecule. These group theoretic conditions imply that $e_{\mu\bar{\nu}}=e_{\bar{\mu}\nu}=0$. The remaining terms in the equation are defined as usual, except that, in this paper, the role of singly and doubly dashed quantities is reversed in order that quantities arising from singly occupied orbitals are singly dashed, and those from doubly occupied orbitals are doubly dashed. Thus:

$$\left.\begin{aligned}
e_{\mu\nu}&=\int\bar{\chi}_\mu(\mathbf{x})[H+V+\mathscr{A}'+\mathscr{A}'']\,\chi_\nu(\mathbf{x})\,d\mathbf{x},\\
e_{\bar{\mu}\bar{\nu}}&=\int\bar{\chi}_{\bar{\mu}}(\mathbf{x})[H+V+\tfrac{1}{2}\mathscr{A}'+\mathscr{A}'']\,\chi_{\bar{\nu}}(\mathbf{x})\,d\mathbf{x},\\
V&=\tfrac{1}{2}\mathscr{V}'+\mathscr{V}'',\\
\mathscr{V}'&=2\sum_{\mu} g_{\mu\mu}(\mathbf{x}),\quad \mathscr{V}''=2\sum_{\bar{\mu}} g_{\bar{\mu}\bar{\mu}}(\mathbf{x}),\\
g_{mn}(\mathbf{x}_i)&=\int\bar{\chi}_m(\mathbf{x}_j)\,r_{ij}^{-1}\,\chi_n(\mathbf{x}_j)\,d\mathbf{x}_j,\\
\mathscr{A}'\psi_n(\mathbf{x})&=-\sum_{\alpha} g_{\alpha n}(\mathbf{x})\,\psi_\alpha(\mathbf{x}),\quad \mathscr{A}''\psi_n(\mathbf{x})=-\sum_{\bar{\alpha}} g_{\bar{\alpha}n}(\mathbf{x})\,\psi_{\bar{\alpha}}(\mathbf{x}):
\end{aligned}\right\} \quad . \quad . \quad . \quad (2.4)$$

H is the operator H_i (1.4) without the subscript.

Neither the form nor the value of Ψ_e is changed if the space orbitals are replaced by a new set,

$$\psi_l = \sum_m t_{lm}\,\chi_m \quad . \; . \; . \; . \; . \; . \; . \; . \qquad (2.5)$$

provided that $t_{\alpha\bar{\beta}}=t_{\bar{\alpha}\beta}=0$. The orbital equations for the ψ_r orbitals have the same form as those for χ_r, except that E_{mn} replaces e_{mn} where

$$E_{mn} = \sum_r \sum_s \bar{t}_{mr}\,t_{ns}\,e_{rs}. \quad . \; . \; . \; . \; . \; . \; . \; . \qquad (2.6)$$

The special set of orbitals for which the E_{ij}-matrix has diagonal form are called *molecular orbitals*. These orbitals have appreciable values throughout the molecule ; and $-E_{ii}$ is the *vertical ionization potential* of the electron in the corresponding orbital. A set of orbitals which transform into each other under the symmetry covering operations of the molecule are said to be *equivalent*. Equivalent orbitals often have a highly localized character, which may lead to very useful approximations.

The ground state of an unsaturated hydrocarbon (all orbitals doubly occupied) can be discussed in the manner above like any other molecule ; but, when the electrons are considered as distributed in doubly occupied orbitals corresponding to bonds, inner shells and lone pairs, there is usually one electron per carbon atom remaining over. These cannot be distributed in doubly occupied, localized, equivalent orbitals without reducing the symmetry of the molecule ; hence, the straight-forward treatment of the ground state is more involved for an unsaturated hydrocarbon than for a saturated one.

The *standard excited state* of an unsaturated hydrocarbon is defined as one in which all the doubly occupied orbitals of bonds, inner shells and lone pairs are σ-orbitals and the one remaining electron per carbon atom is associated with a singly occupied π-orbital, highly localized about each carbon atom. The π-orbitals usually divide into sets of equivalent orbitals. Molecules in the standard excited state may not have an equilibrium configuration, but the stable existence of the molecule in this state is not required by the subsequent use made of its orbitals. The standard excited state is an example of the general case discussed above. The σ-orbitals have all a localized character, and therefore may be assumed, approximately, to be molecular orbitals. By a similar approximation the localized character of π-orbitals gives rise to a simplified $e_{\alpha\beta}$-matrix : in particular, $e_{\alpha\beta}=0$ approximately if α, β are neither equal nor are nearest neighbours (the labelling of the equivalent orbitals and the nuclei coincides conveniently). The π-molecular orbitals are

$$\psi_\mu = \sum_\nu^s t_{\mu\nu}\,\chi_\nu, \quad \mu=1, 2, \ldots . s, \quad . \; . \; . \; . \; . \; . \qquad (2.7)$$

where the χ's are the localized π-orbitals, and $t_{\mu 1}, t_{\mu 2}, \ldots t_{\mu s}$ are the solutions, for each of the possible values, 1, 2, 3, ... s, of μ, of the set of equations,

$$\sum_\nu^s \left(e_{\lambda\nu}-\delta_{\lambda\nu}E_{\mu\mu}\right) t_{\mu\nu}=0, \quad \lambda=1, 2, \ldots . s. \quad . \; . \; . \; . \; . \qquad (2.8)$$

E_{11}, E_{22}, E_{33}, ... , are the solutions for E, arranged in increasing order, of the secular equations

$$|\, e_{\lambda\mu} - \delta_{\lambda\mu} E \,| = 0. \qquad \ldots\ldots \qquad (2.9)$$

Each of the eigenvectors $(t_{\mu 1}, t_{\mu 2}, \ldots . t_{\mu s})$ of (2.8) is normalized to unity, so that, by a general algebraic result, $[t_{\alpha\beta}]$ is a unitary matrix ; and, as $[e_{\alpha\beta}]$ is a real symmetrical matrix, $[t_{\alpha\beta}]$ is real too.

The *standard excited state approximation* to the ground state of an unsaturated hydrocarbon molecule makes use of the molecular orbitals of the same molecule, with the same nuclear configuration, but in the standard excited state : the nuclear configuration need not be an equilibrium configuration of either state. The molecular orbitals of the ground state are taken to be the σ-molecular orbitals of the corresponding standard excited state, doubly occupied, together with as many of the π-molecular orbitals of the standard excited state as are required, also doubly occupied, to accommodate the remaining electrons, the π-orbitals associated with the smaller vertical ionization potential being chosen so as to give the most stable molecule. Thus, only the first half, say $p = \frac{1}{2}s$, of the standard excited state π-orbitals are used in the ground state.

§ 3. THE ENERGY OF AN UNSATURATED HYDROCARBON MOLECULE

The total electronic energy of an unsaturated hydrocarbon is, on the standard excited state approximation,

$$E = \sum_{\bar{\alpha}}^{d} (H_{\bar{\alpha}\bar{\alpha}} + E^{*}_{\bar{\alpha}\bar{\alpha}}) + \sum_{\alpha}^{s/2} (H_{\alpha\alpha} + E^{*}_{\alpha\alpha}). \qquad \ldots\ldots \qquad (3.1)$$

The first summation is the energy due to the σ-electrons and the second is the energy of the π-electrons. The theory of the approximation (Hall 1952 a) gives, by a perturbation treatment,

$$\begin{aligned} E^{*}_{\bar{\alpha}\bar{\beta}} = E_{\bar{\alpha}\bar{\beta}} &+ \sum_{\gamma=1}^{p} [(\psi_{\gamma}\, \psi_{\bar{\alpha}} | G | \psi_{\gamma}\, \psi_{\bar{\beta}}) - \tfrac{1}{2}(\psi_{\gamma}\, \psi_{\bar{\alpha}} | G | \psi_{\bar{\beta}}\, \psi_{\gamma})] \\ &- \sum_{\gamma=p+1}^{2p} [(\psi_{\gamma}\, \psi_{\bar{\alpha}} | G | \psi_{\gamma}\, \psi_{\bar{\beta}}) - \tfrac{1}{2}(\psi_{\gamma}\, \psi_{\bar{\alpha}} | G | \psi_{\bar{\beta}}\, \psi_{\gamma})] \qquad \ldots\ldots \qquad (3.2) \end{aligned}$$

and

$$\begin{aligned} E^{*}_{\bar{\alpha}\bar{\alpha}} = E_{\alpha\alpha} &+ \sum_{\gamma=1}^{p} (\psi_{\gamma}\, \psi_{\alpha} | G | \psi_{\gamma}\, \psi_{\alpha}) \\ &- \sum_{\gamma=p+1}^{2p} [(\psi_{\gamma}\, \psi_{\alpha} | G | \psi_{\gamma}\, \psi_{\alpha}) - (\psi_{\gamma}\, \psi_{\alpha} | G | \psi_{\alpha}\, \psi_{\gamma})] \qquad \ldots\ldots \qquad (3.3) \end{aligned}$$

where

$$(\psi_{l}\, \psi_{m} | G | \psi_{n}\, \psi_{p}) = \int \bar{\psi}_{l}(\mathbf{x}_{i})\, \bar{\psi}_{m}(\mathbf{x}_{j})(1/r_{ij})\, \psi_{n}(\mathbf{x}_{i})\, \psi_{p}(\mathbf{x}_{j})\, d\mathbf{x}_{i}\, d\mathbf{x}_{j}. \qquad \ldots \qquad (3.4)$$

In (3.2) the two summations, being approximately equal, may be neglected ; and similarly, in (3.3) the two summations over the coulomb integrals, $(\psi_{\gamma}\, \psi_{\alpha} | G | \psi_{\gamma}\, \psi_{\alpha})$, cancel approximately : so that

$$\begin{aligned} E \simeq \sum_{\bar{\alpha}}^{d} (H_{\bar{\alpha}\bar{\alpha}} + E_{\bar{\alpha}\bar{\alpha}}) + \sum_{\alpha=1}^{p} (H_{\alpha\alpha} + E_{\alpha\alpha}) + \sum_{\alpha=1}^{p} \sum_{\gamma=p+1}^{2p} (\psi_{\gamma}\, \psi_{\alpha} | G | \psi_{\alpha} \psi_{\gamma}) \qquad \ldots \qquad (3.5) \\ = \mathscr{E}_{\sigma} + \mathscr{E}_{\pi}^{(1)} + \mathscr{E}_{\pi}^{(2)}. \qquad \ldots\ldots\ldots \qquad (3.6) \end{aligned}$$

These contributions to the energy are now considered separately :

(*a*) *The contribution of the σ-electrons* is

$$\mathscr{E}_\sigma = \underset{\substack{\bar{\alpha} \\ \text{(inner shells)}}}{\Sigma} (H_{\bar{\alpha}\bar{\alpha}} + E_{\bar{\alpha}\bar{\alpha}}) + \underset{\substack{\bar{\alpha} \\ (\sigma\text{-bonds})}}{\Sigma} (H_{\bar{\alpha}\bar{\alpha}} + E_{\bar{\alpha}\bar{\alpha}}). \qquad (3.7)$$

$$= U_0 + \sum_{\lambda, \mu} N_{\lambda\mu} U_{\lambda\mu}. \qquad (3.8)$$

U_0, the contribution of the inner shell orbitals, may be assumed constant. $U_{\lambda\mu} = H_{\bar{\alpha}\bar{\alpha}} + E_{\bar{\alpha}\bar{\alpha}}$ where λ, μ are the nuclei at the ends of the σ-bond whose orbital is $\psi_{\bar{\alpha}}$. $N_{\lambda\mu} = 1$, when the nuclei λ, μ are (bonded) nearest neighbours ; otherwise $N_{\lambda\mu} = 0$.

(*b*) *The first contribution of the π-electrons* is

$$\mathscr{E}_\pi^{(1)} = \sum_{\alpha=1}^{p} (H_{\alpha\alpha} + E_{\alpha\alpha}) \qquad (3.9)$$

which, expressed in terms of the equivalent orbitals by eqn. (2.7), is

$$\mathscr{E}_\pi^{(1)} = \sum_{\lambda=1}^{2p} \sum_{\mu=1}^{2p} \left(\sum_{\alpha=1}^{p} \bar{t}_{\alpha\lambda} t_{\alpha\mu} \right) (e_{\lambda\mu} + h_{\lambda\mu})$$

$$= \tfrac{1}{2} \sum_{\lambda=1}^{2p} \sum_{\mu=1}^{2p} p_{\lambda\mu} (e_{\lambda\mu} + h_{\lambda\mu}), \qquad (3.10)$$

where

$$p_{\lambda\mu} = 2 \sum_{\alpha=1}^{p} \bar{t}_{\alpha\lambda} t_{\alpha\mu} \qquad (3.11)$$

is called the *bond order* of the bond between nuclei λ and μ. The nuclear electrostatic interaction energy, i.e. the summation in eqn. (1.8), may be included in $\mathscr{E}_\pi^{(1)}$ by replacing $h_{\lambda\mu}$ by $u_{\lambda\mu}$ as defined by Hall (1952 b). Further, sizeable contributions to (3.10) arose only where either $\lambda = \mu$ (which contributions are independent of the nuclear configuration), or λ, μ are nearest neighbours ; so, approximately,

$$\mathscr{E}_\pi^{(1)} = V_0 + \sum_{\lambda, \mu} N_{\lambda\mu} p_{\lambda\mu} V_{\lambda\mu}, \qquad (3.12)$$

where $2V_{\lambda\mu} = (e_{\lambda\mu} + u_{\lambda\mu})$ and V_0 is a constant.

(*c*) *The second contribution of the π-electrons*,

$$\mathscr{E}_\pi^{(2)} = \sum_{\alpha=1}^{p} \sum_{\beta=p+1}^{2p} (\psi_\gamma \psi_\alpha | G | \psi_\alpha \psi_\gamma) \qquad (3.13)$$

becomes, using (2.7) and writing $(\chi_\alpha \chi_\beta | G | \chi_\gamma \chi_\delta) = (\alpha\beta | G | \gamma\delta)$,

$$\mathscr{E}_\pi^{(2)} = \sum_{\lambda, \mu}^{2p} \sum_{\nu, \omega}^{2p} \left(\sum_{\alpha=1}^{p} t_{\alpha\lambda} t_{\alpha\mu} \right) \left(\sum_{\beta=p+1}^{2p} \bar{t}_{\beta\nu} t_{\beta\omega} \right) (\nu\lambda | G | \mu\omega). \qquad (3.14)$$

But (2.7) is a real unitary transformation, so $p_{\lambda\mu} = p_{\mu\lambda}$ and

$$\sum_{\beta=1}^{p} \bar{t}_{\beta\nu} t_{\beta\omega} + \sum_{\beta=p+1}^{2p} \bar{t}_{\beta\nu} t_{\beta\omega} = \delta_{\nu\omega}. \qquad (3.15)$$

Hence

$$\mathscr{E}_\pi^{(2)} = \tfrac{1}{4} \sum_{\lambda, \mu}^{2p} \sum_{\nu\omega}^{2p} p_{\lambda\mu} (2\delta_{\nu\omega} - p_{\omega\nu}) (\nu\lambda | G | \mu\omega). \qquad (3.16)$$

Only the coulomb integrals, i.e. those for which $\mu=\nu$, $\lambda=\omega$, in this expression have appreciable values (Pariser and Parr 1953, Hall 1954); so

$$\mathscr{E}_\pi^{(2)} \simeq \tfrac{1}{4} \sum_{\lambda,\mu}^{2p} p_{\lambda\mu}\,(2\delta_{\lambda\mu}-p_{\lambda\mu})(\mu\lambda\,|G|\,\mu\lambda)$$
$$=W_0+\sum_{\lambda\neq\mu}^{2p} p^2_{\lambda\mu}\,W_{\lambda\mu}. \quad \dots \dots \quad (3.17)$$

W_0 is a constant, being the contribution to (3.16) for $\lambda=\mu$ and $4W_{\lambda\mu}=(\mu\lambda\,|G|\,\mu\lambda)$. Further coulomb integrals not arising from nearest neighbour equivalent orbitals may be neglected, giving

$$\mathscr{E}_\pi^{(2)} \simeq W_0+\sum_{\lambda,\mu} N_{\lambda\mu}\,p_{\lambda\mu}{}^2\,W_{\lambda\mu}. \quad \dots \dots \quad (3.18)$$

Hence the total energy of the molecule (1.9) is, approximately,

$$\mathscr{E}=\mathscr{E}_0+\sum_{\lambda}^{2p}\sum_{\mu}^{2p} N_{\lambda\mu}\,[U_{\lambda\mu}+p_{\lambda\mu}\,V_{\lambda\mu}+p_{\lambda\mu}{}^2\,W_{\lambda\mu}], \quad \dots \quad (3.19)$$

where $\mathscr{E}_0=U_0+V_0+W_0$ is a constant.

It is now assumed that the functions $U_{\lambda\mu}$, $V_{\lambda\mu}$, $W_{\lambda\mu}$ are: (i) independent of λ, μ; (ii) independent of the particular conjugated hydrocarbon in which they arise; (iii) functions of only the corresponding bond length: then, if they are written as $\mathscr{E}_1$, $\mathscr{E}_2$, $\mathscr{E}_3$ respectively, the total energy of any unsaturated hydrocarbon molecule is

$$\mathscr{E}=\mathscr{E}_0+\sum_{l=1}^{L}[\mathscr{E}_1(r_l)+p_l\,\mathscr{E}_2(r_l)+p_l{}^2\mathscr{E}_3(r_l)]. \quad \dots \quad (3.20)$$

Here r_l and p_l, ($l=1, 2, \dots L$), are the bond lengths and bond orders of the L bonds of the molecule. A necessary condition for an equilibrium configuration of the molecule is that, for $l=1, 2, \dots L$,

$$\frac{\partial\mathscr{E}}{\partial r_l}=\frac{\partial}{\partial r_l}\,\mathscr{E}_1(r_l)+p_l\frac{\partial}{\partial r_l}\,\mathscr{E}_2(r_l)+p_l{}^2\frac{\partial}{\partial r_l}\,\mathscr{E}_3(r_l)$$
$$+\sum_{k=1}^{L}\frac{\partial p_k}{\partial r_l}[\mathscr{E}_2(r_k)+2p_k\,\mathscr{E}_3(r_k)]=0. \quad \dots \dots \quad (3.21)$$

The values of r_1, r_2, $\dots r_L$, for which these equations are true, are the equilibrium bond lengths of the molecule.

§ 4. Bond Orders and Equi-Bond Orders

The calculation of the bond orders of all the bonds of a molecule requires the solution of the equations (2.8) for some of the roots of the secular eqn. (2.9). If the values of $e_{\alpha\beta}$ are known for the molecule concerned, this is a matter of algebra involving no formal difficulty but considerable labour, especially if each $e_{\alpha\beta}$ varies with molecular size. But generally the values of $e_{\alpha\beta}$ are not known. Previous theories, faced with a similar problem, proceeded on the assumptions that $e_{\alpha\alpha}=a$, for all α, $e_{\alpha\beta}=b$ for all α, β which are nearest neighbours and $e_{\alpha\beta}=0$ for all other cases. This greatly simplifies the solution of the secular equation, since, putting $x=(a-E)/b$ and diving each row by b, the determinant has x in the diagonal and either zero or unity elsewhere. Such secular equations can often be solved by special algebraic methods (Rutherford 1947, 1952). In any case, the problem is essentially numerical and the values of the bond orders are independent of the values of a and b. The bond orders of many molecules have been calculated under these assumptions in connection with previous theories.

On the assumptions of the present discussion, bond orders calculated in this manner are the bond orders of a molecule all of whose bonds are equal, since, in the derivation of (3.21), $e_{\alpha\alpha}$, etc. have been assumed to be the same function of bond length, from bond to bond. For this reason, these bond orders are called *equi-bond orders*. Their values depend on the bond in question but are unaffected by the actual size of the molecule, provided all the bonds are equal; they depend on the connectivity of the σ-bonds of the molecule and are essentially a topological property of the molecule. In an actual molecule, bond orders differ from equi-bond orders because of the small variation of the bond lengths; but here it is assumed that these variations in bond order are small compared with the variation of equi-bond order from bond to bond, and that equi-bond orders may be used in (3.21) as good approximations to the actual bond orders. This is equivalent to assuming that p_l depends only on the bond l, and is independent of small variations of the bond length from its equilibrium distance. To avoid confusion, it should be pointed out that this paper establishes a relation between the *equilibrium* lengths of *different* bonds and their respective bond orders, while the above assumption is concerned with the *changes* in bond order of *one particular bond* when all the bond lengths are slightly different from the equilibrium configuration. The numerical values of the bond orders used here are the same as the π-bond orders defined by Coulson (1939), so that not only may the previous calculations of them for several molecules be used, but their application to other topics, e.g. free valance and carcinogens (Coulson 1953), remains the same.

§ 5. BOND ORDER–BOND LENGTH RELATION

Since bond order depends only on the bond, the summation in (3.21) vanishes, giving

$$\frac{d\mathscr{E}_1(r)}{dr}+p\frac{d\mathscr{E}_2(r)}{dr}+p^2\frac{d\mathscr{E}_3(r)}{dr}=0 \quad . \quad . \quad . \quad . \quad . \quad . \quad . \quad (5.1)$$

as the equation relating the equilibrium length r of a bond to the bond order p. This is the new bond order–bond length relation. Its actual form depends on the functions $\mathscr{E}_1(r)$, $\mathscr{E}_2(r)$, $\mathscr{E}_3(r)$, which, though defined in the derivation given here, cannot be expressed easily in analytic form. The best that can be done is to adopt the semi-empirical method and find the form of these functions by fitting the relation (5.1) to experimentally determined values of bond lengths and calculated bond orders.

Let r_0 be a length approximately equal to the mean length of the bonds of unsaturated hydrocarbon molecules. Putting $r=r_0+\rho$, and expanding $d\mathscr{E}_1/dr$, $d\mathscr{E}_2/dr$, $d\mathscr{E}_3/dr$ about $r=r_0$ as

$$\left.\begin{aligned}\frac{d\mathscr{E}_1}{dr}&=a_1+b_1\rho+\dots\\ \frac{d\mathscr{E}_2}{dr}&=a_2+b_2\rho+\dots\\ \frac{d\mathscr{E}_3}{dr}&=a_3+b_3\rho+\dots\end{aligned}\right\} \quad . \; . \; . \; . \; . \; . \quad (5.2)$$

and neglecting terms of second order in ρ, (5.1) becomes

$$r=r_0-\left[\frac{a_1+a_2p+a_3p^2}{b_1+b_2p+b_3p^2}\right]. \quad . \; . \; . \; . \; . \; . \quad (5.3)$$

This is the approximate form of the new bond order–bond length relation. This relation can be fitted to the experimental data by finding the values of a_1, a_2, a_3, b_1, b_2, b_3, for which the expression

$$S=\sum_{l=1}^{n}\left[(a_1+a_2p_i+a_3p_i^2)+\rho_i\,(b_1+b_2p_i+b_3p_i^2)\right]^2 \quad . \; . \; . \quad (5.4)$$

has a minimum value : p_i is the calculated bond order and ρ_i is the experimentally determined value of ρ for each of the n bonds used in the curve fitting. One of the coefficients in (5.3) can be put equal to unity without loss of generality ; here $b_1=1$. The fitting procedure is essentially the ‘ method of least squares ’ applied to (5.1).

The bond lengths of naphthalene and anthracene, obtained by Ahmed and Cruickshank (1953) from earlier x-ray work by Robertson and others (1951), have been used in an attempt to find suitable values of the a's and b's in this manner. The bond orders of naphthalene have been given by Lennard-Jones and Coulson (1939) and of anthracene by Coulson, Dandel and Robertson (1951). It was found that this gave an absurd result : (5.3) had an asymptote in the middle of the range of p considered. The explanation of this failure is the small number of experimental points available, the small range of p involved and the experimental error in the bond length determinations. The bond lengths of many other unsaturated hydrocarbons are known, but with errors about four times those present in the naphthalene and anthracene determinations. These errors are not large, considered as a fraction of the bond length, but they are considerable when regarded as a fraction of the range of variation of the bond lengths involved : this is true, to some extent, even of the naphthalene and anthracene bond lengths. There is, therefore, little to be gained by increasing the number of experimental points and the range of p by including the bonds of other molecules, though some bonds with large bond order may be useful in spite of the errors.

If the bond lengths of anthracene and naphthalene are plotted against the corresponding bond orders, the shape of the bond order–bond length relation is evident (see fig. 1) : this is particularly so if the bridge bond of naphthalene could be disregarded. There is very little difficulty in drawing a smooth curve through these points. Another point, the 'double' bond of ethylene was added to extend the range of the curve. This bond length, following Coulson, Dandel and Robertson, is taken as 1·34 Å, which is a mean of two experimental determinations (1·331 Å due to Thompson, 1·353 Å due to Gallaway and Baker); the bond order is unity (Lennard-Jones and Coulson 1939, Lennard-Jones and Hall 1951). Such a smooth curve was drawn and a number of points on it, equally spaced in the range $p=0·45$ to $p=1·0$, were used in the fitting procedure outlined above, instead of the experimental points. The result is the bond order–bond length relation

$$r=1·40+\left(\frac{2·27p^2-17·38p+9·70}{176·08p^2-186·08p+100}\right), \quad . \quad . \quad . \quad . \quad . \quad (5.5)$$

which is shown in fig. 1. It is a good fit, with the possible exception of the bridge bond of naphthalene, and it follows closely the hand drawn curve.

Fig. 1

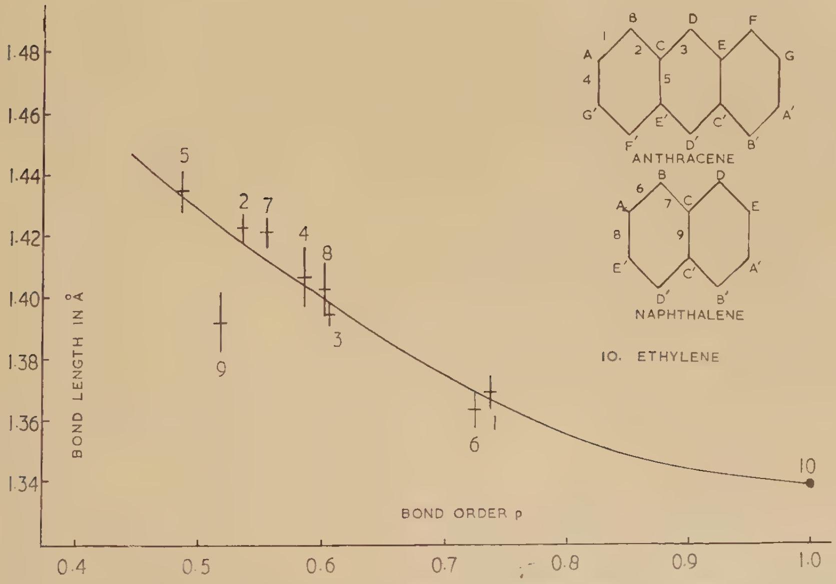

The curve is the bond order–bond length relation given by eqn. (5.5). The points marked are the experimental determined bond lengths given by Ahmed and Cruickshank, with the estimated standard deviation marked off on both sides of the value.

Though this modified procedure is not as satisfactory as a direct fitting, it gives a numerical relation in the form required by the theory. The resulting bond lengths relation is valid only over the range of experimental points used in the fitting. In fact, as p increases (5.5) passes through a minimum and then increases towards its horizontal and only asymptote.

§ 6. Discussion

An important feature of the present theory of bond lengths is the manner in which the notion of bond order occurs in the derivation of the bond order–bond length relation. This notion arises essentially as a parameter in the expression (3.19) for the total energy of a molecule; it is defined, eqn. (3.11), by the molecular orbitals of the standard excited state, and it appears in eqn. (5.1) as the determining parameter for the equilibrium positions of the nuclei. Nowhere is bond order related to the chemical notions of single and double bond: it is only after calculation that it can be asserted that the ethylene 'double' bond has unit π-bond order, and this result is a consequence of the formally unnecessary factor 2 in the definition of bond order. (This factor is included here so that the definition of bond order agrees numerically with Coulson's definition (1939): in his theory the 2 is not without physical significance.) Further, it is not evident that diamond can be regarded as having zero bond order: it is not an unsaturated hydrocarbon, and the molecular orbital treatment of diamond (Hall 1952 c) has no immediate connection with the treatment of unsaturated hydrocarbons upon which this paper is based. There is, therefore, no evident reason to expect the bond order–bond length relation to pass through the diamond bond length for $p=0$. Moreover, the present theory can give no indication of the bond order–bond length relation for values of p lying outside the range of p for which experimentally determined bond lengths are known: in particular, it cannot predict the existence of stable unsaturated hydrocarbons having bonds with very small bond orders. The smallest bond order in a stable molecule known to the author is 0·45 for the 'single' bond of butadiene (Lennard-Jones and Coulson 1939). If unsaturated hydrocarbons with very small bond orders were unstable, the bond order–bond length relation would probably have an asymptote, $p=\text{const.}$, for some small value of p. This does not occur in the present bond order–bond length relation, but there is no reason to suppose that it would not occur in a curve based on more experimental evidence. On the other hand, it is essential to Coulson's theory (1939) that the bond length of diamond lies on the bond order–bond length curve for $p=0$. (In fact, Coulson uses $1+p$ as the variable, adding 1 for the σ-bond orbital.)

From this discussion it is clear that bond order is a concept defined with respect to a particular theory of molecular structure and it should not be assumed that, taken out of this context, it can have any meaning as an intrinsic property of the bond (such as, e.g., length). Though numerically the same, the two concepts of bond order—the one defined here and the other used by Coulson—are essentially different, being imbedded in different theories. Both theories are based on the same mathematical problem of finding the eigenvalues and eigenvectors of the same matrix, but this problem arises for very different reasons in each theory.

ACKNOWLEDGMENTS

The author wishes to thank the Queen's University of Belfast for the award of a Senior Studentship, during the tenure of which he commenced this work in the Department of Theoretical Chemistry, Cambridge. He is indebted for helpful discussions to the late Sir John Lennard-Jones, F.R.S. and Mr. G. G. Hall.

REFERENCES

AHMED, F. R., and CRUICKSHANK, D. W. J., 1952, *Acta Cryst.*, **5**, 852.

CORSON, E. M., 1951, *Perturbation Methods in Quantum Mechanics* (London and Glasgow: Blackie and Sons, Ltd.).

COULSON, C. A., 1939, *Proc. Roy. Soc.* A, **169**, 413; 1951, *Ibid.*, A **207**, 91; 1953, *Advances in Cancer Research*, vol. I (New York: Academic Press Inc.).

COULSON, C. A., DAUDEL, R., and ROBERTSON, J. M., 1951, *Proc. Roy. Soc.* A, **207**, 306.

GALLAWAY, W. S., and BAKER, E. F.. 1942, *J. Chem. Phys.*, **10**, 88.

HALL, G. G., 1952 a, *Proc. Roy. Soc.* A, **213**, 102; 1952 b, *Proc. Roy. Soc.* A, **213**, 113; 1952 c, *Phil. Mag.*, **43**, 338; 1954, *Trans. Faraday Soc.*, **50**, 773.

LENNARD-JONES, Sir J. E., and COULSON, C. A., 1939, *Trans. Faraday Soc.*, **35**, 811.

LENNARD-JONES, Sir J. E., 1951, *Proc. Roy. Soc.* A, **207**, 75.

LENNARD-JONES, Sir J. E., and HALL, G. G., 1951 a, *Faraday Soc. Discussion*, No. 10, p. 18.; 1951 b, *Proc. Roy. Soc.* A, **205**, 357.

PARISER, R., and PARR, R. G., 1953, *J. Chem. Physics*, **21**, 767.

ROBERTSON, J. M., 1951, *Proc. Roy. Soc.* A, **207**, 101.

RUTHERFORD, D. E., 1947, *Proc. Roy. Soc. Edin.* A, **62**, 229; 1952, *Ibid.*, **62**. 232.

THOMPSON, H. W., 1939, *Trans. Faraday Soc.*, **35**, 697.

LXXVII. CORRESPONDENCE

The Bombardment of Chlorine by Nitrogen Ions

By G. W. Greenlees and A. E. Souch
Physics Department, University of Birmingham*

[Received March 17, 1955]

§ 1. Introduction

An investigation has been made of the activities produced by the bombardment of chlorine with the internal nitrogen beam of the 60-in. Nuffield cyclotron. The beam had a continuous energy distribution of maximum energy about 125 MeV with an intensity fall-off by a factor of two for each 10 MeV rise of energy above 50 MeV. A target of fused Li Cl was used. To avoid confusion by activities due to the lithium and oxygen in the target, only activities with mass numbers above chlorine were examined. The target was mounted in a screened probe similar to that described by Checkett *et al.* (1954). A copper screening foil was used.

§ 2. Experimental Method and Results

Chemical separations were made for the elements being investigated and the activities were followed with geiger counters. The decay curves obtained were analysed and the activities present identified by their half-lives. A gross decay curve for the unseparated target was also recorded in an attempt to obtain relative yields.

The identification of the isotopes present by their half-lives was unambiguous after chemical separation except in the case of scandium. The scandium decay curve could be analysed into three half-lives of $\sim$ 90 days, 2·55 days and 3·9 hr. The long lived activity was attributed to ^{46}Sc (85 days) and the 2·55 day activity to ^{44m}Sc (2·4 days). The 3·9 hr. activity could be either or both of ^{43}Sc and ^{44}Sc (3·92 hr. and 4·0 hr. respectively).

The beta-spectrum of the scandium fraction was examined using a simple semi-circular focusing spectrometer with path radius 10 cm. This showed a positron activity with E_{max} $1{\cdot}41 \pm 0{\cdot}07$ MeV in good agreement with the value 1·463 MeV for ^{44}Sc (Bruner and Langer 1950). From the spectrum it was not possible to say if any of the less energetic ^{43}Sc complex spectrum (E_{max} 1·18 MeV) was present.

---

* Communicated by the Authors.

The gamma spectrum of the scandium fraction was examined using a NaI(Tl) crystal and photomultiplier arrangement. This showed a large photopeak at 1·15 Mev which decayed with a half-life of 3·9 hr. indicating that most, if not all, of the 3·9 hr. activity was due to ^{44}Sc (Bruner and Langer 1950, Cuffey 1950). A search was made for the photopeak due to the 0·375 Mev gamma ray from ^{43}Sc (Haskins *et al.* 1952). A small peak was found on the Compton edge of the 0·511 Mev annihilation radiation which decayed with a half-life of about 4 hr. Energy measurements for this peak gave a value 0·385 Mev in good agreement with the accepted value 0·375 Mev. The abundance of ^{43}Sc was computed to be 2% of ^{44}Sc.

^{44m}Sc was identified by its gamma spectrum as well as by half-life meaurements. A mean energy of 0·268 Mev was found for the gamma ray in good agreement with published data (cf. Hollander *et al.* 1953).

Table 1 gives the relative yeilds of the various activities detected. The yields are related to an arbitrary value of 1000 for ^{44}Sc. Those values in brackets are uncertain because of the small activities associated with the long half-lives involved.

Table 1

Activity	Observed $T_{\frac{1}{2}}$	Yield
^{44}Sc	3·9 hrs.	1000
^{44m}Sc	2·55 days	500
^{43}Sc	3·9 hrs.	20
^{46}Sc	90 days	(2400)
^{38}K	10 min.	250
^{38}Cl	35 min.	330
^{39}Cl	52 min.	480
^{49}Cr	39 min.	30–60
^{47}V	41 min.	100–500
^{48}V	16 days	(270)
^{45}Ti	3·2 hrs.	50–220
Ca	—	0

In determining the relative yields no information on the chemical extraction efficiencies was available. These were assumed equal and an attempt was made to check the yields obtained by an analysis of the gross decay curve. Where a range of yield values is given, this indicates discrepancies in the results obtained using different extraction methods and the analysis of the gross decay curve. In general the accuracy of the yields is not better than a factor of two.

§ 3. Discussion

Two possible mechanisms have been suggested to account for the yields of heavy ion reactions : (1) via a compound nucleus (Cohen *et al.* 1954) and (2) by a direct interaction of the ‘ stripping ’ or ‘ buckshot ’ type (Chackett *et al.* 1954). The present results give a qualitative fit with either mechanism. More detailed experiments with monoenergetic beams are required to determine the relative importance of the two processes.

Using the heavy ion beams available from a 60-in. cyclotron, semi-classical wavelength considerations suggest that high values of incident angular momentum would be involved in the reactions. This is borne out by the scandium results where ^{44}Sc and ^{44m}Sc are produced in approximately equal amounts despite the high spin difference between the two levels of ^{44}Sc.

Heavy ion bombardments may prove a useful means of exciting high spin isomeric states not readily produced in normal reactions. By such means it may be possible to produce as yet undetected isomeric states which are expected from shell structure considerations.

ACKNOWLEDGMENTS

The authors wish to thank members of the cyclotron crew for making the bombardments under difficult conditions, Dr. K. F. Chackett for his help in devising chemical separation procedures and Dr. R. G. Freemantle for help with the target preparation.

One of us (A. E. S.) wishes to thank the Department of Scientific and Industrial Research for financial support covering the period of this work.

REFERENCES

BRUNER, J. A., and LANGER, L. M., 1950, *Phys. Rev.*, **79,** 606.
CHACKETT, K. F., FREMLIN, J. H., and WALKER, D., 1954, *Phil. Mag.*, **45,** 173.
COHEN, B. L., REYNOLDS, H. L., and ZUCKER, A., 1954, *Phys.. Rev.*, **96,** 1617.
CUFFEY, W. H., 1950, *Phys. Rev.*, **79,** 180.
HASKINS, J. R., DUVAL, J. E., CHENG, L. S., and KURBATOV, J. D., 1952, *Phys. Rev.*, **88,** 876.
HOLLANDER, J. M., PERLMAN, I., and SEABORG, G. T., 1953, *Rev. Mod. Phys.*, **25,** 469.

LXXVIII. REVIEWS OF BOOKS

X-Ray Diffraction by Polycrystalline Materials. (London: Institute of Physics.) [Pp. 725.] Price 63*s*.

This work, sponsored by the x-ray Analysis Group of the Institute of Physics is issued as one of the volumes of the series Physics in Industry published by the Institute. Although it deals with only one branch of crystal analysis, the study of polycrystalline materials, the volume of 32 chapters and an appendix of useful data has been compiled by 28 British and 3 American authors, each qualified to write with authority on one or more of the many aspects of the subject which are covered.

Space does not permit of a detailed review of this comprehensive and wholly admirable work. Its general nature can be judged from the fact that ten of the authors work in industrial laboratories, nine in Universities, five in Colleges of Technology, four in Government Establishments, two in Research Associations and one in the Royal Institution.

The last nine chapters of the book are in the form of essays showing how the methods described in the earlier chapters can be applied in many different scientific fields. The technical editors Messrs. Peiser, Rooksby and A. J. C. Wilson are to be congratulated on the satisfactory completion of a formidable task, presented in the customary high quality of publications of the Institute of Physics. It is clear that it will remain a standard work of reference for many years to come.
A. M. T.

Advances in Electronics and Electron Physics, Vol. VI, 1954. [Pp. xi+538.] (Academic Press, New York.) $11.80.

This volume continues the series *Advances in Electronics* under an expanded title which is thought to describe its contents more accurately. Certainly the net is cast wide, to include "Metallic Conduction at High Frequencies and Low Temperatures" (A. B. Pippard); "Relaxation Processes in Ferromagnetism" (Elihu Abrahams); "Physical Properties of Ferrites" (J. Smit and H. P. J. Wijn); "Space Charge Limited Currents" (H. F. Ivey); "A Comparison of Analogous Semiconductor and Gaseous Electronics Devices" (W. M. Webster); "The Electron Microscope—A Review" (M. E. Haine); "Travelling-Wave Tubes" (R. G. E. Hutter); "Paramagnetism" (J. Van Den Handel). Indeed the variety of topics may be so great that few individuals will care to pay this price just for the one or two articles in which they are interested. The production is lavish, including name and author indices to the whole volume; one wonders whether it might not be better to publish the articles separately and cheaply, perhaps in paper covers, the whole being bound together only in a library edition.
J. M. Z.

Superfluids: Macroscopic Theory of Superfluid Helium, Vol. II. By F. London. [Pp. xvi+217.] (Chapman & Hall.) Price 64*s*.

At the time of his death in March 1954 Fritz London was still at the height of his intellectual powers. This posthumous second volume of *Superfluids* is a lasting memorial to the importance of his contributions to, and the depth of his understanding of, the problem of liquid helium, which he first began to investigate about 1936 and which remained his chief interest until the end. Although both volumes purport in their titles to be concerned with macroscopic theory, of superconductivity and superfluid helium respectively, they do in fact differ considerably in their approach. The former was indeed almost wholly taken up with the macroscopic description of superconductors without more than the most general observations on the possible microscopic explanation of the phenomena. The latter, on the other hand, devotes considerable space to genuinely microscopic matters, such as the atomic structure of the liquid and the extent to which it may resemble a degenerate Bose–Einstein gas. This difference reflects the different approaches which have been made to the two problems: repeated failure to achieve a microscopic theory of superconductivity has encouraged the development of a phenomenological picture, while with liquid helium the phenomenological treatment has tended to arise from more or less successful attempts at formulating a microscopic theory. It is only natural that the distinction between microscopic and macroscopic should have become somwehat blurred. Nevertheless the emphasis of the second volume is still predominantly macroscopic in so far as the most important single topic treated is the two-fluid model of helium, originally suggested by Tisza. The model is presented with historical truth as springing from London's analogy of the λ-point with the temperature at which a Bose–Einstein gas becomes degenerate. At the same time the alternative development by Landau and later workers, arising out of the quantum theory of a fluid continuum, is dealt with in lucid detail. There seems to be little doubt now that the two-fluid model gives an adequate description of superfluid helium, and there is general agreement on the form of the hydrodynamical equations so far as the linear terms are concerned. It is in the non-linear, particularly dissipative, effects that discrepancies between theory and experiment become apparent. These matters are given a full treatment, which constitutes a very valuable section of the book. There is also a detailed discussion of the prcperties of liquid helium–3 and mixtures of the two isotopes.

So long as a complete solution of the problem of liquid helium is wanting, it would be rash to assert that all the conclusions of the book will stand the test of time. Nevertheless so much of the theory developed is so firmly based that it is most unlikely to be modified except in matters of detail, and this last book of London's seems destined to occupy for many years a place of honour in the literature of low temperature physics.

A. B. P.

BOOK NOTICES

The Language of Taxonomy—an application of symbolic logic to the study of classificatory systems. By JOHN R. GREGG, Associate Professor of Zoology, Columbia University. [Pp. ix+70.] Columbia University Press (London: Geoffrey Cumberlege). Price 20*s*.

Mathematics and Plausible Reasoning. Volume I: Induction and Analogy in Mathematics; Volume II: Patterns of Plausible Inference. By G. POLYA. [Vol. I, pp. xvi+280; Vol. II, pp. x+190.] Princeton University Press (London: Geoffrey Cumberlege). Price: Vol. I, 42*s*., Vol. II, 35*s*.; Vols. I and II, 70*s*.

Functionals of Finite Riemann Surfaces. By M. SCHIFFER and D. C. SPENCER. [Pp. x+451.] Princeton University Press (London: Geoffrey Cumberlege). Price 63*s*.

Contributions to the Theory of Partial Differential Equations. Edited by L. BERS, S. BOCHNER and F. JOHN. Papers read at the Conference on Partial Differential Equations sponsored by the National Academy of Sciences—National Research Council, October 1952. [Pp. 257.] Princeton University Press (London: Geoffrey Cumberlege). Price 32*s*.

[*The Editors do not hold themselves responsible for the views expressed by their correspondents.*]